Julius-Maximilians-
UNIVERSITÄT
WÜRZBURG

Charge Transport and Recombination Dynamics in Organic Bulk Heterojunction Solar Cells

Dissertation zur Erlangung des
naturwissenschaftlichen Doktorgrades
der Julius-Maximilians-Universität Würzburg

vorgelegt von
Andreas Baumann
aus Rothenburg ob der Tauber

Würzburg 2011

Eingereicht am: 11. Mai 2011
bei der Fakultät für Physik und Astronomie

1. Gutachter: Prof. Dr. Vladimir Dyakonov
2. Gutachter: Prof. Dr. Bert Hecht
der Dissertation.

1. Prüfer: Prof. Dr. Vladimir Dyakonov
2. Prüfer: Prof. Dr. Bert Hecht
3. Prüfer: Prof. Dr. Bernd Engels
im Promotionskolloquium.

Tag des Promotionskolloquiums: 02. August 2011

Doktorurkunde ausgehändigt am:

» Falls Gott die Welt geschaffen hat, war seine Hauptsorge sicher nicht, sie so zu machen, dass wir sie verstehen können. «

Albert Einstein (1879-1955)

Kurzfassung

Der Ladungstransport in ungeordneten organischen "bulk heterojunction" (Heterogemisch, Abk.: BHJ) Solarzellen stellt einen kritischen Prozess dar, der den Wirkungsgrad wesentlich beeinflusst. Aufgrund der großen Nachfrage neuer, vielversprechender Materialien für die organische Photovoltaik, ist es um so wichtiger nicht nur ihre photophysikalischen sondern auch deren elektrischen Eigenschaften zu charakterisieren. Gerade letztere erfordern experimentelle Messmethoden, die an funktionsfähigen Solarzellen angewandt werden können.

Zur experimentellen Untersuchung des Landungstransportes in organischen Solarzellen werden in dieser Arbeit die Methoden der transienten Photoleitfähigkeit, auch bekannt als "Time-of-Flight" (TOF), sowie die transiente Ladungsextraktionsmethode "Charge Carrier Extraction by Linearly Increasing Voltage" (CELIV) verwendet. Gerade Letztere ermöglicht es an Dünnschichtsystemen von nur wenigen 100 nm, eine typische Schichtdicke bei organischen Solarzellen, den Ladungstransport aber auch die Rekombination von Elektronen und Löchern zu untersuchen. Entscheidend für eine vielversprechende funktionsfähige organische BHJ Solarzelle ist dabei eine günstige Morphologie, die eine effiziente Generation von Ladungsträger, sowie deren Abführung zu den Elektroden erlaubt. Dabei wird in dieser Arbeit der Einfluss der räumlichen, als auch der der energetischen Unordnung der photoaktiven Schicht auf den Ladungstransport und der Rekombination der Ladungsträger untersucht. Das weit verbreitete Materialsystem bestehend aus Poly-3-(Hexyl) Thiophen (P3HT) und [6,6]-Phenyl C_{61} Buttersäure Methylester ($PC_{61}BM$) dient dabei als Donator–Akzeptor Referenzsystem. Neuartige Donator- bzw. Akzeptor-Materialien und deren Potential für künftige Anwendungen in der organischen Photovoltaik werden hinsichtlich ihrer Ladungsträgereigenschaften mit dem Referenzmaterialsystem verglichen.

Im Zuge der Kommerzialisierung organischer Solarzellen bzw. Solarmodulen ist die Anfälligkeit der Zellen gegenüber äußeren Umwelteinflüssen, wie Sauerstoff oder Wasser, in den Vordergrund des wissenschaftlichen Interesses gerückt. Dementsprechend wird in dieser Arbeit auch der Einfluss von synthetischer Luft auf den Transport und die Rekombination von Ladungsträgern und somit auf den Wirkungsgrad der Solarzelle untersucht und diskutiert.

Schließlich wird im Rahmen dieser Arbeit eine Erweiterung der photo-CELIV Messmethode vorgestellt. Diese ermöglicht es die Lebensdauer und den Transport von Ladungsträgern in organischen Dünnschicht-Solarzellen unter realen Arbeitsbedingungen, d.h. Beleuchtung unter einer Sonne bei Raumtemperatur, zu bestimmen.

Abstract

The charge transport in disordered organic bulk heterojunction (BHJ) solar cells is a crucial process affecting the power conversion efficiency (PCE) of the solar cell. With the need of synthesizing new materials for improving the power conversion efficiency of those cells it is important to study not only the photophysical but also the electrical properties of the new material classes. Thereby, the experimental techniques need to be applicable to operating solar cells.

In this work, the conventional methods of transient photoconductivity (also known as "Time-of-Flight" (TOF)), as well as the transient charge extraction technique of "Charge Carrier Extraction by Linearly Increasing Voltage" (CELIV) are performed on different organic blend compositions. Especially with the latter it is feasible to study the dynamics—i.e. charge transport and charge carrier recombination—in bulk heterojunction (BHJ) solar cells with active layer thicknesses of 100–200 nm. For a well performing organic BHJ solar cells the morphology is the most crucial parameter finding a trade–off between an efficient photogeneration of charge carriers and the transport of the latter to the electrodes. Besides the morphology, the nature of energetic disorder of the active material blend and its influence on the dynamics are discussed extensively in this work. Thereby, the material system of poly(3-hexylthiophene-2,5-diyl) (P3HT) and [6,6]-phenyl-C_{61}butyric acid methyl ester ($PC_{61}BM$) serves mainly as a reference material system. New promising donor or acceptor materials and their potential for application in organic photovoltaics are studied in view of charge dynamics and compared with the reference system.

With the need for commercialization of organic solar cells the question of the impact of environmental conditions on the PCE of the solar cells raises. In this work, organic BHJ solar cells exposed to synthetic air for finite duration are studied in view of the charge carrier transport and recombination dynamics.

Finally, within the framework of this work the technique of photo-CELIV is improved. With the modified technique it is now feasible to study the mobility and lifetime of charge carriers in organic solar cells under operating conditions.

Contents

Chapter 1
Introduction

The tremendous amount of CO_2 (carbon dioxide) produced over many years by fuel power plants and its dramatic impact on climate changes especially in the last decade rises the demand for sustainable energy resources. Besides wind and bio mass power, the photovoltaic (PV) technologies are an important renewable energy technology. In the year 2005 almost 84 million tons of released CO_2 could be avoided by using renewable energies in Germany [1]. Although solar power has up to now only a small contribution to that economy, the European Photovoltaic Industry Association forecasts an overall percentage of the electricity needs of 10% until year 2035.

The power generation from solar irradiation is based on the photovoltaic effect, which was first observed by Becquerel in 1839 [2]. Due to absorption of electromagnetic radiation, electrons are excited from the valence band into the conduction band. An electron–hole pair—so called exciton—is created, which is the prerequisite for a photocurrent generation. Since the first crystalline silicon (Si) solar cell was developed in Bell Laboratories by Chapin *et al.* in 1954 [3] with a power conversion efficiency (PCE) of around 6%, photovoltaic cells made from inorganic semiconductors have been studied extensively. Up to now, the efficiency has been increased to around 25% [4], which is already very close to the theoretically predicted upper limit of 30% for Si estimated by W. Shockley and H. J. Queisser [5]. The so-called Shockley–Queisser limit can be estimated by two considerations: First, only photons are absorbed with energies above the absorption edge of the semiconductor. For Si the band gap is about 1.1 eV. Thus, about half of the photon flux of the sunlight cannot be used for conversion to electrical power. Second, all energy above the energy band gap of the semiconductor is lost, as there is no way to capture this excess energy other than heating of the crystal. So, for single junction Si solar cells a theoretical limit of the performance can be calculated to be around 30%.

Silicon is an indirect semiconductor, which is one of the major disadvantages of the Si-based PV. The light absorption is much weaker in an indirect compared to a direct semiconductor, such as gallium arsenide (GaAs). Thus, to absorb 90% of the incoming light it takes around 1 μm of GaAs, but 100 μm of Si.[6] The diffusion length of the minority carriers, which are responsible for the photocurrent in inorganic solar cells, has to be at least twice the thickness of the semiconductor. For Si this results in a predicted cell thickness of around

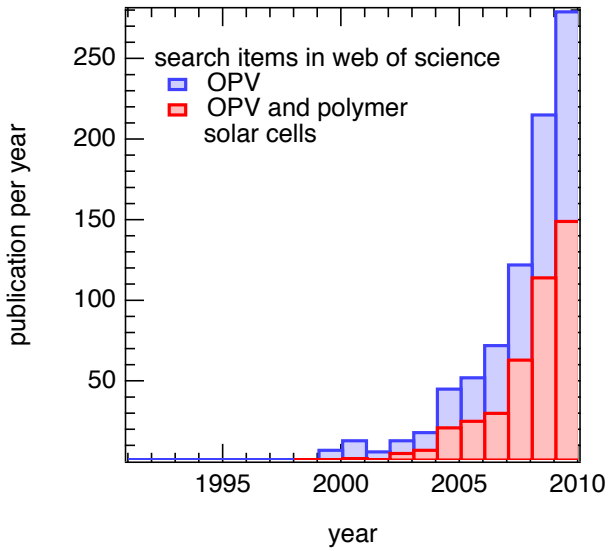

Figure 1.1: Number of publications per year in the field of OPV as a search item in Web of Science.

200 μm, which is quite a huge amount of material consumption compared to several hundreds of nm used in thin film technologies. Furthermore, the material has to be crystalline and of very high purity. One question for the near future will be the source of highly purified silicon for solar cells. Almost 50% of the module costs is related to the costs of processing silicon wafers. In the past, the PV industry just used the rejected material of the semiconductor industry, which was available for low costs.[6] However, this implies a dependence which is only viable if both industrial sectors grow with the same rate. Therefore, thin film technologies became more and more attractive. Besides thin film silicon photovoltaics, especially CIGS ($Cu(In,Ga)(S,Se)_2$) solar cells have drawn a lot of attention with PCE values of around 20.3% [4]. However the usage of rare elements like Indium (In) and Gallium (Ga) are one of the major disadvantages which has to be considered in case of CIGS solar cells.

Besides the conventional photovoltaic based on inorganic semiconductors, the field of organic photovoltaics (OPV) as part of the 3rd generation PV has become very interesting for scientists in the last decade. This is also reflected especially in the increase of publications since the year 2000 (see Figure 1.1), which indicates a highly emerging research field.

In the year 2000 Alan Heeger together with Alan MacDiarmid and Hideki Shirakawa were awarded with the Nobel prize in chemistry due to their discovery and the development of conductive polymers. This was a very strong impetus for organic semiconductors and their application in electronic devices, such as organic solar cells (OSC) and organic light emitting diodes (OLED).

Whereas OLEDs have already been implemented successfully in the market, e.g. in mobile phones or TV flatscreens, organic solar cells still have to catch up. However, due to their similarities scientists in the field of OPV can adopt lot of background knowledge from OLED research. In Figure 1.2 an overview of the developments in OPV is given. Especially, in the last three years, the PCE of organic solar cells has been increased almost twofold. For a promising commercial launch, however, the module efficiency values have to achieve at least 10%. For comparison, dye sensitized solar cells (DSSC) being a serious competitor for OSC are also depicted in Figure 1.2. The efficiency of DSSC haven't increased the last ten years.

In general, the field of OPV can be divided in two major areas: solar cells, which are based on small molecules and those based on conjugated polymers. Whereas the former need to be evaporated in ultra high vacuum, polymer solar cells can be made from solution. Especially due to their solution processability organic solar cells have a promising potential for low cost fabrication. The use of already implemented printing techniques or roll–to–roll processes allow for large scale applications with less material consumption. The future goal for low cost photovoltaics is to reach values around 1 € per Watt peak. It is commonly believed that organic photovoltaics has the best potential to produce electricity at much less than 1 € per Watt peak.[7] However, there are still some efforts needed to gain a deeper understanding in the working principle of organic BHJ solar cells, especially in the charge transport and loss mechanisms like charge carrier recombination. The aim of this work is to address the issues of charge transport and charge carrier recombination in organic BHJ solar cells and how they influence finally the power conversion efficiency. The conjugated polymer poly(3-hexylthiophene-2,5-diyl)(P3HT) blended with the fullerene [6,6]-phenyl-C_{61}butyric acid methyl ester ($PC_{61}BM$) is used as a reference material system. Besides the charge carrier mobility studied in the pure materials and its blend composition, the loss mechanisms in BHJ solar cells will be shown to be strongly dependent on the morphology within the bulk of the material system.

First of all, an overview will be given showing the major historical breakthroughs in the field of OPV, whereas the PCE has been increased from far below 1% to more than 8% nowadays. Before the materials used in organic bulk heterojunction solar cells are presented the fundamental processes in organic BHJ solar cells from light absorption to charge extraction are introduced. Finally, the experimental techniques used in this work are highlighted and the experimental results discussed extensively.

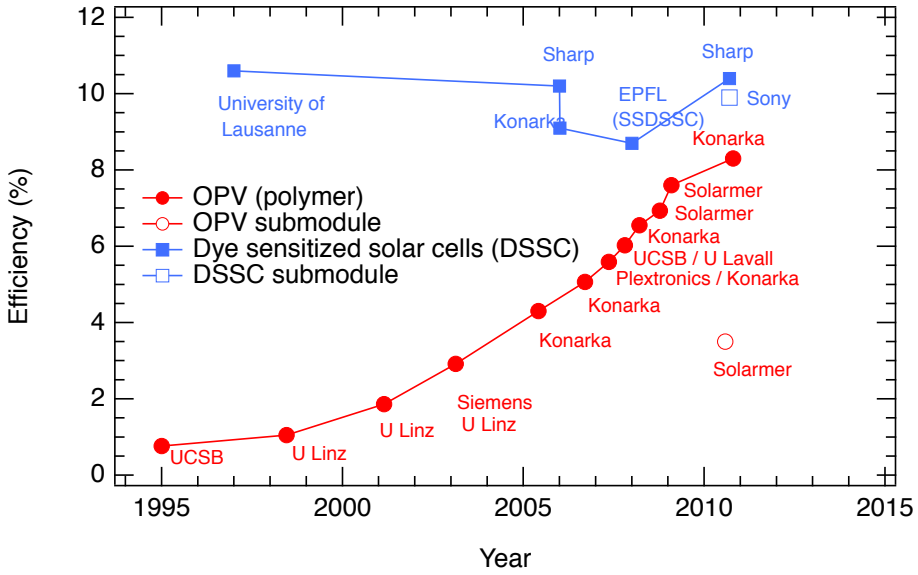

Figure 1.2: Development of the organic photovoltaics (OPV) and dye sensitized solar cells (DSSC): Power conversion efficiency (PCE) as single, module and tandem cells (after Ref. [8]).

Chapter 2

Organic Photovoltaics

2.1 Developments in the Field of Organic Photovoltaics

Several reviews can be found in literature, which give an overview of the milestones and principles in organic photovoltaics, such as presented by Deibel *et al.* [9] and Brabec *et al.* [8], both of which will build a fundamental basis for the following review.

Since the discovery of their conductivity polymers were amongst others spotlighted for the field of photovoltaics. As polymers exhibit usually a high absorption coefficient in the visible spectrum of the sunlight, thin films in the range of 100–200 nm are sufficient to harvest enough photons for energy conversion. The first organic solar cells consisting of a single polymer layer, however, had power conversion efficiency values far below 1% [10]. One of the reasons for their poor performance are the relatively strong exciton binding energies in organic semiconductors. The generated singlet excitons being formed on the polymer chain are strongly Coulomb bound with binding energies between 0.5 eV and 1 eV and called Frenkel excitons. In order to separate these Frenkel excitons either a sufficiently large thermal energy is needed or the excitons have to be dissociated at the contacts within their lifetime. Both processes are rather unlikely in an organic solar cell: The thermal energy is not high enough under operating conditions and the polymer film thickness is usually much larger than the exciton diffusion length. Without being separated singlet excitons recombine radiatively by emitting a photon (photoluminescence).

An important milestone for the field of OPV was the introduction of a second semiconductor layer on top of the polymer film forming a so-called organic bilayer solar cell structure (Figure 2.1(a)). Due to high electron affinity an electron can be now transferred from the polymer to the the second semiconductor. The latter provides sufficient energy for an electron to overcome the exciton binding energy, as the electron moves to a state of much lower energy (see Figure 2.1(b)). The light absorbing polymer is called donor, as it delivers the electron to the electronegative semiconductor, which accepts the electron and is thus called acceptor. The hole remains on the donor. However,

the charge transfer and hence the separation of an exciton can only occur, if the exciton reaches an donor–acceptor interface within its lifetime and if the difference between the energy of the electron sitting on the donor and sitting on the acceptor is larger than the exciton binding energy. The distance corresponding to the exciton lifetime may be referred to as the exciton diffusion length. After dissociation of the exciton the charge carriers, even though located on different molecules, are still Coulomb bound due to a week screening of the electric field in organic semiconductors forming a so-called polaron pair. Consequently, a further step is needed to overcome this Coulomb attraction and separate the bound charge carriers to finally get free polarons, which can then be extracted at the electrodes. A polaron is defined as a charge in combination with a distortion of its environment. Due to strong electron–phonon interaction a charge sited on an organic molecule often causes a deformation of the whole molecule. This implies that the charge transport becomes more difficult and the mobility of a charge carrier becomes lower.[11] The dissociation of polaron pairs can be achieved either by an electric field or by the energetic disorder of the organic semiconductors [12]. The first organic bilayer solar cell, which was built of a two layer structure of copper phthalocyanine (donor) and a perylene tetracarboxylic derivative (acceptor), was presented by W. Tang *et al.* [13]. With this structure a PCE of around 0.95% could be achieved, which was so far the highest reported efficiency value in the new field of organic photovoltaics. As in a bilayer organic solar cell only a

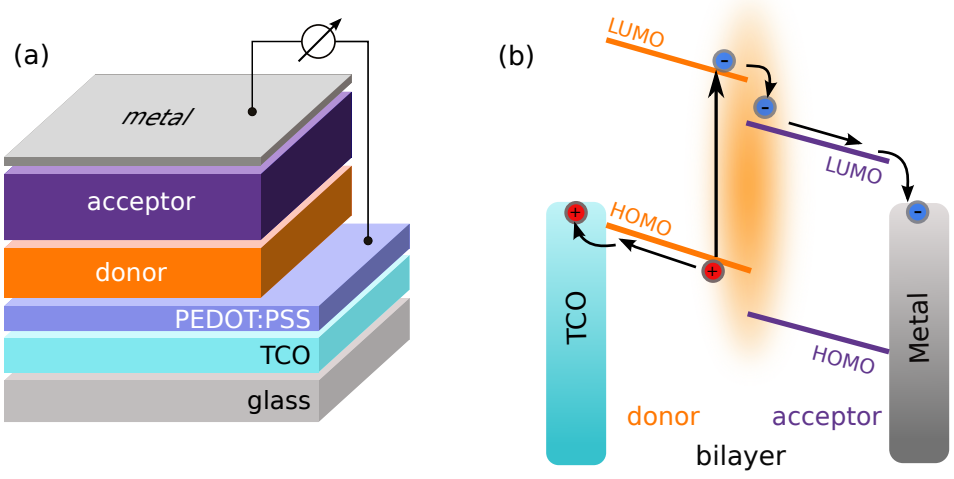

Figure 2.1: (a) Architecture and (b) energy diagram of an organic bilayer solar cell consisting of a donor and an acceptor layer.

single planar interface is formed between the donor and the acceptor only a

very small region compared to the bulk is sensitive for converting sunlight in photocurrent.

The concept of bulk heterojunction (BHJ) circumvent the problem of low exciton diffusion length, as many spatially distributed donor–acceptor interfaces are formed throughout the bulk of the solar cell (Figure 2.2(a)). Such organic bulk heterojunction solar cells can be achieved either by spin-coating of both compounds, which are already mixed in solution, or by co-evaporating small molecules. In 1995 Yu *et al.* [14] mixed the conjugated polymer poly[2-methoxy-5-(2'-ethyl-hexyloxy)-1,4-phenylenevinylene] (MEH-PPV) together with the soluble fullerene derivative [6,6]-phenyl-C_{61}butyric acid methyl ester ($PC_{61}BM$) reaching efficiency values still below 1%, which was the first reported solution processed bulk heterojunction solar cell system.[8] BHJ solar cells offer the great ability that photogenerated excitons can be dissociated very efficiently in the bulk. However, in case of a very fine intermixing of donor–acceptor interfaces the polaron pair dissociation and finally the charge transport to the respective electrodes due to missing percolation pathways become more difficult, as will be shown later in this work. The morphology plays a very important role for the performance of a bulk heterojunction solar cell. In the last years, several methods have been introduced to optimize the phase segregation of donor and acceptor compound, such as the choice of solvent [15], the thermal treatment [16] of the solution processed polymer:fullerene solar cell or by putting additives [17] to the blend solution. Thereby, all methods aim to achieve a more favorable structure in terms of electron–hole pair dissociation and charge transport. As a consequence, the PCE was increased manyfold, e.g. due to thermal annealing from around 1% to above 3%.

It is still an ongoing process of improving the performance of bulk heterojunction solar cells by tailoring the phase separation as well as looking for novel material systems. The highest efficiency reported so far for solution processed organic bulk heterojunction solar cells is as high as 8.3% [4].

A more detailed description of the fundamental processes taking place within a bulk heterojunction solar cell will be given in the next section.

2.2 Operational Principles of Organic Bulk Heterojunction Solar Cells

As was already briefly depicted above, the conversion of sunlight into electrical power in organic solar cells is somewhat different and more complicated compared to those based on inorganic semiconductors. In the following, the important steps will be highlighted from the beginning of light absorption

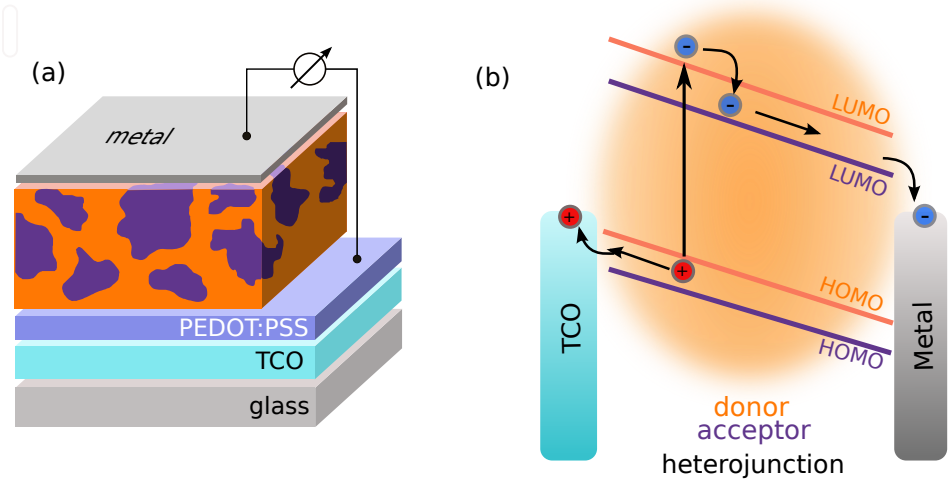

Figure 2.2: (a) Device architecture and (b) energy diagram of an organic bulk heterojunction solar cell; Due to well distributed donor–acceptor interfaces the whole bulk of the solar cells contributes to the generation of charge carriers and thus to the conversion of light to electric power.

and exciton generation to free polarons being extracted at the electrode. A detailed review of the fundamental processes in an operating organic bulk heterojunction solar cell was given by Deibel *et al.* in 2010 [9]. These processes are summarized in Figure 2.3.

Exciton Dissociation

Due to high absorption coefficients of the polymer exceeding 10^7 m^{-1}, a thin layer of a few hundreds of nm is sufficient to gain a satisfying absorption yield for power conversion. After light absorption by the polymer an electron–hole pair is formed on the polymer chain. In contrast to Mott–Wannier excitons generated in inorganic semiconductors with binding energies of around 25 meV, the generated Frenkel excitons in organic semiconductors possess rather huge binding energies in the range of 500 meV due to a small dielectric constant—$\varepsilon \approx 3$–4—and hence a small screening length.

For efficient dissociation the generated excitons have to diffuse to a donor–acceptor interface to overcome the binding energy [19, 20]. If the exciton is further away from the interface than its diffusion length, it will recombine radiatively by photoluminescence (see Figure 2.4). A prerequisite for excitons to dissociate is that the charge transfer to the acceptor molecule has to be energetically favorable, i.e. the energy gain is larger than the exciton binding energy. Actually the energy gain can only roughly be described by the energy

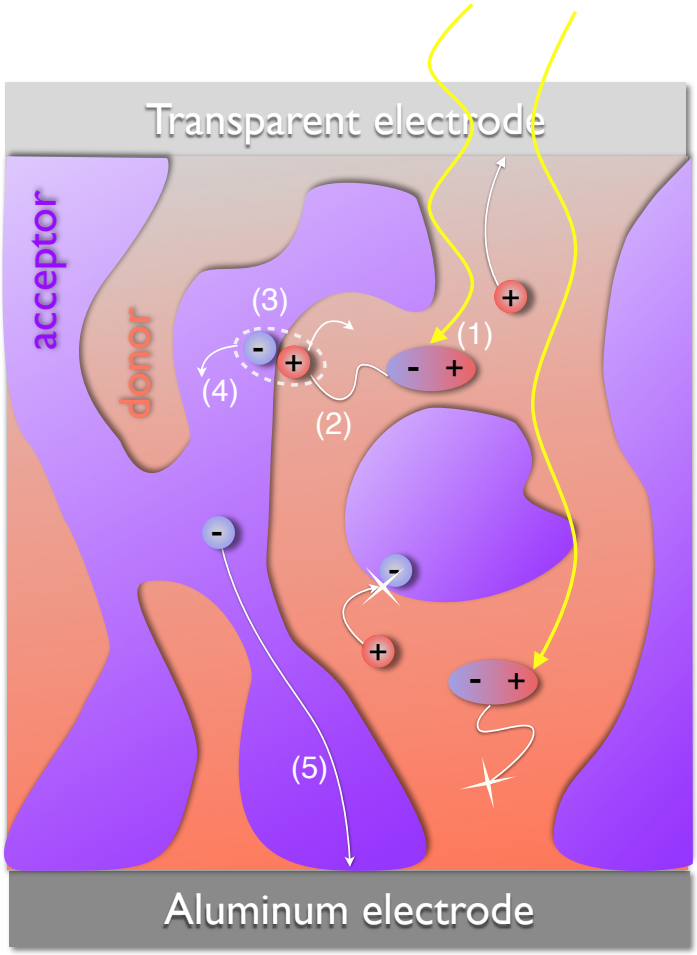

Figure 2.3: Overview of fundamental processes in organic bulk heterojunction solar cells: (1) Singlet exciton generation (2) Exciton diffusion to a donor–acceptor interface (3) Exciton dissociation creating a bound polaron pair (4) Polaron pair dissociation (5) Charge transport to the electrodes. (After Ref. [18]).

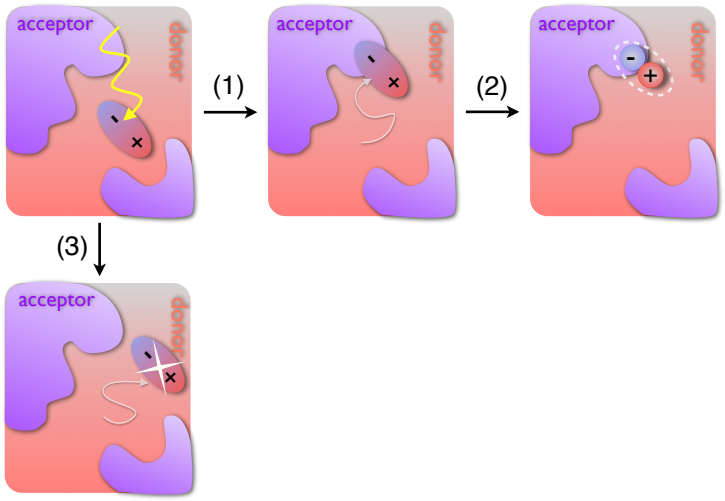

Figure 2.4: Exciton dissociation: Photogenerated exciton will diffuse to a donor–acceptor heterointerface (1) and be separated (2) or recombine radiatively by photoluminescence (3).

offset between the LUMO of the donor and the LUMO of the acceptor, as the LUMOs are energy levels of uncharged molecules—not occupied by a charge carrier—and thus not describing charged molecules or optical transitions.[21]

Polaron Pair Dissociation

After dissociation of a singlet exciton, the electron and the hole are still Coulomb bound residing on two different material compounds, i.e. acceptor and donor material, respectively [22]. The formation of a polaron pair is the intermediate step from a photogenerated exciton to a pair of free polarons [23].

A commonly used model to describe the dissociation probability of two charges is the Braun–Onsager model. In 1938 Onsager calculated the probability to separate a Coulomb bound pair of ions oppositely charged with a given initial distance with the aid of an external electric field [24]. Later, Braun extended the model of Onsager, as he was taking into account the finite lifetime of the initial bound states. Furthermore, he applied the model to the dissociation of charge transfer states in donor–acceptor systems [25]. Up to now the Braun–Onsager model is the most commonly used model to describe the polaron pair dissociation probability in organic solar cells[26, 27, 28, 29]. A bound polaron pair has either the possibility to be dissociated into free charges with a rate k_d or recombine to the ground states with a constant rate given by the inverse of the lifetime $k_f = \tau_{PP}^{-1}$. Finally, free charges can meet and generate a bound polaron pair with a rate k_r (see Figure 2.5) again. Note

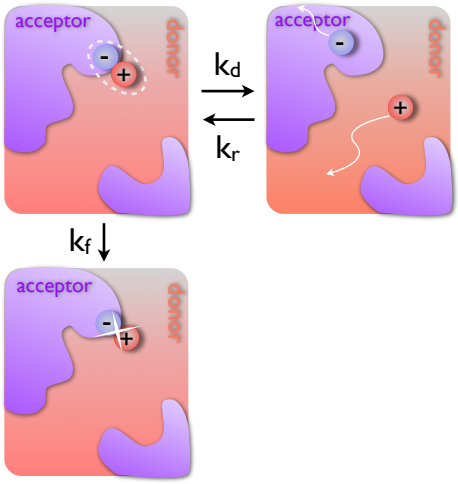

Figure 2.5: Schematic overview of the polaron pair dissociation process: Bound polaron pairs can either be dissociated into free polarons with the rate k_d or recombine radiatively with rate k_f to the ground state. The rate k_r accounts for free polarons met again forming a bound polaron pair. (After Ref. [9])

that the recombination of charge carriers in the Braun–Onsager model can only occur via a bound polaron pair. So if free charge carriers recombine, they will first build a Coulomb bound pair.

The probability for dissociation of a bound polaron pair is given by the equation

$$P_d(F) = \frac{k_d(F)}{k_d(F) + k_f} \quad , \tag{2.1}$$

where F is the electric field and $k_f = \tau^{-1}$ is the recombination rate of the polaron pair to the ground state. The probability $P_d(F)$ contains the charge carrier mobility μ as well as the polaron pair recombination rate k_f in linear dependence, so that the $\mu\tau$–product has a great impact on the dissociation yield [9].

A drawback of the Braun–Onsager model is that the model does not account for energetic disorder or high local charge carrier mobility along polymer chains [30, 31, 32]. However, it was shown recently by Deibel *et al.* [33] that the conjugation length of the polymer has an important impact on the polaron pair dissociation. They used Monte Carlo simulations considering energetic disorder and an effective conjugation length. In contrast to Braun–Onsager theory, they found a qualitatively good agreement for the dissociation yields between 20% and 75%.

Polaron pairs might also be lost due to an extraction of charge carriers

at the wrong electrode. This is in analogy to the process found in literature in conjunction with electron and hole blocking layers [34, 35, 36, 37]. As polaron pairs are still attracted by Coulomb interaction, they can even move against the electric field, when the latter is not much higher as the energetic disorder of the system. This behavior may be observed in disordered organic systems as a negative field dependent charge transport [38, 39]. However, as this process has been predicted only by Monte Carlo simulations [40] but is hard to be determined experimentally, the importance of this loss mechanism is difficult to estimate.

Finally, polaron pair dissociation might also be influenced by the excess energy which is available after the exciton dissociation. The Durrant group found a direct relationship between the photogenerated polaron density and the energy offset of the HOMO of the donor and the LUMO of the acceptor ($\mathrm{HOMO}_D - \mathrm{LUMO}_A$) [41]. This implicitly indicates that the excess energy gained after the dissociation of an exciton serves the polaron pair with additional kinetic energy, such that the Coulomb attraction can be overcome. Following this assumption, a smaller energy offset between the HOMO of the donor and the LUMO of the acceptor would also lead to an enhanced driving force for polaron pair separation. However, as the $\mathrm{HOMO}_D - \mathrm{LUMO}_A$ gap is directly proportional to the open circuit voltage of the bulk heterojunction solar cell it is not straight forward to increase the photocurrent. Rather, a trade-off between high photocurrent and open circuit voltage may have to be found to optimize the performance of organic bulk heterojunction solar cells.

Charge Carrier Transport and Recombination

Those polarons, which have successfully been separated, need to be transported to the respective electrode. In contrast to a band transport in crystalline semiconductors, the charge transport takes place by a so called *hopping* process between two neighboring localized energy states, which will be discussed more in detail in Chapter 3. As a consequence of the localized charge transport in a disordered environment, the charge carrier mobility in bulk heterojunction solar cells, or generally in all disordered organic semiconductors ($\approx 10^{-3}$ cm^2/Vs), is many orders of magnitude smaller compared to the mobility obtained in well ordered crystalline inorganic semiconductors (up to 10^3 cm^2/Vs). Thereby, the holes usually hop on the donor and the electrons on the acceptor material. The difficulty in establishing a unified theoretical model has hindered a complete understanding of the transport mechanism incorporating both, a macroscopic and a microscopic point of view [42]. Thereby, the charge carrier mobility defined as the proportionality constant between the

drift velocity of charges v_d and the applied electric field F

$$\mu = \frac{v_d}{F} \tag{2.2}$$

is one of the key parameters of interest.

On their way to the collecting electrode polarons can also undergo recombination resulting in a loss of photocurrent. In organic solar cells two main loss mechanism are distinguished, i.e. *geminate* and *non-geminate* recombination, which will be discussed more in detail in Chapter 4. Whereas geminate recombination is defined as a loss mechanism between two charges bound by Coulomb interaction after photogeneration, it is called non-geminate if two oppositely charged carriers recombine, which originate from two different excitons. Typical time scales reported for geminate recombination in organic donor–acceptor solar cells are in the range from hundreds of picoseconds up to around 100 ns [43, 44, 45, 46, 47], whereas non-geminate recombination occurs in a time range from μs to ms.

Charge Carrier Extraction and Surface Recombination

If the charge carriers survived the exciton dissociation, polaron pair separation and the transport to the electrodes without recombining non-geminately, they can be extracted at the electrode. The charge extraction process depends strongly on charge carrier concentration at steady state conditions determined by the device architecture. Thereby, the carrier concentration at the metal–organic interface is influenced by surface recombination, which again has an impact on the charge extraction process [9]. Scott and Malliaras [48] as well as Nelson *et al.* [49] have proposed the surface recombination to limit the performance of organic solar cells, i.e. the recombination at the organic/metal electrode interface. Surface recombination does not necessarily imply a loss of charge carriers except the case when both carrier types are extracted at the same electrode. A better way of describing surface recombination velocity is to think of an extraction rate of charge carriers at the electrodes. If the velocity is low the charge carriers cannot leave the device quickly enough so that a space charge region will be built at the contacts making the charge extraction process worse.[9]

2.3 Current–Voltage Characteristics and Solar Cell Parameters

The most important parameter describing the performance of a solar cell is the power conversion efficiency η, which is generally defined as the ratio between

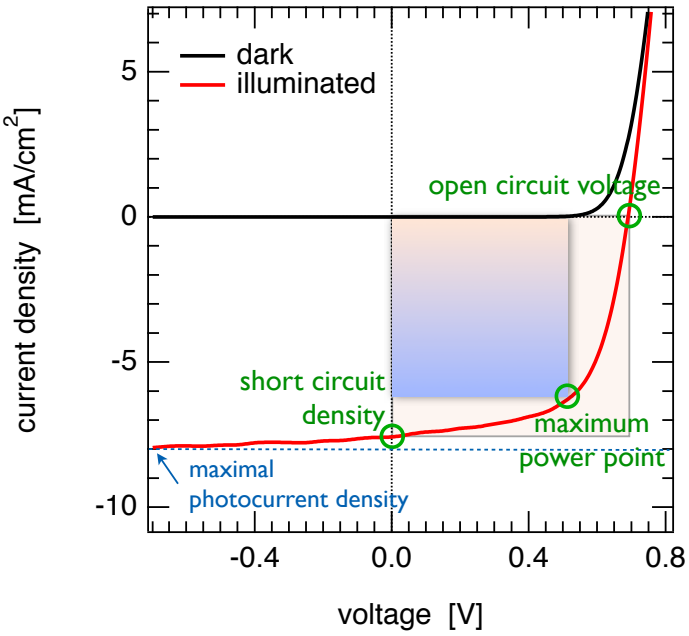

Figure 2.6: Characteristic current density–voltage (J–V) curve of an organic bulk heterojunction solar cell (here P3HT:bis-$PC_{61}BM$ 1:1).

the maximum power point P_{mpp} achieved by the solar cell and the incident radiant power P_L

$$\eta = \frac{P_{mpp}}{P_{\mathrm{L}}} \quad . \tag{2.3}$$

P_{mpp} can be calculated from characteristic parameters of the solar cells, i.e. the open circuit voltage V_{oc}, the short circuit current density j_{sc}, and the fill factor FF (see Figure 2.6). V_{oc} is defined as the point at which the current under illumination intercepts the voltage axis and hence is the voltage at which no net current is flowing. The short circuit current density on the other hand is the current flowing under illumination when no external voltage is applied to the solar cell. The fill factor is given by the ratio between the maximum power and the product of V_{oc} and j_{sc}. In other words, it describes the "squareness" of the current density–voltage (J–V) characteristics of the solar cell. The power conversion efficiency in equation (2.3) can be rephrased as follows:

$$\eta = \frac{P_{mpp}}{P_L} = \frac{V_{mpp} \cdot j_{mpp}}{P_L} = \frac{V_{oc} \cdot j_{sc} \cdot FF}{P_L} \quad , \tag{2.4}$$

with the current density j_{mpp} and the voltage V_{mpp} at maximum power point.

The solar cell parameters j_{sc}, FF, and V_{oc} are influenced by all of the above mentioned processes, i.e. the important steps from exciton generation

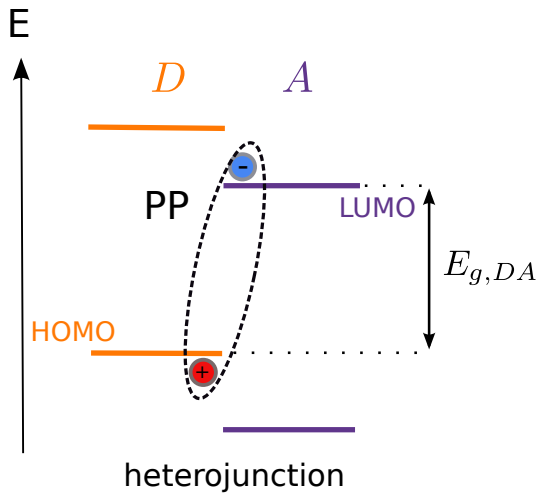

Figure 2.7: After exciton separation at a donor–acceptor heteroninterface the polarons are still bound by Coulomb interaction forming a bound polaron–pair (PP). The maximum energy available in a BHJ solar cell, which is given by energy band gap of the polymer, is reduced to $E_{g,DA}$, i.e. the energy difference between the LUMO of the acceptor and the HOMO of the donor.

and dissociation to the final extraction of free polarons at the electrodes. Whereas the fill factor and the short current density are mainly dominated by the steps from photogeneration of excitons to the gain of a photocurrent by the charge extraction, the open circuit voltage is related to the energetics of an organic solar cell. The maximum energy available in an illuminated organic solar cells is the energy of the singlet exciton. As these strongly bound excitons have to be dissociated into free polarons the theoretically obtained maximum of the open circuit voltage is reduced to the voltage defined by the so-called charge transfer (CT) state: the bound polaron pair (PP), which is directly related to the donor–acceptor interface [50] (see Figure 2.7). It was shown for polyphenylvinylene-based polymers that V_{oc} depends almost linearly on the effective band gap between the donor and acceptor $E_{g,DA}$ [51, 52]. However, in polyfluorene based devices, with higher V_{oc} values compared to polyphenylvinylene based solar cells, the work function difference of the metal contacts were found to influence the open circuit voltage [53]. Thus, the open circuit voltage in a bulk heterojunction solar cells is either limited by the contacts or the bulk depending on the which energy is smaller the difference of the work functions of the electrodes or the effective band gap $E_{g,DA}$, respectively. Even though a linear dependence of the V_{oc} on the difference between the HOMO and LUMO of donor and acceptor was found, a constant offset of around 0.3 V has to be included to correctly describe V_{oc} for a vast range of

donor–acceptor combinations [54]

$$V_{oc} = \frac{1}{q} \mid HOMO_D - LUMO_A \mid -0.3V \quad . \tag{2.5}$$

Vandewal *et al.* were able to observe the weak quantum efficiency of polaron pairs and hence the effective band gap of the blend material using Fourier transform photocurrent spectroscopy measurements, where they even found an offset of 0.43 V [55]. The reduced open circuit voltage compared to its theoretical maximum value is related to the quasi-Fermi level splitting, which cannot exceed the energy of the charge transfer state but can be lowered for some reasons. Deibel *et al.* [21] showed very recently that the open circuit voltage is limited due to radiative and non-radiative recombination. Under open circuit conditions the energy bands are not necessarily flat. Generally, a weak band bending between the donor and the acceptor material can be thought of. For the case of very fine intermixing of the donor and acceptor material the corresponding bands are expected to be parallel to each other as shown in Figure 2.2. In contrast, bilayer solar cells can reveal a strong band bending, as the donor and the acceptor are only connected at a planar heterointerface [9]. Besides the band bending, the open circuit voltage is also influenced by the injection barriers at the electrodes influencing the quasi-Fermi levels. A general equation can be given as

$$V_{oc} = \frac{E_{g,DA}}{q} + BB_D + BB_A - \Delta\Phi_C - \Delta\Phi_A \quad , \tag{2.6}$$

with the effective band gap $E_{g,DA}$ between the donor and the acceptor at the interface, the elementary charge q, the band bending in the donor layer BB_D and the acceptor layer BB_A, which can be both positive or negative. $\Delta\Phi$ accounts for the injection barriers from the anode into the donor or cathode into the acceptor, respectively.

In order to optimize the open circuit voltage V_{oc} in organic BHJ solar cells, the difference between the CT state—$E_{g,DA}$—and the open circuit voltage has to be reduced. This can be done for example by increasing the LUMO level of the acceptor [56, 57]. However, the reduction is limited as there is still a driving force needed for efficient exciton dissociation without electron back transfer. Furthermore, minimizing the recombination will help to reach a maximum possible open circuit voltage.

Even though the charge carrier mobility in organic bulk heterojunction solar cells is more than a million times smaller compared to crystalline silicon, it is amazing that the power conversion efficiency recently reached more than 8% [4]. To give an answer for that and further upcoming questions related to the quite remarkable performance of organic solar cells, was a main goal of this work.

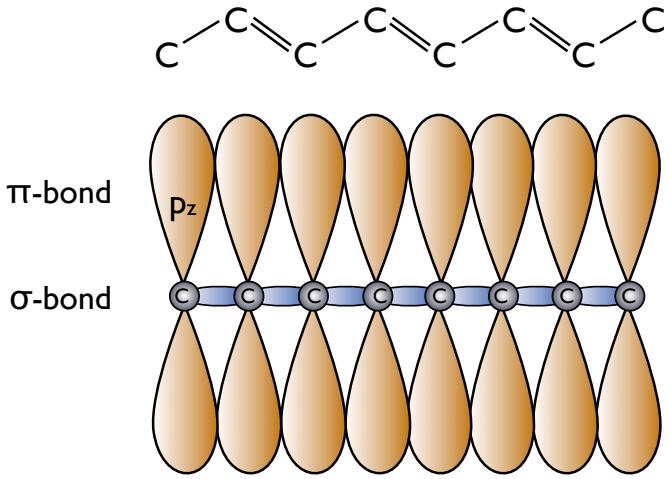

Figure 2.8: (Top) Alternating single and double carbon bonds and (bottom) the resulting configuration of the electronic sp^2 hybrid orbitals.

In the following, the two material classes—the donor and acceptor—for organic BHJ solar cells will be introduced.

2.4 Donor Materials

In solution processed organic BHJ solar cells usually a conjugated polymer is used as the donor material . Polymers in general are macromolecules with huge molecular weight ($>$ 10.000 mg/mol) [58], which are built of long chains of repeating chemical units, called monomers. A homo polymer is characterized by only one monomer, whereas copolymers results from the polymerization of more than one type of monomer. Depending on their structure polymers can have an isolating but also semiconducting character. The electronic structure of an organic semiconductor is based on so-called conjugated π-electrons. The ground state of a carbon atom is in the configuration $1s^2 2s^2 2p^2$. Due to hybridization the $2s^2 2p^2$ form four new orbitals energetically favored. The four sp^3 orbitals are oriented towards the corners of a regular tetrahedron allowing a strong degree of overlap in bond formation with another atom.

Conjugated polymers are characterized by their alternating single and double bonds of carbon atoms, which are hybridized in sp^2 configuration. Three orbitals formed by one s and two p orbitals ($p_x p_y$) are oriented planar, whereas the residual p_z orbital is located perpendicular to the σ-bond plane (see Figure 2.8). Two neighboring p_z orbitals are able to overlap and build a so-called π-bond with delocalized electron wave function above and below the σ-electrons in the bond plane. The overlapping π-electron wave functions to-

gether form a π-band. Since the delocalized orbitals are half-filled, one might expect metallic behavior due to a finite density of states (DOS) at the Fermi level [42]. However, this does not happen due to the appearance of a band gap between the filled bonding states—π-band or highest occupied molecular orbital (HOMO)—and the empty anti bonding states—π^*-band or lowest unoccupied molecular orbital (LUMO)—lowering the energy of filled states on account of Peierls instability [59]. The Peierls theorem, as was shown by Rudolph Peierls in 1955, states that a one-dimensional system—in this case the long carbon chain—with an incompletely filled band distorts in a way as to open up a gap at the Fermi level [60]. A band gap of 1–3 eV between the HOMO and the LUMO is responsible for the semiconducting properties of such organic compounds. In Figure 2.9 the chemical structures of some representative conjugated polymers are shown.

The chain of a conjugated polymer is not stretched indefinitely, but makes twists and coiled structures. Thus, the delocalization length of the π-cloud of electrons is limited to a definite length, also known as conjugation length, which is bounded by an energy barrier created by defects [61]. Furthermore, the conjugation lengths of a conjugated polymer obey random distributions leading to alternating energies of the π-electrons. This can be seen in broad and featureless absorption and emission spectra, often observed for conjugated polymers (see Figure 2.10). However, some conjugated polymers reveal also a crystalline phase besides the amorphous nature. Such crystallinity is strongly related to a well ordered polymer chain conformation.

Apart from charge delocalization, an important factor for charge transport in conjugated polymers are inter-chain interactions, π-π stacking as well as the role of side groups. In contrast to the intra-chain interaction, where the transport occurs along the polymer chain, the charges move perpendicular to the polymer chains along the π stacks. Thereby, the delocalization of π-electrons along the polymer backbone is not sufficient for charge transport.

2.5 Acceptor Materials

Since their first use in organic bulk heterojunction solar cells in 1995 [14], fullerene derivatives have been widely used as acceptor materials being a n-type semiconductor. The most commonly used fullerene derivatives are the [6,6]-phenyl-C_{61}butyric acid methyl ester ($PC_{61}BM$) and [6,6]-phenyl-C_{71} butyric acid methyl ester ($PC_{71}BM$). They consists mainly of a C_{60} or C_{70} cage with an additional side chain to allow for solubility in organic solvents (Figure 2.11). Both are used as electron acceptors in organic BHJ solar cells in this work. The reason for their ability to accept electrons from the donor is based

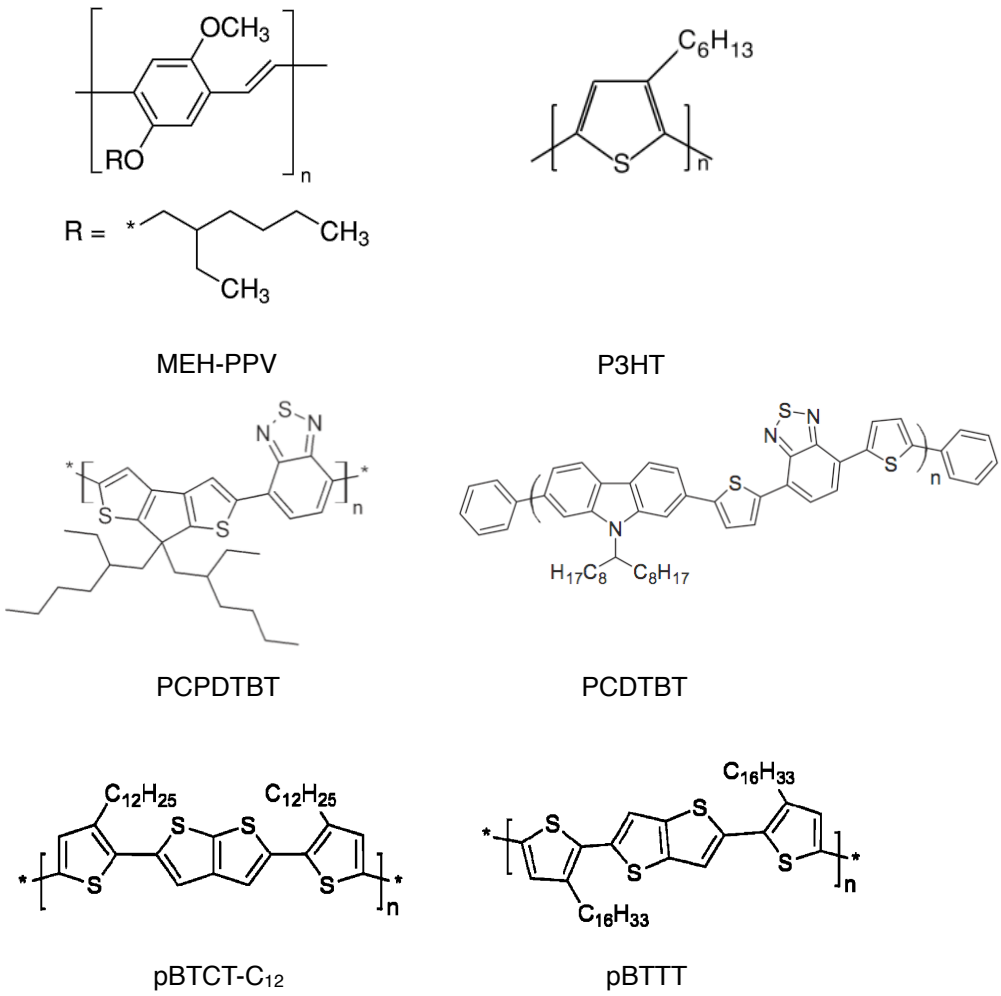

Figure 2.9: Some representative conjugated polymers: poly[2-methoxy-5-(2'-ethyl-hexyloxy)-1,4-phenylenevinylene] (MEH-PPV), poly(3-hexylthiophene-2,5-diyl) (P3HT), poly[2,6-(4,4-bis-(2-ethylhexyl)-4H-cyclopenta[2,1-b;3,4-b']dithiophene)-alt-4,7-(2,1,3-benzothiadiazole)] (PCPDTBT), poly[[9-(1-octylnonyl)-9H-carbazole-2,7-diyl]-2,5-thiophenediyl-2,1,3-benzothiadiazole-4,7-diyl-2,5-thiophenediyl] (PCDTBT), poly(2,5-bis(3-alkylthiophen-2-yl)thieno[2,3-b]thiophene) (pBTCT-C_{12}), poly(2,5-bis(3-tetradecylthiophen-2-yl) thieno[3,2-b]thiophene) (pBTTT).

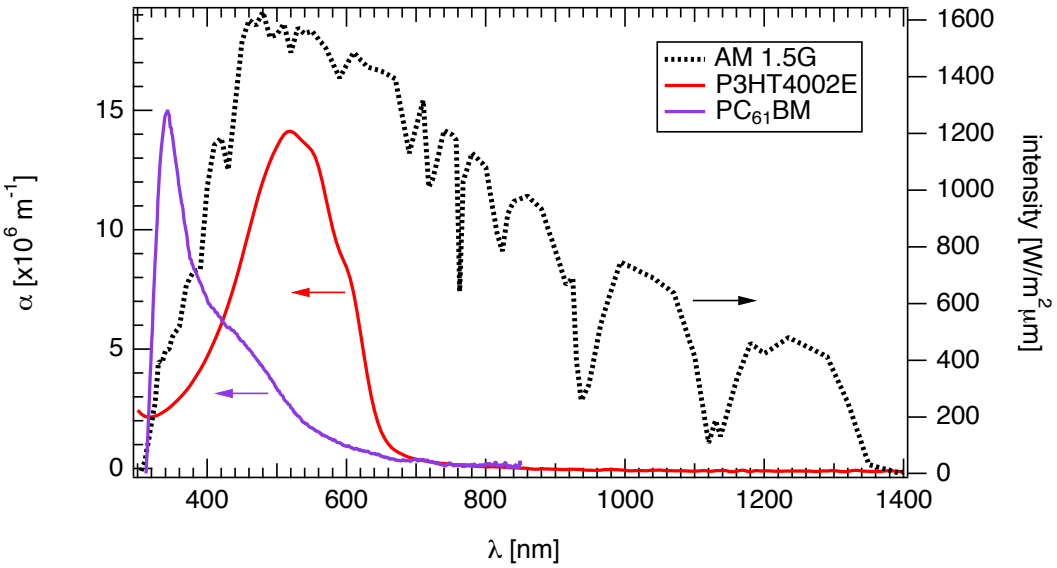

Figure 2.10: Absorption coefficient α (left axis) of the conjugated polymer P3HT4002E and the fullerene $PC_{61}BM$as a function of the wavelength λ; AM1.5 G solar spectrum (right axis) is also shown.

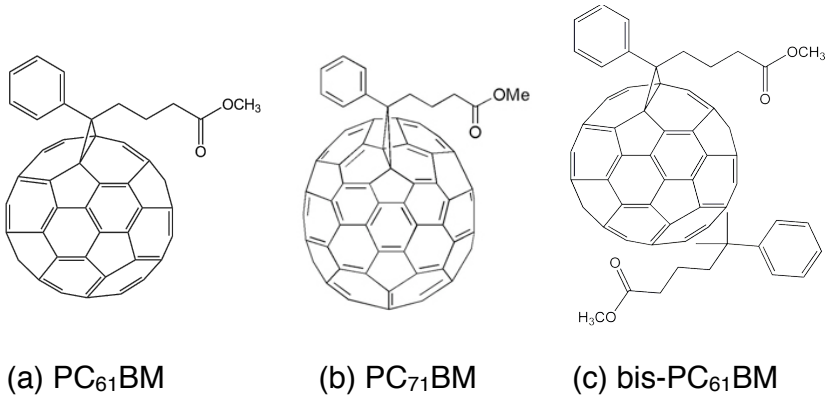

(a) $PC_{61}BM$ (b) $PC_{71}BM$ (c) bis-$PC_{61}BM$

Figure 2.11: Fullerene Derivatives: (a) [6,6]-phenyl-C_{61}butyric acid methyl ester (b) [6,6]-phenyl-C_{71} butyric acid methyl ester (c) bis-[6,6]-phenyl-C_{61}butyric acid methyl ester.

on several factors. Fullerenes have appropriate LUMO levels with respect to most of the used conjugated polymers, so that an electron can easily be transferred from the polymer to the fullerene.[62] Consequently, fullerenes exhibit ultrafast (sub-ps) forward photoinduced electron transfer when combined with conjugated polymers like MDMO-PPV or P3HT [63]. Due to three dimensional symmetry, fullerenes can isotropically (in case of C_{60} cage) or relatively isotropically (in case of C_{70} cage) accept electrons, which is favorable in three dimensional bulk heterojunction structures. Moreover, fullerenes exhibit good electron mobilities (up to 1 cm^2/Vs) [64], in addition to the extended exciton diffusion length, which has been estimated in pure C_{60} to be of the order of 40 nm [65].

In order to avoid energy transfer instead of charge transfer between the donor and acceptor it is important that the HOMO level is low enough, which is true for C_{60} and C_{70}.
However, there are of course also disadvantages in using fullerene derivatives in organic bulk heterojunction solar cells. One of these drawbacks is the insolubility in solvents other than aromatic and even in those the solubility is limited. Furthermore, the relatively low optical absorption in the solar spectral range limits the photon harvesting. For $PC_{71}BM$, however, the absorption width is broadened due to an asymmetrical shape of the molecules absorbing also in the visible range. By adding more side chains to the fullerene cage bisadducts of the fullerene can be obtained like bis-$PC_{61}BM$ [66] shown in Figure 2.11(c). The addition of a side chain will increase the LUMO level of the fullerene and hence lead to an increase in the open circuit voltage of the solar cell. However, as a major drawback it will also enhance the energetic disorder, as a close packing of the fullerene cages will be distorted [67]. A comparative study of the charge transport and recombination dynamics in P3HT:$PC_{61}BM$ and P3HT:bis-$PC_{61}BM$ BHJ solar cells will be presented later in Chapter 8.

In the past several years, efforts have been made to find alternative acceptor materials, which, for example, contribute more strongly to the absorption of solar sunlight. As V_{oc} is related to the energetic difference between the LUMO of the acceptor and the HOMO of the donor, this difference has to be increased as much as possible as already mentioned above (see Figure **XXX**). However, even though the band gap $E_{g,DA}$ can be larger than 1 eV, V_{oc} might be limited well below 1 V due to charge carrier recombination. Therefore, it is of particular importance to understand the recombination processes in the bulk in order to improve the solar cell performance.

Remarkably, even after 15 years of extensive research for acceptor materials, $PC_{61}BM$ is still one of the best performing acceptors and being certainly the most widely used electron acceptor for organic photovoltaics devices.[8]

Chapter 3

Charge Transport in Organic Disordered Materials

In this chapter, some of the models describing the transport in organic disordered systems will be presented, one of which is the commonly used Gaussian disorder model (GDM).

Many organic semiconductors like π-conjugated polymers are disordered and amorphous in nature. Due to the absence of three dimensional periodical lattice structure the transport cannot be described by classical semiconductor models, such as transport in bands. Instead, the spatial and energetic disorder in organic semiconductors lead to the formation of localized states [68], whereas charge carriers may proceed from one state to another by a hopping process. Depending on the distance between the hopping sites and their energy, some of the hopping steps will be easy and some more difficult. In case of a large energetic distance between two neighboring hopping sites the charge carrier may considered to be trapped, even if no trap states—such as chemical defects—are are present in the organic semiconductor pope1999book.

Inorganic well ordered semiconductors offer a quasi free transport of charge carriers within delocalized states, i.e. the conduction and valence band for electrons and holes respectively, with a characteristic temperature dependent charge carrier mobility: At low temperatures the transport is limited by Coulomb repulsion of equally charged carriers with the a temperature behavior of $\mu \propto T^{3/2}$, whereas at high temperatures scattering at phonons leads to a temperature dependence of $\mu \propto T^{-3/2}$ [69]. In organic disordered materials the charge carrier mobility exhibits also a temperature dependence, which can ,however, more described by thermally activated processes. Furthermore, in the early 1970s a field dependent charge carrier mobility, similar to Poole–Frenkel [70], was found experimentally by Gill when studying the charge transport in molecularly doped polymers by using the experimental technique of transient photoconductivity, also known as time-of-flight (TOF) (see Section 6.1). He proposed an empirical formula describing the experimental observations he made on the polymer polyvinylcarbozole to be

$$\mu(E,T) = \mu_0 \exp\left(-\frac{\Delta_0 - \beta\sqrt{F}}{kT_{eff}}\right), \quad \frac{1}{T_{eff}} = \frac{1}{T} - \frac{1}{T_0} \quad , \tag{3.1}$$

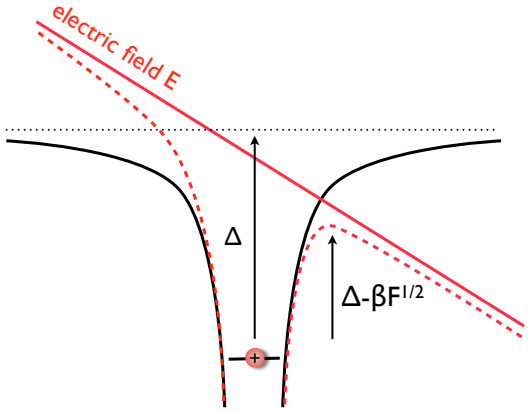

Figure 3.1: Poole–Frenkel effect: A charge carrier trapped in a Coulomb potential can be released due to barrier lowering.

where μ_0 is the zero field mobility, F is the field strength, β is the field activation parameter and Δ_0 the activation energy. A Poole–Frenkel like behavior describes a charge carrier trapped in a Coulomb potential well, whereas the barrier is lowered in the direction of the applied electric field (see Figure 3.1).

As was already suggested by Gill—even though not physically understood—at a certain temperature T_0, a negative field dependence of the charge carrier mobility μ can be observed. Indeed, in disordered organic semiconductors sometimes a negative dependence of the charge carrier mobility on the electric field F is observed experimentally, i.e. a decreasing μ with increasing F. The reason for this behavior is not completely understood yet, the answer of which, however, is often related to the hopping mechanism in a Gaussian density of states (GDOS) distribution [39]. Thereby, it may be originated from the influence of diffusion on the charge carrier mobility, although μ is actually a drift parameter.

3.1 Variable Range Hopping

The hopping transport mechanism is generally characterized by a combination of tunneling from one site to the next neighboring state and a thermally activated process. The former depends on the transfer integral between the corresponding wave functions.[9] Marcus proposed in the mid 1950s a hopping rate describing a jump from site i to site j by [71, 72]:

$$\nu_{ij} = \frac{\mid I_{ij} \mid^2}{\hbar} \sqrt{\frac{\pi}{\lambda k T}} exp\left(-\frac{(\Delta G_{ij} + \lambda)^2}{4\lambda k T}\right) \quad , \tag{3.2}$$

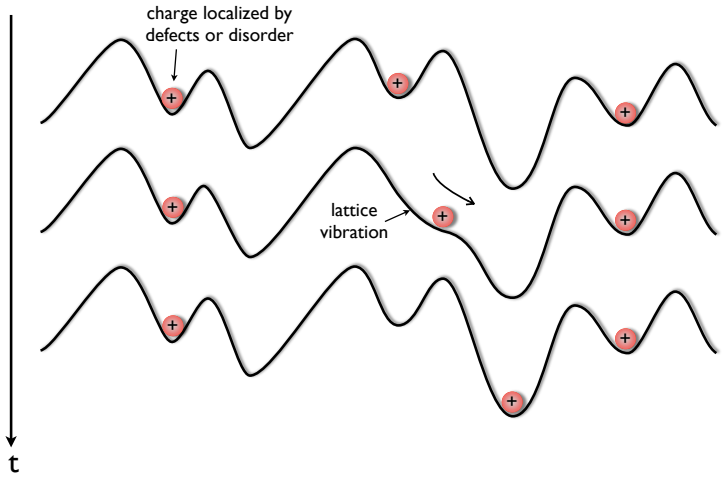

Figure 3.2: Hopping transport in an irregular lattice. Charge carriers localized on a defect site can only move from one site to another when energetically activated by a lattice vibration (after Ref. [11]).

with the transfer integral I_{ij}, i.e. the wave function overlap between site i and site j, which is equivalent to the tunneling. λ represents the reorganization energy related to the relaxation of the molecule upon charge transfer (polaron relaxation), kT is the thermal energy and ΔG_{ij} is the energy difference between the two sites i and j. In 1956 Conwell [73] and Mott [74] proposed the concept of hopping transport in order to describe impurity band conduction in organic semiconductors. Only a few years later, in 1960, Miller and Abrahams calculated the transition rate ν_{ij} for a phonon assisted hopping process from an occupied state i with an energy E_i to an unoccupied state j with energy E_j [75] to be:

$$\nu_{ij}(E_i, E_j, R_{ij}) = \nu_0 \exp(-2\gamma R_{ij}) \begin{cases} \exp\left(-\dfrac{E_j - E_i}{kT}\right) & E_j > E_i \\ 1 & E_j < E_i \end{cases} . \quad (3.3)$$

ν_0 is the maximum hopping rate, also known as attempt–to–escape frequency, R_{ij} is the spatial distance between the states i and j, γ is the inverse localization radius being proportional to the transfer integral, k the Boltzmann constant and T the temperature. The first exponential term in Equation (3.3) describes the overlap of the wave function of the states i and j representing again the tunneling contribution, whereas the second exponential term accounts for the temperature dependence of the phonon density. As can be seen, for jumps upwards in energy also a Boltzmann term is used in analogy to the Marcus theory, even though the energy difference ΔE_{ij} usually considers only energetic disorder, but not the polaron relaxation. Both hopping rates

proposed by Marcus and Miller–Abrahams were applied in Monte-Carlo simulations [76, 77, 78] or hopping master equations [79, 80] to gain insight into the macroscopic charge transport properties in disordered materials, where analytic solutions are difficult to find.

3.2 Gaussian Disorder Model (GDM)

A famous model describing the transport of charge carriers in an energetic disordered environment was given in 1993 by Heinz Bässler [77]. Due to fluctuations in conjugation lengths and structural disorder the charge transporting sites of polymers are spread in energy. From absorption measurements, Gaussian shaped spectra has been revealed for many polymers [77]. Thus, charge transport sites in disordered systems are often described by a Gaussian density of states (GDOS) distribution, given by

$$g(E) = \frac{N_t}{\sqrt{2\pi\sigma^2}} \exp\left(-\frac{E^2}{2\sigma^2}\right) \quad . \tag{3.4}$$

N_t reflects the density of localized states and σ the standard deviation of the density of states being also representative for the degree of disorder of the material. Bässler described in his Gaussian disorder model (GDM) [77] the transport in disordered organic systems by a hopping process in a system with energetic and spatial disorder being uncorrelated to each other and both characterized by a GDOS distribution. The hopping rate between two neighboring sites was assumed to obey the Miller–Abrahams equation (Equation (3.3)). From Monte-Carlo simulations, he found the charge carrier mobility to depend on temperature T and the electric field F:

$$\mu = \mu_\infty \exp\left\{-\left(\frac{2\sigma}{3kT}\right)^2\right\} \begin{cases} \exp(C[(\frac{\sigma}{kT})^2 - \Sigma^2]\sqrt{F}), & \Sigma \geq 1.5 \\ \exp(C[(\frac{\sigma}{kT})^2 - 2.25]\sqrt{F}), & \Sigma < 1.5 \end{cases} \quad , \tag{3.5}$$

assuming a Gaussian density of states distribution of the width 2σ (see Figure 3.3). σ/kT is defined as the energetic disorder parameter and Σ as the spatial disorder parameter. C and the factor $2/3$ are scaling factors from parametric fits. The results are in good agreement with the empirical equation found by Gill in 1972 (Equation (3.1)). Consequently, the parametric GDM model is commonly used in literature, even though it is assumed that the site energies are distributed independently with no correlations among them. However, using the GDM the Poole–Frenkel like field dependence of the charge carrier mobility can only be explained in a narrow field range. Five years later, Novikov and Dunlap [81] extended the GDM model, as they

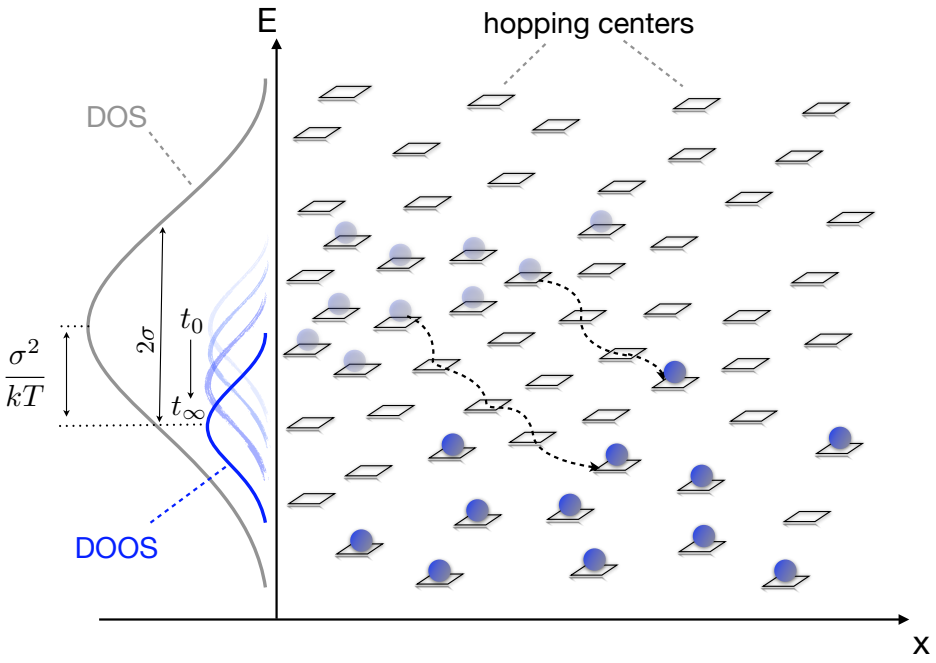

Figure 3.3: Hopping processes in an energetic landscape of site energies distributed by a Gaussian density of states distribution (GDOS). Charge carriers tend to relax down in energy during their hopping motion.

proposed a correlated disorder model (CDM), where the spatial and energy disorders depend on each other. They took into account that a changing environment for a given molecule will have an influence on its energetic position, which was not considered in the model presented by Bässler. Using CDM, it is then possible to reconcile to a wider range of validity of the Poole–Frenkel law even down to low and intermediate fields.

Even though a Gaussian shape of the DOS was found from absorption measurements [82], the actual shape maybe somewhat different. Thereby, often a combination of a Gaussian DOS and an exponential DOS is supposed [83], whereas the latter describes the tail states of the DOS [84, 85, 86].

3.3 Multiple Trapping and Release (MTR) Model

Another extension to the GDM was given by Pasveer *et al.* in 2005 [79]. Previously, it was observed experimentally that the charge carrier mobility depends on the concentration of the charge carriers in amorphous organic

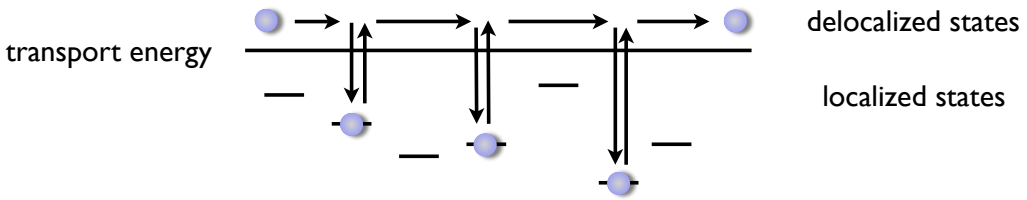

Figure 3.4: Overview of the multiple transport and release model: Charge carriers get trapped in states below the transport energy E_{tr} during their transport. They can only contribute again to the transport if released from the trap state to a state above E_{tr}.

semiconductors [87, 88], which was assigned to a filling of the Gaussian density of states, where lower states act as traps [89]. Using a hopping master equation approach and fitting parametrically an empirical description for the carrier concentration dependent mobility was found [79], which is sometimes termed as the enhanced Gaussian disorder model. In this context, the concept of the transport energy has to be considered [90, 91, 92]. Thereby, the transport energy can be compared with the mobility edge [91] in amorphous inorganic semiconductors. Charge carriers tend to relax in energy—in other words thermalize—to an equilibrium state, which is defined as the transport energy E_{tr} (see Figure 3.3), where the character of relaxation changes: After a hop to a state below E_{tr}, the charge carrier prefers to hop upward towards E_{tr}. These processes above and below E_{tr} resample multiple trapping and release (MTR) processes (Figure 3.4), where E_{tr} plays the role of the mobility edge [90]. For a given temperature, this equilibrium state is on average σ^2/kT below the centre of density of states distribution (see also Figure 3.3). It has been shown by Monte-Carlo simulation [93] and analytically [91, 92] that a carrier will most probably jump from a currently occupied state to a hopping site belonging to the effective transport energy level E_{tr} given by the transcendental equation [92]:

$$\int_{-\infty}^{E_{tr}} dE \;\; g(E)(E_t - E)^3 = \frac{6}{\pi}(\gamma kT)^3 \tag{3.6}$$

Charge carriers below E_{tr} mostly do not contribute to the transport and are considered to be trapped. Keeping this picture in mind, the MTR model adapted from trap-rich inorganic semiconductors such as amorphous silicon (a-Si) is often used to describe the charge transport in organic semiconductors in equivalence to a band transport including trapping events.

However, the transport in a blend consisting of two material compounds, as

is the case in BHJ solar cells, is even more complicated to describe. Compared to single material devices an additional spatial disorder in the bulk has to be taken into account. For an efficient charge transport in a BHJ percolated pathways have to exist in order to connect both material phases with the corresponding electrodes.

On their way to the electrodes charge carriers may also undergo loss mechanisms such as recombination, which will be discussed in the following chapter.

Chapter 4

Charge Carrier Recombination

Now, the loss mechanism of charge carrier recombination in organic bulk heterojunction solar cells will be discussed in detail. Before focusing on organic disordered systems, an overview of the four main types of charge carrier losses, which can occur in semiconducting materials in general, will be highlighted.

If two oppositely charged carriers meet each other within a distance, which is smaller than the Coulomb capture radius r_c, they are most likely lost due to recombination. Thereby, r_c is defined as the point where the Coulomb energy of the two charge carriers is of the order of the thermal energy. Thus, thermal fluctuations will lead to the complete separation of the two charge carriers [94]. If the recombination is associated with the emission of a photon it is called radiative, otherwise non-radiative if only phonons are emitted [11]. Whereas in inorganic semiconductors the Coulomb attraction is rather small (in the order of kT at room temperature; 25 meV) due to high dielectric constant of about $\varepsilon \approx 11$–12, charge carriers in organic semiconductors with $\varepsilon \approx 3$–4 suffer from a four times higher Coulomb force. Moreover, charge carrier recombination in inorganic semiconducting crystalline materials will mostly occur at trap states in the band gap of the crystal caused e.g. by impurities or grain boundaries, also known as Shockley–Read–Hall recombination. Due to the typically high purity of crystalline materials this kind of loss mechanism, however, is not a limiting factor of the solar cell performance. This might be different in organic disordered materials.

In 1978 Mott discussed four main types of recombination mainly considering inorganic systems [95, 11]:

1. **Auger recombination:** This kind of recombination is generally a rather unusual process, where three particles are involved. Mott distinguishes between two cases:

    a. In the presence of localized states:
    A hole (or electron) is trapped at a defect, and the countercharge recombines with the trapped charge forming a transient trapped charge-transfer (CT) state. If another free electron collides with the trapped CT state, an Auger process can take place, in which all the recombination energy is used to impart kinetic energy to the free electron.

   b. band-to-band:
      Here, holes and electrons recombine directly, giving their excess energy to another atom that can ionize.

2. **Recombination at defects – radiative** Here, the recombination can take place at an impurity of a crystal imperfection being radiative or non-radiative. This loss mechanism is often used to describe the recombination in organic crystals but also in inorganic ordered semiconductors and is known as Shockley–Read–Hall recombination.

3. **Recombination with multi-phonon emission** This is an non radiative recombination process describing a more general problem of non radiative decay of a free or trapped excitons in organic crystals.

4. **Recombination energy loss by cascade** In general, this process addresses the recombination of charge carriers with excess kinetic energy, which eventually meet each other within the Coulomb capture radius r_c. If the charge carriers at that point loose energy due to phonon emission, the probability of recombination increases exponentially. However, the charge carriers have a chance to escape even in the absence of an external assisting field.

In the following, the possible recombination dynamics taking place in an organic bulk heterojunction solar cell consisting of two materials intermixed on the nm-scale will be discussed.

4.1 Charge Carrier Recombination in Organic Bulk Heterojunction Solar Cells

As described in the previous chapter, the charge transport in disordered organic semiconductors cannot be characterized by a classical band transport, but by hopping processes between localized states. Thus, the loss mechanisms cannot be described by a classical band–band recombination [9].

We distinguish between two recombination processes in organic solar cells, the geminate and non-geminate recombination (see Section 2.2). The recombination of two oppositely charged carriers is called geminate, if the charge carriers are generated from the same precursor state. In contrast, the recombination of two oppositely charged carriers, which originate from two different polaron pair dissociation processes and hence from different precursor states, is known as a non-geminate process.

Looking first at the dynamics for polaron pairs, Koster *et al.* [96] found a simplified equation for charge losses in organic solar cells. The continuity equation for polaron pairs PP can be described as follows:

$$\frac{d\mathrm{PP}}{dt} = G_{\mathrm{PP}} - k_f \mathrm{PP} - \underbrace{k_d \mathrm{PP}}_{G} + R \quad , \tag{4.1}$$

where G_{PP} is the polaron pair generation rate. For ideal exciton dissociation this is equal to the singlet exciton generation rate. k_f is the polaron pair recombination rate to the ground state (geminate), k_d is the dissociation rate from a polaron pair to a free polaron. The term k_dPP corresponds to the generation rate G of free polarons being a loss mechanism of polaron pairs. In contrast, the recombination rate of free polarons R always leads to the generation of a polaron pair, which is considered in this equation by a positive sign. Consequently, the dynamics of two polarons after polaron pair dissociation can now be described again by the continuity equation (here for electrons):

$$\frac{dn}{dt} = -\frac{1}{q}\frac{dj_n}{dx} + G - R \quad , \tag{4.2}$$

with the concentration of electrons n and the spatial derivative of the current j_n, the elementary charge q, the optical generation rate G and the recombination rate R of polarons. By using Equation (2.1) as $k_d = k_f(P_d/1 - P_d)$ and coupling Equation (4.1) and (4.2) by assuming steady-state conditions, where the time derivates are zero, the continuity equation becomes

$$\frac{1}{q}\frac{dj_n}{dx} = P_d G_{PP} - (1 - P_d)R \quad . \tag{4.3}$$

This expression implies that the charge carriers are not necessarily lost after recombination, but first form a bound polaron pair, which can either again dissociate into free polarons or decay to the ground state [96]. Only in the latter case, the polarons are lost.

Considering the recombination rate R in organic BHJ solar cells, generally two processes can be thought of, a first order (n^1) and a second order process (n^2):

$$R = \frac{n}{\tau} + k_{br} n^2 \quad , \tag{4.4}$$

with the charge carrier concentration n and the recombination coefficients $1/\tau$—with the charge carrier lifetime τ—and k_{br}. The first term in Equation (4.4) can be assigned to a monomolecular recombination, where the decay of the charge carrier concentration is given by a constant lifetime τ. A bimolecular recombination process is given by the second term in Equation (4.4). In this case, the lifetime of the charge carriers is not constant, but

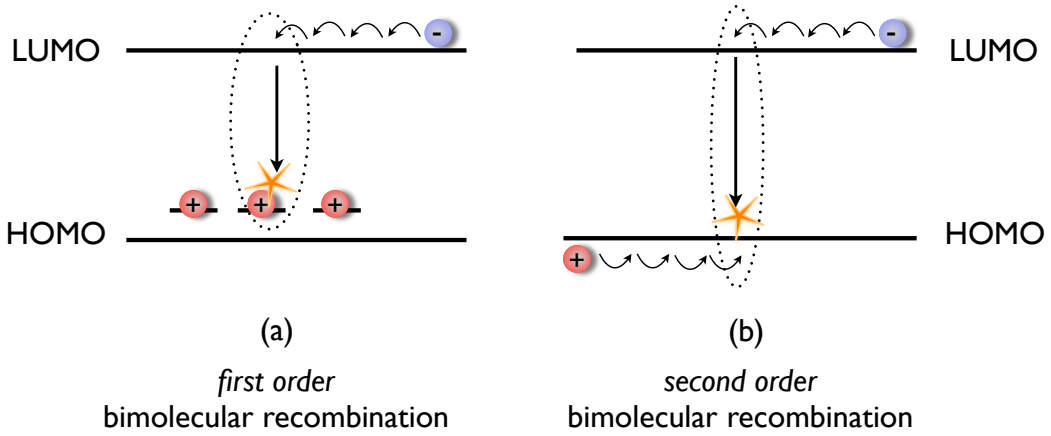

Figure 4.1: Bimolecular recombination (non-geminate) of different order: (a) first order recombination with only one type of charge carrier being mobile (minority) and the other type being trapped (majority); (b) bimolecular recombination with both charge carriers being mobile (both being equal in equal number).

depends on the charge carrier concentration n with $\tau = 1/(k_{br}n)$. In analogy, the geminate recombination process, as defined above, can be described by a monomolecular recombination rate and the non-geminate process by a bimolecular recombination rate. However, the definitions of monomolecular and bimolecular recombination is not consistent in literature. Thereby, the term monomolecular recombination is also used to describe the recombination of two charge carriers residing on one molecule and bimolecular recombination as a process, where the two oppositely charged carriers are located on two different molecules, which is already implied by their names. Here, the charge carrier recombination is defined more in a mechanistic sense instead of being described by the recombination rate.[97]

In this work, the polaron recombination is assigned to bimolecular recombination, whereas the recombination order is defined by the decay of the charge carrier concentration n. Thereby, the bimolecular recombination rate does not necessarily be of second order (see Figure 4.1). If a mobile charge carrier, for example, recombines with a trapped charge carrier, the process is described by a first order, if the trapped charges exceeds the number of mobile ones. In this case, the number of trapped charge carriers being in excess decays exponentially with a lifetime of $1/\tau$ (Figure 4.1(a)). In contrast, if the concentration of trapped charge carriers is lower or comparable to the free mobile ones, the bimolecular recombination is indeed described by a second

order process [9] (Figure 4.1(b)).

A theory, which is commonly used in literature to describe the recombination dynamics in organic BHJ solar cells, is the model introduced by Langevin in 1903 [98]. This kind of recombination can be classified by a bimolecular recombination process and will be explained in the following more in detail.

4.2 Langevin Recombination

Langevin suggested a model to describe the recombination dynamics of two oppositely charged ions in a large reservoir [98]. He proposed that the charge carrier recombination is a random process and kinetically bimolecular, if oppositely charge carriers are produced statistically independent of each other. An important initial requirement is that the mean free path of the carriers has to be less than the Coulomb capture radius r_c of one carrier by the other. This condition is fulfilled in narrow-band conductors with charge carrier mobilities less than 1 cm^2/Vs. Consequently, the scattering length is of the order of the lattice parameter. The limiting factor for recombination of an electron and a hole is proportional to the direct recombination rate and the finding of each other. Whereas in high mobility semiconductors the former process is dominant, the low charge carrier mobility limits the recombination rate in disordered organic semiconductors. The process of finding each other is limited by diffusion proportional to the charge carrier mobility when considering Einstein relation [11]

$$D = \frac{kT}{q} \cdot \mu \quad , \tag{4.5}$$

with the diffusion constant D. In Figure 4.2 a schematic overview of the Langevin recombination process is given. We assume the hole as to be fixed and electrons being mobile with a mobility $\mu = \mu_e + \mu_h$. Both charge carriers are attracted by the Coulomb force. If no external electric field is present, the electron can only circumvent recombination if the thermal energy is sufficient to overcome the Coulomb attraction. The Coulomb capture radius r_c can be calculated.

$$E_c = E_{th} \tag{4.6}$$

$$\frac{e^2}{4\pi\varepsilon\varepsilon_0 r_c} = kT \tag{4.7}$$

$$r_c = \frac{e^2}{4\pi\varepsilon\varepsilon_0 kT} \tag{4.8}$$

For $\varepsilon = 3.4$ a radius of $r_c \approx 17$ nm can be obtained at room temperature. If an electron moves within r_c a recombination probability of one is assumed.

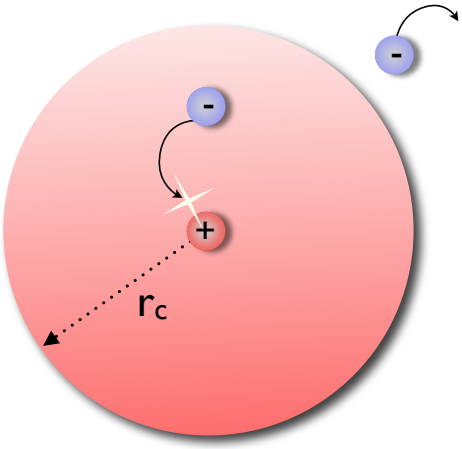

Figure 4.2: Schematic drawing of the Langevin model: A hole, which is considered to be immobile, describes a Coulomb capture radius r_c (defined by the balance of the Coulomb attraction and the thermal energy). If the mobile electron will reach the hole within that distance r_c they will recombine.

This problem was first analyzed by Onsager in 1938 [24]. Therefore, r_c is also known as the Onsager radius [94]. Considering a drift current, which is defined as

$$j_e = \frac{e^2}{4\pi\varepsilon\varepsilon_0 r_c^2} n\mu \quad , \tag{4.9}$$

an electron recombination current can be calculated, which corresponds to a current I_e flowing into the sphere of radius r_c

$$I_e = j_e \cdot 4\pi r_c^2 = \frac{q^2}{\varepsilon\varepsilon_0}\mu n = \gamma q n \quad , \tag{4.10}$$

with the Langevin recombination coefficient

$$\gamma = \frac{q}{\varepsilon\varepsilon_0}\mu \quad . \tag{4.11}$$

The recombination is proportional to the charge carrier mobility μ of electron and hole. Thus, for low conductivity materials the finding of each other is the limiting factor for recombination, as was already mentioned above.

The recombination rate described by the Langevin model is generally given by

$$R_L = \gamma \cdot (np - n_i^2) \quad , \tag{4.12}$$

with the intrinsic charge carrier concentration n_i^2, which is usually much smaller than the product np.

If we apply now the Langevin model to organic bulk heterojunction solar cells a major discrepancy can be found. The bulk of these solar cells consists of two materials blended together and hence two reservoirs exist, whereas the transport of electrons and holes is usually restricted to only one material phase. Consequently, a deviation from the Langevin can be expected, which will be discussed more in details in the experimental part of this work.

Chapter 5

Sample Preparation

As the material compounds of bulk heterojunction solar cells are solved in organic solvents, such as chlorobenzene and chloroform, several techniques can be used to manufacture organic solution based solar cells, including also mass printing techniques like roll–to–roll printing. For lab usage, usually the techniques of spin coating and doctor blading are used to deposit the organic active material on the chosen substrate, like glass or plastic foils. In the following, the roadmap of an organic BHJ solar cell, as studied in this work, will be presented from the single materials and substrates to the operating device.

A BHJ solar cell is built up in a diode configuration, as shown in Figure 5.1. The sputtered indium tin oxide (ITO) substrates are first structured by a wet chemical lithography step before further used in the process. On the structured ITO a thin layer (around 30–40 nm) of poly(3,4-ethylendioxythiophene): polystyrolsulfonate (PEDOT:PSS) is spin coated in air on top serving as a hole transporting layer, which is treated thermally afterwards for 10 minutes at 130 °C in a water free environment, i.e. usually in a nitrogen glove box system. All upcoming processing steps will be made in the inert atmosphere of a two chamber nitrogen glove box. The donor and the acceptor are solved in an organic solvent such as orhto-dicholorbenzene, chlorobenzene or chloroform. After being mixed together in a desired ratio the blend solution is spin coated on top of the baked PEDOT:PSS/ITO substrate layer. Usually, layer thicknesses from a few tenth of nm up to a few hundred of nm can be obtained just by varying the concentration and/or the speed of the spin coater (rpm: rounds per minute). If the organic layer is treated with an additional heating step after deposition, the solar cell is called *annealed*, otherwise without any further heating procedure it is called *pristine*. Finally, a metal contact as the counter electrode to the ITO electrode is evaporated thermally on top of the organic layer in a high vacuum evaporation chamber attached to the glove box system at pressures below 10^{-7} mbar. Several metals can be used as electrode material depending on the blend composition. Thereby, the metal has to be chosen carefully not to negatively affect the performance of the solar cells, e.g. to get a reduced V_{oc} [99, 100]. In order to get reliable good PCE values for organic BHJ solar cells often a buffer layer is evaporated on top of the organic material before metal deposition [101]. For the reference material

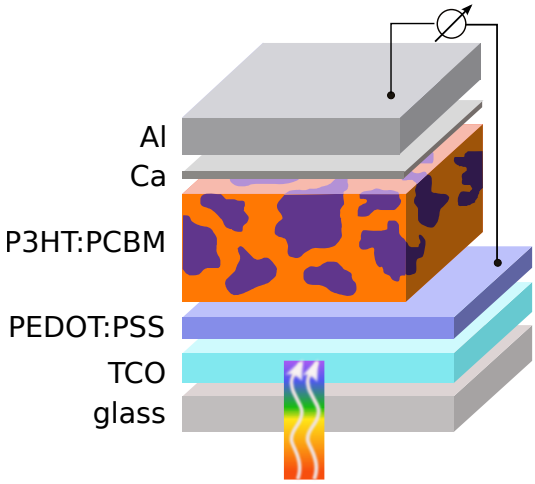

Figure 5.1: Layer structure of a typical solution processed organic bulk heterojunction solar cell studied in this work. In this case P3HT blended with PCBM was used as the active layer of the solar cell.

system P3HT:$PC_{61}BM$ the combination of Ca/Al as well as LiF/Al can be used, whereas fill factors up to 70% can be obtained. Evaporating Al directly on top of the organic layer results in rather low FF and thus in limited PCE values. The reason might be related to a badly formed organic/metal interfacial contact [102, 103]. Al atoms after evaporation are highly mobile on top of the surface trying to find a thermodynamical favorable place. Some Al atoms might also penetrate deeper into the organic layer due to pinholes in the sheet structure decreasing the active layer thickness. Finally, the solution processed organic bulk heterojunction solar cells were characterized inside the glove box system by measuring the external quantum efficiency and the J–V characteristics.

So, the samples were processed and characterized in clean environment without any oxygen or water exposure during the processing steps. For charge transport measurements, however, the samples had to be transferred in air for a short time to a optical helium closed-cycle cryostat. Current–voltage measurements in the glove box system before transferring to the cryostat and thereafter in the cryostat were performed to ensure no degradation of the solar cells has occurred during transportation.

If not mentioned otherwise, the samples used in this work were processed according to the recipe described above.

Chapter 6

Experimental Techniques

In this chapter, the experimental techniques used in this work will be explained in detail, which are focused on the investigations of the charge transport and recombination mechanisms in organic BHJ solar cells.

The transport of charge carriers inside the bulk of an organic solar cell to the corresponding electrodes is one of the important prerequisites for an operating solar cell. A commonly used technique to determine the bulk mobility of electrons and holes is the transient photoconductivity experiment, also known as time-of-flight (TOF). However, the TOF method can only be applied to rather thick samples (d $>$ 1 μm). For thin film structures the experimental technique of charge extraction by linearly increasing voltage (CELIV) is often used to determine the bulk charge carrier mobility. As organic solar cells usually consists of active organic layers in the range from 80 nm to 200 nm, the technique of CELIV is advantageous compared to TOF. The major drawback of the CELIV method, however, is that the polarity of the charge carriers cannot be discriminated. In contrast, in the TOF experiment electrons and holes can be distinguished by the direction of the applied electric field.

In the following, both experimental methods will be introduced in more detail. The temperature measurements were performed in an optical closed–cycle helium cryostat (50 K–300 K). A sketch of the experimental setup can be seen in Figure 6.1. For photogeneration of charge carriers either a Nd:YAG (neodymium-doped yttrium aluminium garnet) laser (EKSPLA PL-2210) or a pulsed white light emitting diode (LED) is used. The extraction voltage pulse is applied to the sample by an arbitrary function generator (Agilent 81150A), whereas the current is acquired by a digital storage oscilloscope (Agilent Infiniium DSO90254A) after being amplified by a current–voltage amplifier (FEMTO DHPCA-100) or voltage–voltage amplifier (FEMTO DHPVA-200).

6.1 Transient Photoconductivity

In the TOF experiment, diode-like sample structures are probed, whereas the studied material with a certain dielectric permittivity ε is sandwiched between two electrodes, of which at least one needs to be semi-transparent for laser illumination. Depending on the applied electric field both types of charge

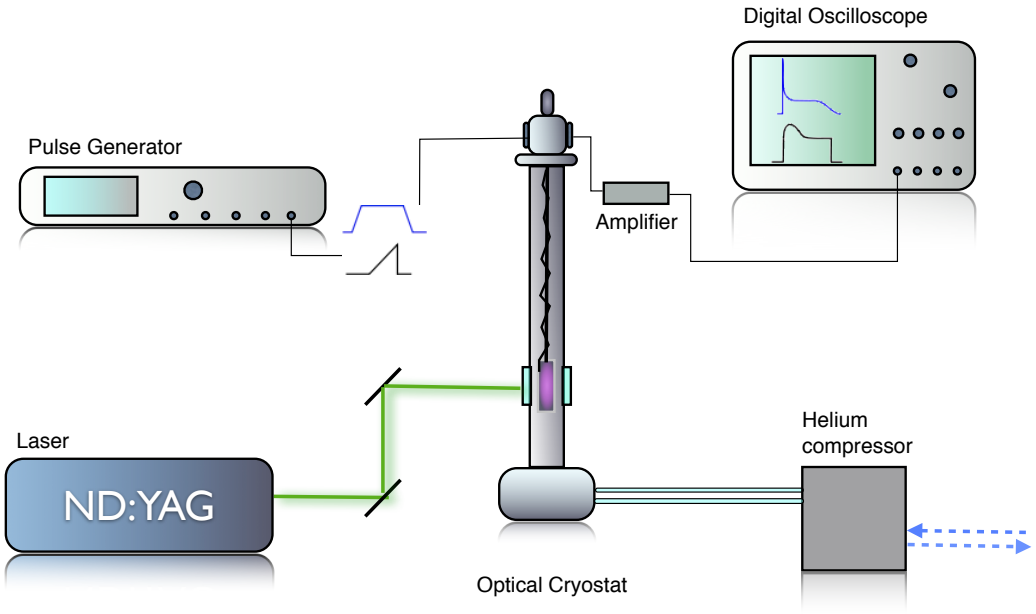

Figure 6.1: Scheme of the experimental setup for charge carrier transport and recombination measurements.

carriers—electrons and holes—can be measured separately. In Figure 6.2 a schematic overview of the experimental TOF technique is given. In excitonic semiconductors, as studied in this work, a pulsed laser flash generates electron–hole pairs in the vicinity of the illuminated electrode. These excitons are separated by an applied electric field, by defects or at interfaces. Due to the direction of the applied electric field one type of charge carriers is already extracted at the front electrode, whereas the complementary charge carriers hop through the bulk of the sample in field direction and will be extracted at the counter electrode. The resulting current can be measured with a digital storage oscilloscope. At time t_{tr}, when the charge carriers arrive at the counter electrode, the photocurrent drops to the dark level. From t_{tr} the charge carrier mobility can be calculated:

$$\mu = \frac{d}{t_{tr} \cdot F} \quad , \tag{6.1}$$

where d corresponds to the thickness of the active layer and F to the applied electric field [104]. The direction of the applied electric field determines, whether holes or electrons are extracted at the counter electrode. The absorption profile of the investigated material has to be measured to ensure a sufficient small penetration depth of the laser compared to the sample thickness. Otherwise, the sample thickness d in Equation (6.1) cannot be used

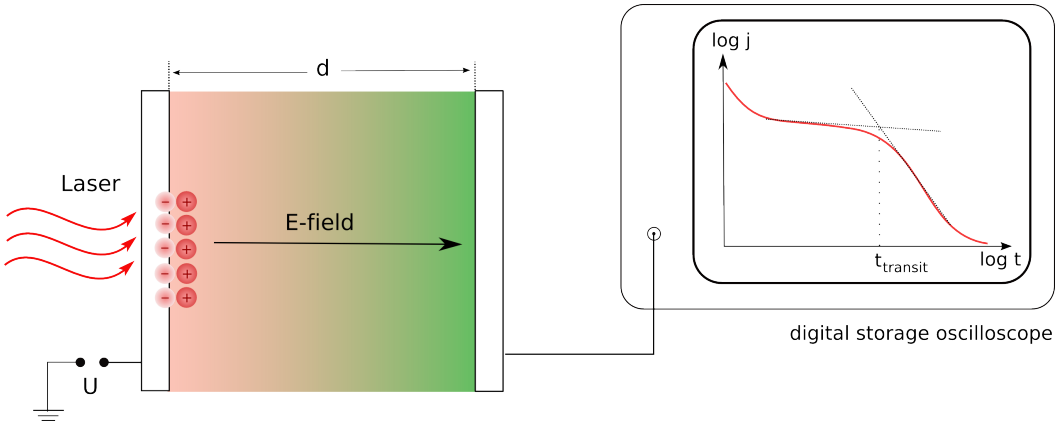

Figure 6.2: Schematic overview of the transient photoconductivity experiment, also known as TOF. Generated electron–hole pairs are separated by extracting one type of charge carrier at the front electrode. The residual charge carrier type is dragged through the active layer and extracted at the counter electrode.

to determine the mobility of the studied charge carriers. As a consequence, the laser wavelength has to be adjusted to the absorption maximum of the material system. For the polymer P3HT, the absorption coefficient α at a wavelength of 500 nm is $1.3{\times}10^7$ m^{-1}, so that the absorption depth of a 500 nm laser is around 77 nm.
In order to get reliable results from the TOF measurement, several prerequisites have to be fulfilled:

1. The diode has to be biased in reverse direction to avoid high dark current flowing through the device distorting the photogenerated charge carrier package.

2. The electrodes have to be at least semitransparent to ensure charge generation by laser excitation.

3. The charge Q of the photogenerated charge carriers should be less than 5% of the charge CU stored at the two electrodes of the sample ($Q \ll CU$). C is the capacitance of the sample and U the applied voltage. The photogeneration can be adjusted by varying the laser intensity.

4. Only low conductivity materials can be investigated, so that the transit time t_{tr} is much smaller than the dielectric relaxation time τ_σ ($t_{tr} \ll \tau_\sigma$). Otherwise, free intrinsic charge carriers are available throughout the whole sample, which will redistribute the electric field within the

bulk. Moreover, these charge carriers falsify the transit time t_{tr} and can recombine with the photogenerated excess charge carriers. $\tau_\sigma = \varepsilon\varepsilon_0/\sigma$ is the relaxation time and σ the conductivity of the material.

5. The electrodes have to be chosen as such that at least one blocking contact is formed in order to avoid charge injection which would distort the homogenous electric field.

6.2 Charge Carrier Extraction by Linearly Increasing Voltage (CELIV)

The technique of charge carrier extraction by linearly increasing voltage is a transient extraction technique used to determine the charge carrier mobility and charge carrier density within thin film devices. Compared to the method of TOF, samples with thicknesses less than 1 μm can be studied. As organic solar cells usually have active layer thicknesses in the range from 80 nm to 200 nm, the CELIV technique is an appropriate method to study charge transport in those systems. The CELIV technique was first introduced by Petravichyus *et al.* in 1975 [105], where they studied the hole drift in high resistivity p-type CdSe crystal plates. Juška *et al.* used it to study the charge transport in microcrystalline silicon [106] complementary to the previously used technique of TOF. Especially problems related to the restrictions of the TOF method could be solved using the technique of CELIV, e.g. that the material dielectric relaxation time τ_σ should be longer than the delay time t_{delay} or τ_σ larger than t_{tr}. If the latter limitations is not fulfilled the number of equilibrium charge carriers is sufficient to redistribute the electric field within a time shorter than the transit time. A schematic overview of the measurement techniques can be seen in Figure 6.3. One of the great advantages of the CELIV method compared to other experimental techniques is that the charge carrier mobility and the charge carrier concentration in the bulk can be determined simultaneously.

To get an expression for the charge carrier mobility from the CELIV transient the continuity, the current and Possion equation have to be considered, which yields in a Riccatti-type first order differential equation

$$\frac{dl(t)}{dt} + \frac{\sigma}{2\varepsilon\varepsilon_0 d} l^2(t) = \frac{\mu A t}{d} \quad , \tag{6.2}$$

with the extraction depth $l(t)$, the voltage slope $A' = V_p/t_p$ the charge carrier mobility μ and the device thickness d. e is the elementary charge, n the charge carrier concentration, ε_0 the vacuum permittivity and ε the dielectric constant of the studied material. This equation has been either solved

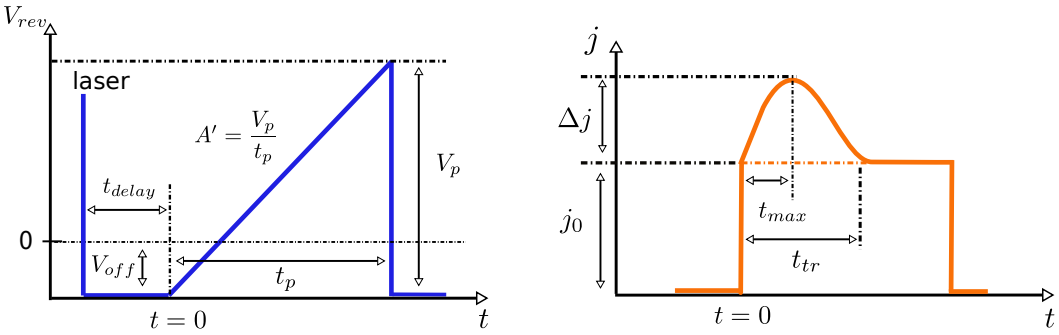

Figure 6.3: Photo-CELIV characteristics: (left) Linearly increasing voltage pulse being applied to the sample after laser excitation. (right) Current transient as a response to the applied voltage pulse.

numerically [107] or analytically for a low ($\tau_\sigma \gg t_{tr}$) and a high ($\tau_\sigma \ll t_{tr}$) conductivity approximation [106]. The equation found by Juška *et al.* [106] for the medial conductivity case, which is widely used in literature, is

$$\mu = \frac{2d^2}{3A' t_{max}^2 (1 + 0.36 \frac{\Delta j}{j_0})} \quad , \tag{6.3}$$

with the numerical factor 0.36 to account for electric field redistribution. However, this equation is only valid if the current density at maximum charge extraction (Δj) equals to the current step due to capacitive response of the device (j_0) [108]. Otherwise, the relative error made by calculating the mobility increases above 5% [109]. It was suggested that the numerical factor has to be replaced by 0.21 to get a more reliable result over a wider range of conductivity [110].

$$\mu = \frac{2d^2}{3A' t_{max}^2 (1 + 0.21 \frac{\Delta j}{j_0})} \quad . \tag{6.4}$$

Lorrmann *et al.* [109] extended the simplified theory to a full analytical description of the Riccatti equation, which allows now to computationally evaluate mobility μ and charge carrier density n from CELIV measurements also on medial and high conductive materials over a wide range of experimental parameter settings (e.g. $\Delta j / j_0 > 1$). Especially in organic devices such as organic solar cells they proved that the validity of the low and high conductivity approximation is rather limited [109]. From their calculations they

found a more appropriate equation for the charge carrier mobility to be

$$\mu = \frac{d^2}{2A' t_{max}^2} \left[\frac{1}{6.2 \cdot (1 + 0.002 \frac{\Delta j}{j_0})} + \frac{1}{1 + 0.12 \frac{\Delta j}{j_0}} \right] \quad . \tag{6.5}$$

t_{max} accounts for the maximum position of the CELIV extraction peak, Δj for the extraction peak height and j_0 is the saturation current (initial current step) (see Figure 6.3). Thereby, Equation (6.5) describes a fit to the analytic description, whereas the relative error made by calculating the charge carrier mobility never exceeds 5% [109].

The charge carrier concentration extracted from the bulk of the diode in the CELIV experiment can be calculated by integrating the current transient. In the CELIV experiment, only intrinsic charge carriers are considered. If a laser is used to generate additional charge carriers, the method is called photo-CELIV. To ensure that the photogenerated charge carriers will not leave the bulk by the internal electric field V_{bi} before charge extraction by the reverse voltage pulse, an offset bias voltage V_{off} in forward direction has to be applied to the sample to compensate for V_{bi} [108]. By shifting the delay time t_{delay}—defined as the time between laser excitation and voltage pulse (see Figure 6.3)—to larger times the photogenerated charge carriers have more time to diffuse within the bulk of the solar cells and thus to recombine. Thus, due to recombination processes within the active area, less charge carriers can be extracted at long delay times, which result in a decrease of the CELIV extraction peak. Using photo-CELIV the charge transport and recombination dynamics can be monitored in the bulk of an organic BHJ solar cell.

In Figure 6.4 a simplified energy diagram of an BHJ solar cells is shown for the two different conditions in a photo-CELIV experiment. First, a laser flash generates charge carriers, whereas an offset bias is applied to compensate V_{bi}. Generated excitons will be dissociated at a donor–acceptor interface into free polarons via polaron pairs. Free polarons diffusing within the bulk of the solar cells may recombine during the delay time if they reach an oppositely charged carrier. After t_{delay} the residual charge carriers are extracted by the triangular voltage pulse.

However, there are also disadvantages, which have to be kept in mind, when performing CELIV measurements. All transient methods are limited by the RC time of the circuit and so is the CELIV technique. The RC limitation might result in an underestimation of t_{max} and thus in an imprecise charge carrier mobility μ, as is illustrated in Figure 6.5. When studying organic BHJ solar cells the capacitance of the circuit is mainly determined by the sample geometry and not by the cable and connectors. The thickness of

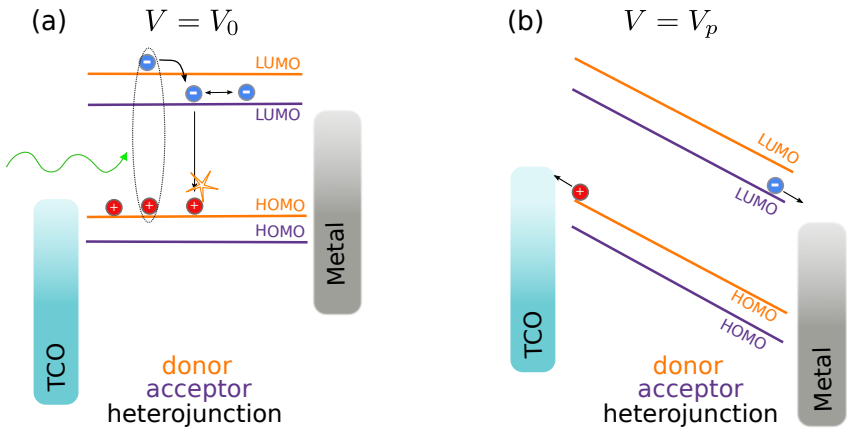

Figure 6.4: Energy band diagrams of a BHJ solar cell during a photo-CELIV experiment. (a) The case when the internal electric field is compensated, so that the photogenerated charge carriers are not extracted by the field during $0 \leq t \leq t_{delay}$ ($V_0 > V_{oc}$). (right) For $t > t_{delay}$ the applied voltage pulse (linearly increasing in time) extracts the charge carriers by tilting the HOMO and LUMO of the donor and acceptor.

the studied organic layers are usually in the range of 100–200 nm with a dielectric constant of $\varepsilon = 3$–4, which results in a capacitance in the range of hundreds of pF to even nF depending on the device area. Thus, even with low current amplification the RC time can be as high as hundreds of ns to even μs. To minimize RC effects first the device area has to be designed as small as possible. As explained above, a constant offset voltage V_{off} in forward direction has to be applied to the solar cell to study the recombination dynamics within the bulk. Consequently, the photocurrent and hence a charge loss at the time when the laser hits the solar cell is impeded. Due to the illumination of the solar cell by a short intense laser pulse ($\sim$ ns, $\sim$ 10 μJ) a rather high offset voltage is needed for this compensation, which is larger than the open circuit voltage V_{oc}. In dark conditions this constant offset voltage implies a constant current flow in forward direction, which is caused by charge carriers injected into the bulk due to non-blocking contacts. These charge carriers will increase the capacitance of the solar cell, which will affect the current transient even more by the RC time. As will be seen in the experimental part (Chapter 8) the RC time can even be increased ten fold due to charge carrier injection. Furthermore, injected charge carriers may also interact with photogenerated charge carriers influencing the recombination dynamics.

To account for this major drawback, we extended the photo-CELIV experiment to optimize the technique for extracting the highest obtainable charge

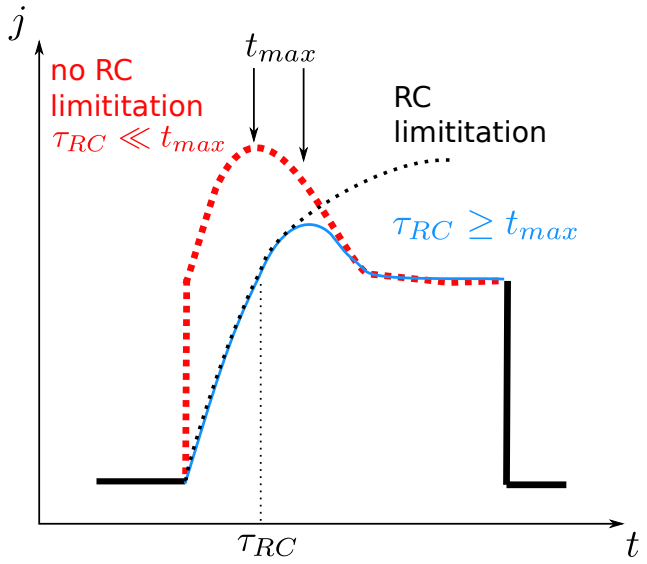

Figure 6.5: RC limitation in CELIV experiment. Due to τ_{RC} the maximum CELIV peak position is falsified.

carrier mobility and the reliable charge carrier concentration by avoiding charge injection. The method is called OTRACE (open circuit corrected transient charge extraction by linearly increasing voltage) and will be explained in the following.

6.3 Open Circuit Corrected Transient Charge Extraction by Linearly Increasing Voltage (OTRACE)

In an illuminated solar cells no current is flowing at $V = V_{oc}$, whereas under dark conditions no current is flowing at $V = 0$ as the solar cell is in the thermodynamical equilibrium. Under open circuit conditions ($V = V_{oc}$) the generation rate G is equal to the recombination rate R. By switching off the light $G = 0$ and the voltage drops from V_{oc} to zero with time due to the recombination of photogenerated charge carriers. In Figure 6.6 the transient of the open circuit voltage V_{oc} is illustrated. It can be seen that the voltage, which has to be applied during the photo-CELIV experiment to compensate for charge extraction at the electrodes, should not be constant, but rather a function of time. With a constant offset bias being applied to the solar cell during the delay time t_{delay} charge carriers will not only recombine but are also swept out of the device due to varying open circuit conditions, which are

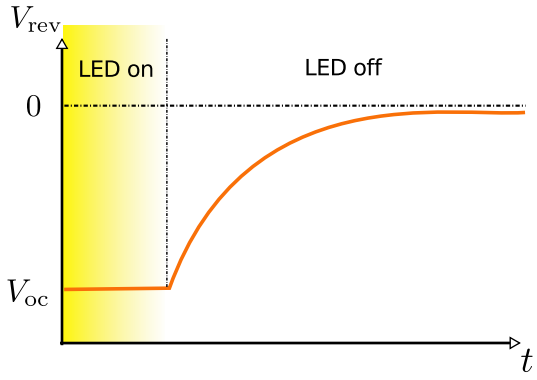

Figure 6.6: An example for a transient of the open circuit voltage V_{oc}. When switching off the light the voltage drops to zero due to charge carriers recombining within the active layer.

not considered.

In the extended transient charge extraction method OTRACE, first a V_{oc} transient is acquired, which is further used as an input for the offset voltage $V_{off}(t)$ for field compensation in the photo-CELIV experiment. This will lead to a more accurate measurement of the charge carrier recombination dynamics in the bulk of the solar cell. In this case, the compensation of the internal electric field during t_{delay}, when photogenerated charge carriers need to be kept in the device, is optimal. Furthermore, by using a pulsed white light emitting diode (LED) as a source for photogeneration of charge carriers in contrast to a laser, solar cell operating conditions can be approached. Thereby, the LED light pulse has to be applied long enough to create steady-state conditions in the illuminated solar cell. A schematic overview of the modified transient extraction technique is illustrated in Figure 6.7. For comparison, the applied voltage pulse in case of the conventional photo-CELIV technique is also shown on top.

The V_{oc} transient is acquired by a digital storage oscilloscope using a high impedance adapter (1 GΩm), which prevents the current flow and hence fulfill the requirements for open-circuit conditions.

A detailed comparison of the novel OTRACE technique and the conventional photo-CELIV experiment will be presented in Chapter 11, which will especially highlight the major advantages of the new technique.

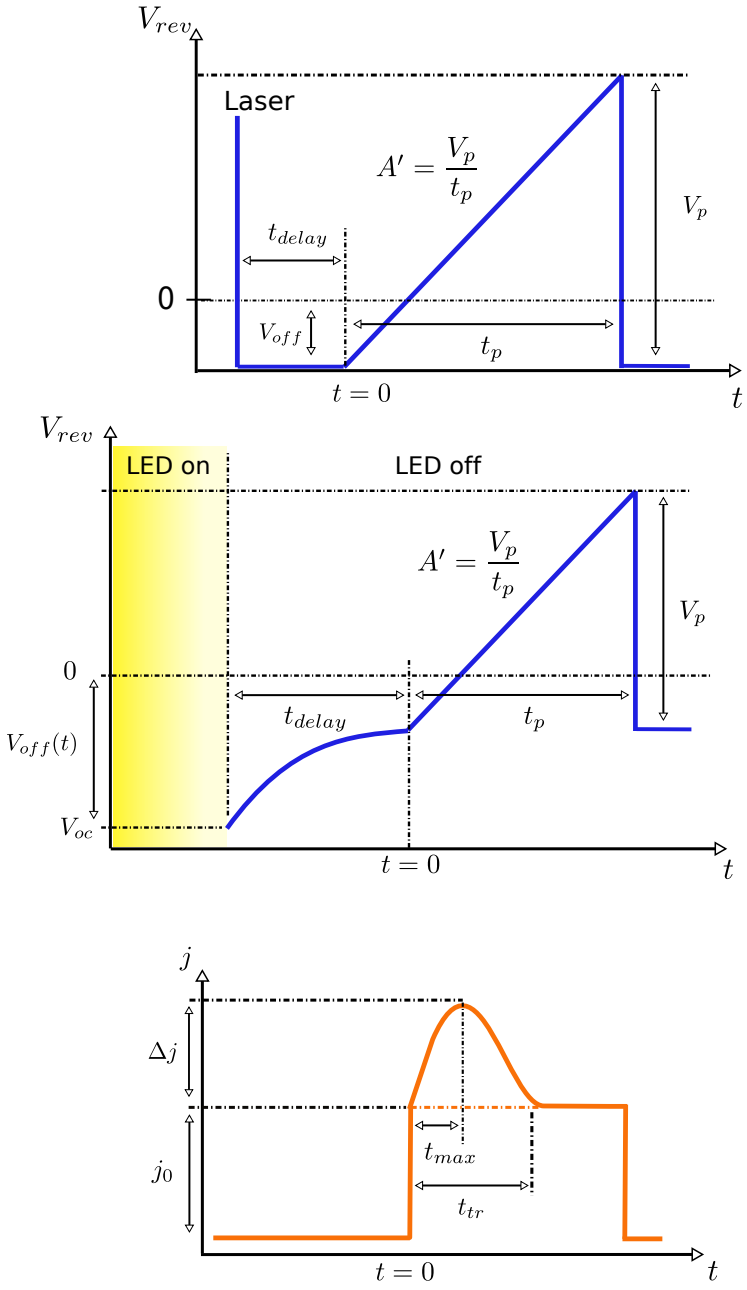

Figure 6.7: Overview of the technique of open circuit corrected transient charge extraction by linearly increasing voltage (OTRACE) compared to the conventional technique: (top) The applied voltage in the conventional CELIV method for comparison. (middle) Voltage pulse tailored by a combination of the V_{oc} transient for field compensation and the CELIV technique for charge extraction of residual charge carriers. (bottom) Current transient as the response to the linearly increasing voltage pulse (see also transient in Figure 6.3).

Chapter 7

Charge Transport in P3HT:$PC_{61}BM$ blends probed by Transient Photoconductivity

In this chapter, the charge transport measurements in pure P3HT as well as blended with $PC_{61}BM$ are presented. The technique of TOF was applied to thick samples in the range from 1 to 10 μm. The ratio between P3HT and $PC_{61}BM$ was varied, whereas both the electron and hole mobility was investigated in the regime of non dispersitivity and low charge carrier concentration.

Part of the results discussed in this chapter is published in Paper 3.

7.1 Introduction

The mobility of photogenerated charges is one of the crucial factors determining the performance of organic solar cells [29], its impact being more complex than following any "faster equals better" stereotype. A high charge carrier mobility may be beneficial for organic solar cells reaching high power conversion efficiency values. However, from macroscopic simulations—solving the drift, diffusion and continuity equations considering injection barriers for electrons and holes—it could be revealed that at a certain charge carrier mobility the power conversion efficiency even decreases with increasing mobility (see Figure 7.1) [29, 111]. Nevertheless, one of the important prerequisites for a well-performing BHJ solar cell is that the respective mobilities for transporting electrons on the fullerene and holes on the conjugated polymer are rather balanced, in order to avoid a space charge building up. As the blend of two different material types cannot be described by a simple superposition of the single material properties, a prediction of the bipolar charge transport in a solar cell is not straightforward. Tuladhar et al. [112] investigated the dependence of the charge carrier mobility in poly[2- methoxy-5-(3',7'- dimethyloctyloxy)-1,4-phenylenevinylene (MDMO-PPV) with varying $PC_{61}BM$ content using transient photoconductivity method (TOF). They found an increase of the mobility for both carrier types with an increasing fullerene fraction. Additionally, ambipolar transport was found in $PC_{61}BM$ embedded in an insu-

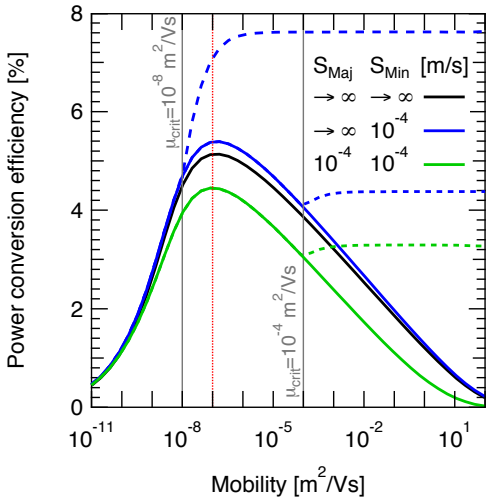

Figure 7.1: PCE versus μ (here equal for electrons and holes) deduced from macroscopic simulations. Under the assumption of capped Langevin recombination (vertical lines), finite minority surface recombination velocities (S_{Min}) enhances the solar cell efficiency to a saturated level at higher mobilities (dashed lines). Finite minority surface recombination velocities (S_{Maj}) lead to a reduction of the efficiency. (from Ref. [111]).

lating polystyrene matrix. For the nowadays more relevant combination of P3HT:$PC_{61}BM$, field effect transistor (FET) experiments were reported in literature, observing an ambipolar transport in a limited range of blend ratios [113, 114]. However, field effect measurements consider neither photogenerated charges nor low carrier concentrations. Using the TOF technique, Huang et al. [115] found an anomalous transition from dispersive to nondispersive and back to dispersive transport for an increasing $PC_{61}BM$ fraction. The authors, however, used films with a thickness of around one micrometer, and do not comment on the observed dispersivity which might be influenced by the layer thickness [116]. Furthermore, they did not report in this context on the ratio dependent electron and hole mobilities, which would have been of particular interest.

7.2 Experimental

In contrast to spin coating the active layer, as described in Chapter 5, the samples were prepared by slow drying a mixture of P3HT:$PC_{61}BM$ made from solution in chlorobenzene on PEDOT:PSS covered ITO/glass substrates. Thus, active layer thicknesses ranging from 2 μm to 9 μm were obtained depend-

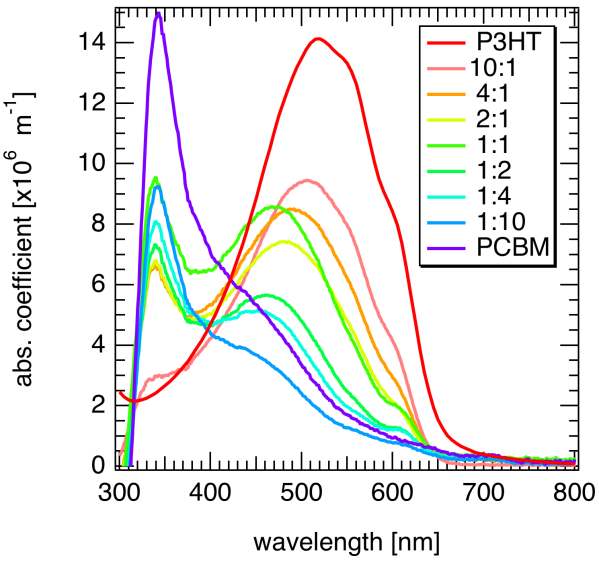

Figure 7.2: Absorption coefficient α of the studied ratios from 10:1 P3HT:$PC_{61}BM$ to 1:10. α for the pure materials are also shown

ing on the blend ratio and the concentration of the chlorobenzene solution, as monitored by a Dektak profilometer. A semitransparent aluminum anode (thickness $d \approx 20$ nm) was evaporated thermally. P3HT was purchased from Rieke Metals, $PC_{61}BM$ from Solenne. All materials were used without further purification. The TOF experiments were performed at different electric fields in the range between $3 \cdot 10^4$ V/cm and $4 \cdot 10^6$ V/cm using the setup shown in Figure 6.1. Instead of using a Nd:YAG laser, carriers were generated by a short 5 ns nitrogen laser pulse equipped with a dye unit ranging from 335 nm to 500 nm in order to ensure sufficient absorption, as we found that samples with more than 50% $PC_{61}BM$ show a blue shift of the maximum absorption, as can be seen in Figure 7.2. The penetration depth of the laser was calculated to be less than 10% of the sample thickness. For measuring electrons at the Al electrode, the laser was illuminating the ITO electrode and vice versa for detecting holes at the ITO electrode. An overview of the investigated samples is given in Table 7.1. The mobility μ was calculated from the transit time of the charge carriers, the sample thickness d and the electric field F according to Equation (6.1). To justify the measurements the quantum yield for the generation of electrons and holes in the TOF experiment was estimated. With an energy of around 30 μJ/cm^2 on the sample, including losses at Al and ITO electrode, a number of incident photons of about $7{\times}10^{17}$ m^{-2} can be expected. On the other hand, the number of extracted charges can be calculated to be around $6{\times}10^{16}$ m^{-2}, which is comparable to concentrations existing in

Table 7.1: The P3HT:$PC_{61}BM$ (D:A) ratio, the $PC_{61}BM$ content x, the concentration c of the used chlorobenzene solution, the determined thickness d of the investigated samples, the absorption coefficient α and the used laser wavelength λ are shown.

D:A	x	c g/l	d μm	α m^{-1}	λ nm
1:0	0	10	2.2	1.3×10^7	500
10:1	0.09	20	8.5	9.4×10^6	500
4:1	0.2	20	4.8	8.4×10^6	500
2:1	0.33	20	5.6	7.2×10^6	500
1:1	0.5	20	4.2	7.7×10^6	500
1:2	0.66	30	6.0	7.0×10^6	335
1:4	0.8	30	4.3	7.7×10^6	335
1:10	0.9	30	6.5	8.6×10^6	335

related experiments on the studied material system, such as photo-CELIV measurements at similar laser intensities [117]. Thus, depending on the internal quantum efficiency, between 10 and 50% of the generated charges are extracted in the TOF experiment within the time frame of the measurements. All experiments were performed at room temperature.

7.3 Results and Discussion

Before the result of the blend samples are presented, the charge transport in pure P3HT samples with different regioregularities (RR) is compared. It is an ongoing process of not only purifying the polymers for organic electronic applications but also improving the quality of regioregularity and hence the ability of ordering and crystallization of the polymer, as was mentioned in Section 2.4. A better alignment of the polymer chains will lead to a longer conjugation length and finally to a better charge transport of electrons and holes. In Figure 7.3 the current transients from a TOF experiment on pure P3HT (4002E, RR 93%) for electrons and holes are shown. From the transit time t_{tr} a mobility of around $1.8 \cdot 10^{-4}$ cm^2/Vs for electrons and holes can be calculated. Even though P3HT 4002E is usually used as an hole conducting material an electron mobility of the same order as the one for holes could be observed in the experiment. This ambipolar transport behavior was already observed previously [118]. Thereby, the detection of an electron transport in

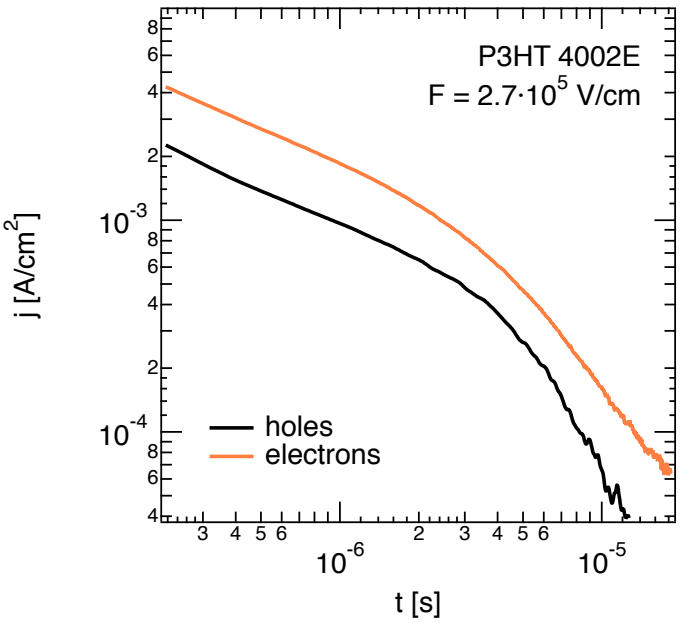

Figure 7.3: Current transients from a TOF experiment on a pure P3HT 4002E diode structure with a thickness of $d = 2.23$ μm. The electron and hole mobility can be determined to be around $1.8{\cdot}10^{-4}$ cm^2/Vs.

P3HT was found to critically depend on the purity of the polymer. In Figure 7.4(a) the hole transients for various electric fields and in Figure 7.4(b) the deduced electron and hole mobility of P3HT (P200) with a regioregularity (RR) of 98% are shown as a function of the applied electric field. As expected, the more ordered polymer structure leads to an increased charge carrier mobility of $\mu = 1 \times 10^{-3}$ cm^2/Vs, which is almost one order of magnitude higher compared to P3HT with RR of 93%.

In the following of this chapter, the result on the transport studies in the blend mixture of the polymer P3HT (4002E, RR 93%) and the fullerene $PC_{61}BM$ are presented, whereas the ratio between the donor and the acceptor is varied from 90% P3HT and 10% $PC_{61}BM$ to 10% P3HT and 90% $PC_{61}BM$.

Figure 7.5 shows the current transients of electrons and holes for the studied blend ratios at different electric fields. The arrows in the two graphs indicate the observed transit times in the measured transients. For both types of carriers, a Poole–Frenkel-like behavior was observed. Furthermore, for almost all studied blend ratios a negative electric field dependence of the charge carrier mobility—for both electrons and holes—was obtained. The negative field dependence can be attributed to a relatively large spatial disorder of the charge transport sites [115, 119]. According to Equation 3.5, μ decreases with increasing F, when the spatial disorder parameter Σ exceeds the energetic

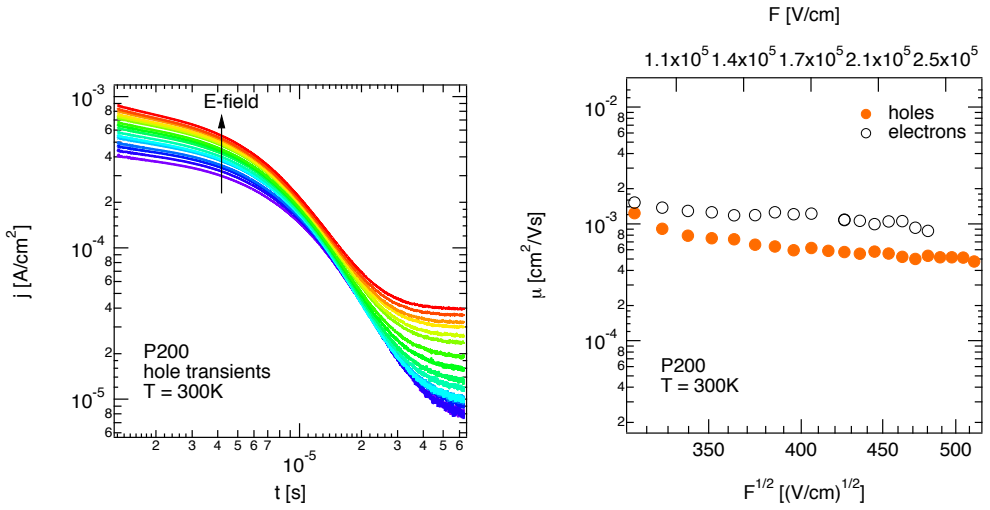

(a) (b)

Figure 7.4: (a) Hole transients detected in a P3HT (P200, RR 98%) by TOF measurements and (b) charge carrier mobility of electrons and holes as a function of the square root of the electric field $F^{1/2}$.

disorder parameter σ/kT. Especially in a blend system, where two materials are intermixed, faster routes as well as dead-ends are present for both charge carriers in the bulk. Thereby, the faster routes whose direction is not aligned with the direction of the external electric field are diminished at high electric fields. The charge carriers are forced to make the difficult jumps, which results in a decreasing charge carrier mobility with increasing electric field [120, 38]. In contrast, in the pure polymer P3HT almost no dependence of the charge carrier mobility on the electric field is observed. Thereby, self-organization in P3HT films was found to result in a lamella structure consisting of two-dimensional conjugated sheets, which are formed by interchain stacking [121]. This self-organization in a lamella structure leads to a high order of the charge transport sites, whereas the charge carrier mobility increases with the degree of order as was shown for P3HT with RR of 98%. Moreover, in the studied range of electric fields μ is constant, which can be explained by the many pathways being present in the highly ordered polymer film.

Furthermore, double transients for both charge carrier types were found (see Figure 7.5): For $x = 0.66$, two extraction signals in the hole current transients can be seen. The same is true for the electron current transient for $x = 0.8$ and $x = 0.5$. Note that these transit times shift with the electric field, which is a clear indication that a field dependent charge carrier mobility instead of an artefact is measured, as can be seen in Figure 7.6.

In Figure 7.7 the current transients for electrons are shown for a

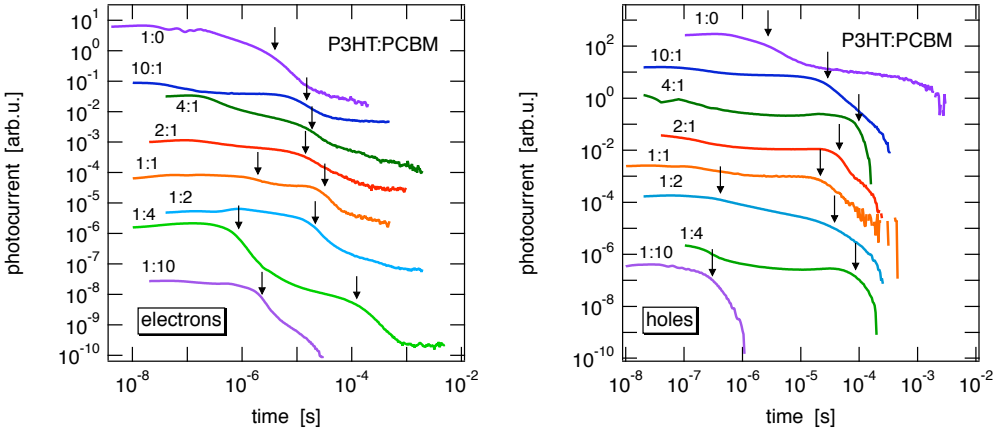

(a) electron TOF transients (b) hole TOF transients

Figure 7.5: (a) Electron and (b) hole current transients for the different blend ratios at electric fields from about $3 \cdot 10^4$ V/cm to $4 \cdot 10^6$ V/cm; the arrows in the graph indicate the field dependent transit times.

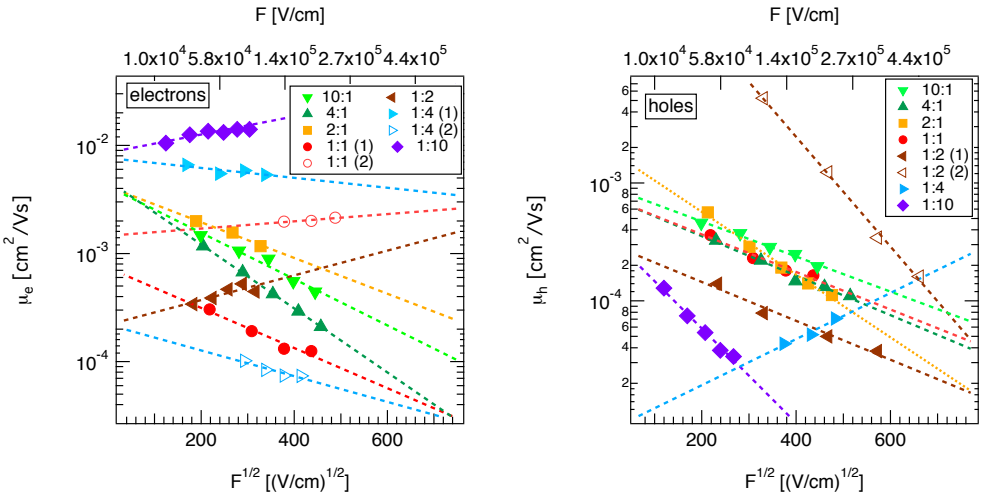

(a) (b)

Figure 7.6: (a) Electron and (b) hole mobility as a function of the square root of the electric field $F^{1/2}$ deduced from TOF measurements on P3HT:PCBM samples with different ratio. (1) and (2) indicates the two characteristic transit times observed in the corresponding ratio.

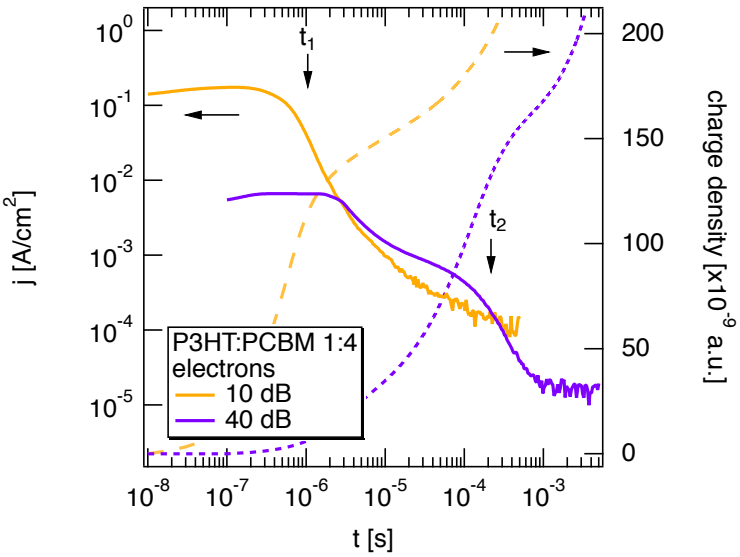

Figure 7.7: Current transient for electrons from a TOF experiment on P3HT (4002E):$PC_{61}BM$ 1:4 sample. Two transit times are observed; for t_2 a higher amplification was used. On the right axis the extracted charge density determined by integrating the current transient is shown.

P3HT:$PC_{61}BM$ 1:4 ratio (x=0.8) probed in two different acquisition ranges with two different transit times. Thus, to get a more complete picture of the charge transport a large time range has to be studied.

In order to compare the ratio dependent electron and hole mobility the values were interpolated at an electric field of 2.5×10^5 V/cm. The result can be seen in Figure 7.8, showing the electron and hole mobility as a function of $PC_{61}BM$ content x. A very similar dependence on the $PC_{61}BM$ fraction was found by plotting mobilities at other electric fields. A bipolar transport for the whole range of the studied P3HT:$PC_{61}BM$ ratios can be found. The electron mobility increases strongly with raising $PC_{61}BM$ concentration above 50% with $\mu = 2.3 \cdot 10^{-2}$ cm^2/Vs for $x = 0.9$. The value is comparable to the one reported for $PC_{61}BM$ embedded in an insulating matrix [112]. Below 50%, the electron mobility remains almost constant or decreases slightly. In contrast, the hole mobility slightly decreases with increasing $PC_{61}BM$ content in the blend for $x < 0.25$, which might be related to a distortion of the semi-crystalline packing of P3HT. Below 75% $PC_{61}BM$ concentration the hole mobility varies little with adding $PC_{61}BM$ content. Interestingly, we observe an increased hole mobility at 90% $PC_{61}BM$ content of about $7.3 \cdot 10^{-3}$ cm^2/Vs, which is comparable to the high electron mobility found in the same device. From the percolation theory [122, 123] a threshold can be estimated, at which

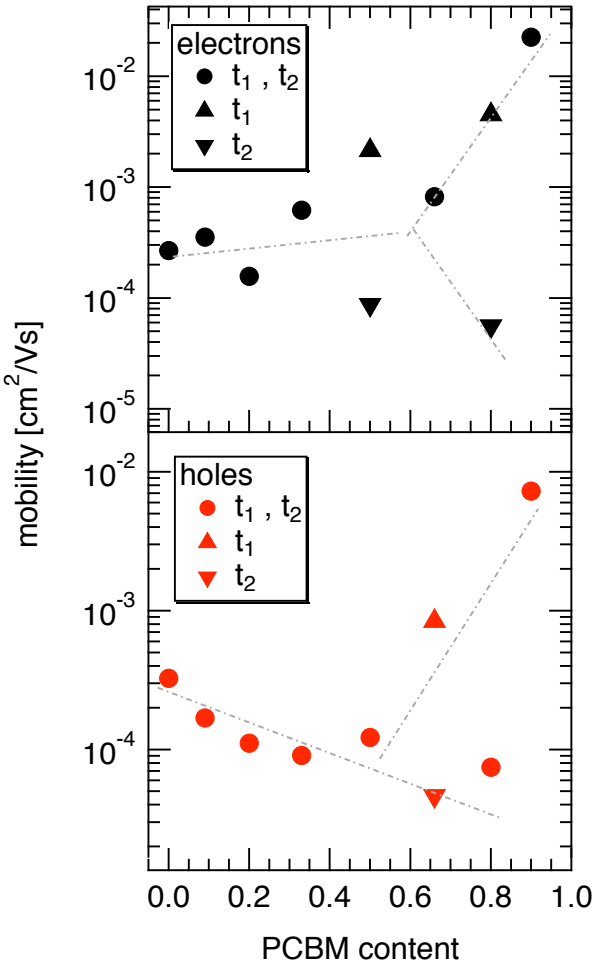

Figure 7.8: Electron and hole mobilities in P3HT:$PC_{61}BM$ blend films versus $PC_{61}BM$ concentration at T=300K; mobility values were obtained by interpolating the Poole-Frenkel like field dependent mobility at an electric field of $2.5 \cdot 10^5$ V/cm; for $x = 0.8$ and $x = 0.5$ a double transient for electrons and for $x = 0.66$ for holes can be detected; circles denote transients with only one transit time and the triangles those with two transit times t_1 and t_2 observed. Guides to the eye are included (dashed lines).

a material will build a persistent pathway to the corresponding electrode. For spheric molecules like $PC_{61}BM$ a threshold of around 17–20% is obtained, whereas elongated snake like molecules like conjugated polymers percolate already at a polymer content of 2%. Thus, the hole mobility might result from holes hopping on the polymer P3HT even in the P3HT:$PC_{61}BM$ 1:10 ratio. In this case, the hole mobility would be an order of magnitude higher compared to the one in pure polymer film, which can only hardly be explained. Tuladhar *et al.* [112], however, reported from an ambipolar transport in $PC_{61}BM$with a comparable electron and hole mobility, which would explain the observed high hole mobility in the P3HT:$PC_{61}BM$ 1:10 ratio being comparable to the electron mobility.

The mechanism responsible for double transients, signified by two different transit times (Figure 7.7 and 7.5), originates from slower charges being hindered in the extraction process by an energy barrier. Two potential explanations come to mind. First, the slow charge carriers become trapped in deep states during their hopping transport. Depending on the activation energy needed to leave these states, the charge transport of the trapped fraction of carriers is delayed as compared to the faster charge carrier package. These trap states can be caused e.g. by isolated P3HT molecules embedded in a percolated $PC_{61}BM$, where holes can be trapped, or $PC_{61}BM$ molecules in a P3HT environment as electron traps. Second, the different mobilities can be due to electrons not only being transported on the $PC_{61}BM$, but—once overcoming the energy barrier to hop onto the polymer phase—also on the donor material, and vice versa. We exclude the case of charge trapping, as we would expect the mobility to be lower than the one we calculate from the second transit time t_2. Furthermore, we find from Monte Carlo simulations [124, 125] performed on a system with sites distributed by a GDOS without traps, that an increased phase separation in the blend leads to TOF transients with two clearly distinguishable transit times. In contrast, randomly distributed phases in the blend show only one single transit time (see Figure 7.9). Thus, a blend consisting of two ambipolar materials, which are well phase separated in the bulk, are able to transport both types of charge carriers in the donor as well as the acceptor phase. Finally, we note that double transients were also observed in liquid crystals being due to electronic and ionic contributions [126].

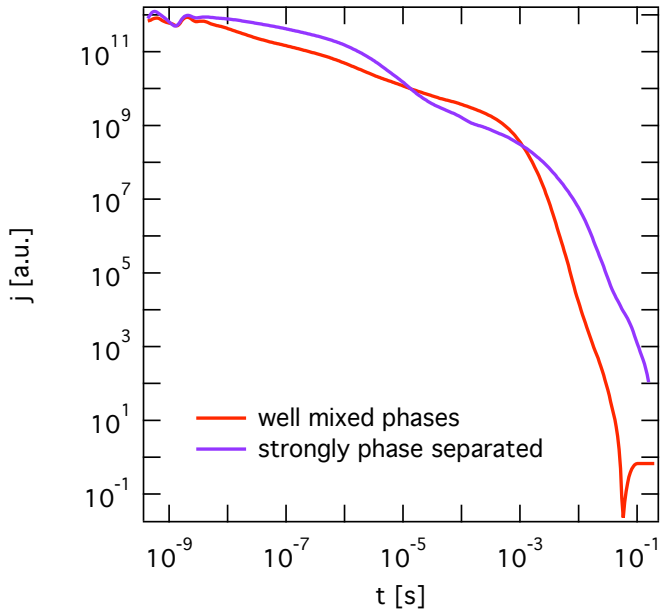

Figure 7.9: Current transients revealed by Monte Carlo simulations of a TOF experiment assuming a blend structure with well mixed phases and one with strongly phase separated domains. For the latter clearly two characteristic kinks are obtained (after Ref [125]).

7.4 Conclusion

The electron and hole mobility in P3HT:$PC_{61}BM$ samples with variable ratio were investigated using the transient photoconductivity technique. A bipolar charge transport was found for all studied devices ranging from pure polymer to polymer:fullerene with 90% $PC_{61}BM$ content. With a $PC_{61}BM$ concentration smaller than 50% the electron mobility remained nearly constant, whereas the hole mobility slightly decreased for less than 25% $PC_{61}BM$ fraction. For more than 50% $PC_{61}BM$, both electron and hole mobility increases. In P3HT:$PC_{61}BM$ 1:4 and 1:1 devices two transit times in the electron current transients are observed, as well as in the hole current transients for an weight ratio of 1:3 polymer to fullerene. It is proposed that the slower carriers have to overcome a barrier before they can leave the sample, leading to longer extraction times. Although the origin for the observation of such double transients is unresolved yet, two possible explanations were given: (a) decreased mobility due to trapping of carriers; (b) bipolar transport, with energetic activation barriers for electrons hopping on P3HT and holes on $PC_{61}BM$. For charge carrier trapping, in principle a lower mobility than experimentally observed is expected. Moreover, Monte Carlo simulations supported the conclusion that

double transients may occur if two ambipolar materials mixed together are well separated and thus form both percolated pathways for efficient charge transport. In the sample with the highest $PC_{61}BM$ content of 90% a high hole mobility of approximately $7.3 \cdot 10^{-3}$ cm^2/Vs could be determined, comparable to the high electron mobility of $2.3 \cdot 10^{-2}$ cm^2/Vs found in the same device. Furthermore, an ambipolar transport in pure P3HT with an electron and hole mobility in the range of $1.8 \cdot 10^{-4}$ cm^2/Vs was revealed. With an enhanced regioregularity in P3HT both the hole and electron mobility found to be increased by almost one order in magnitude to 1×10^{-3} cm^2/Vs.

Chapter 8

Effect of Energetic Disorder on the Charge Transport and Recombination

In the previous chapter the bulk transport properties of P3HT as the donor material and $PC_{61}BM$ as the acceptor material were discussed. For a weight ratio of around 1:1 P3HT:$PC_{61}BM$ an almost balanced mobility of electrons and holes was found at room temperature. In this chapter, the charge carrier mobility and the charge carrier concentration are studied in pristine and annealed P3HT:$PC_{61}BM$ and P3HT:bis-$PC_{61}BM$ bulk heterojunction solar cells by the photo-CELIV technique. Thereby, bis-$PC_{61}BM$ leads to an increased open circuit voltage and is assumed to be cost cutting in the large-scale production compared to the widely used $PC_{61}BM$. The two side groups on the C_{60} cage, however, are expected to influence the morphology and thus the energetic disorder of the blend, which will affect the transport and recombination of charge carriers.

8.1 Introduction

The concept of bulk heterojunction solar cells is one of the most promising design architectures for a well performing organic solar cell with state of the art PCE values above 8% [4]. Polyphenylvinylene (PPV) based bulk heterojunction solar cells have been used reaching power conversion efficiency values up to 2.5% [15]. With polythiophenes, such as poly(3-hexylthiophene-2,5-diyl)(P3HT), a new class of donor materials was found exhibiting hole mobilities in the range of 10^{-8} m^2/Vs (see Chapter 7), which is at least one order of magnitude higher than in PPV. Using this material composition a PCE of up to 4.4% can be reached [127] with an improved PCE by a factor of almost 2, due to a better ordering of the conjugated polymer and increased hole mobility [118, 29]. Bulk heterojunction solar cells based on blends of P3HT and phenyl-C_{61} butyric acid methyl ester ($PC_{61}BM$) belong to the most studied candidates for this application in the last several years. In this blend system

Table 8.1: Solar cell parameters of the studied P3HT:$PC_{61}BM$ 1:0.8 and P3HT:bis-$PC_{61}BM$ 1:1 pristine and annealed are shown.

P3HT:$PC_{61}BM$ 1:0.8	V_{oc} mV	J_{sc} mA/cm^2	FF %	PCE %
pristine	625	2.9	56	1.0
annealed	565	10.2	67	3.86
P3HT:bis-$PC_{61}BM$ 1:1				
pristine	715	5.0	44	1.57
annealed	690	7.6	62	3.25

a deviation from Langevin recombination dynamics (see also Chapter 4) was reported in literature [128, 117].

In this chapter, the charge carrier mobility and the charge carrier concentration in P3HT:$PC_{61}BM$ is studied simultaneously using the technique of photo-CELIV. To further investigate the influence of the energetic disorder on the polaron transport and recombination dynamics in BHJ solar cells we also use an altering acceptor material, i.e. bis-$PC_{61}BM$ being the bisadduct analogue to $PC_{61}BM$ with an additional side chain at the fullerene cage [66]. Thereby, the addition of side chains raises the energy of the LUMO of the acceptor leading to a higher open–circuit voltage compared to P3HT:$PC_{61}BM$, but hinders a close packing of the fullerenes, which induces more disorder [67, 129].

8.2 Experimental

BHJ solar cells made of a mixture of P3HT and $PC_{61}BM$ or bis-$PC_{61}BM$, respectively, are processed on ITO structured glass substrates and characterized by using a solar simulator with respect to Section 5. Both, pristine and annealed blend films were studied. In Figure 8.1 the J–V curves of the illuminated BHJ solar cells are shown. The respective solar cell parameters are listed in Table 8.1.

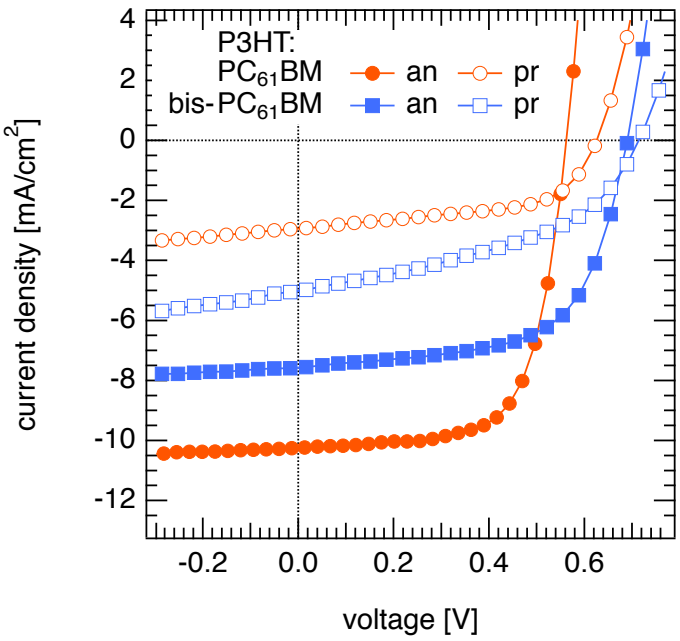

Figure 8.1: J–V characteristics of the illuminated P3HT:$PC_{61}BM$ 1:0.8 and P3HT:bis-$PC_{61}BM$ 1:1 pristine and annealed BHJ solar cells. The corresponding solar cell parameters can be found in Table 8.1.

8.3 Results

In Figure 8.2 current transients from photo-CELIV on an annealed P3HT:$PC_{61}BM$ blend device at $T = 150$ K are shown for different delay times t_{delay}. A constant offset voltage of 0.76 V in forward direction superimposed to the extraction voltage pulse was applied to the solar cell during the measurement to account for the internal electric field. The extraction voltage pulse was $V_p = -6$ V at a pulse width of $t_p = 1$ ms. As can be seen, with increasing t_{delay} the corresponding photo-CELIV peak decreases. Note that even in the dark without any laser excitation a CELIV peak can be detected. We assign this extracted charge carriers to equilibrium charges, which are injected into the bulk due to non-ideal blocking contacts.

Therefore, in order to consider only the photogenerated charge carrier concentration, the illuminated photo-CELIV transients are subtracted from the dark CELIV transient measured with the same parameter settings as a reference.

The result can be seen in Figure 8.3, where the photogenerated charge carrier concentration n_{ext} extracted from the bulk for a pristine and an annealed P3HT:$PC_{61}BM$ BHJ device is plotted as a function of t_{delay} for two different temperatures, $T = 150$ K and $T = 275$ K. At low temperatures n_{ext}

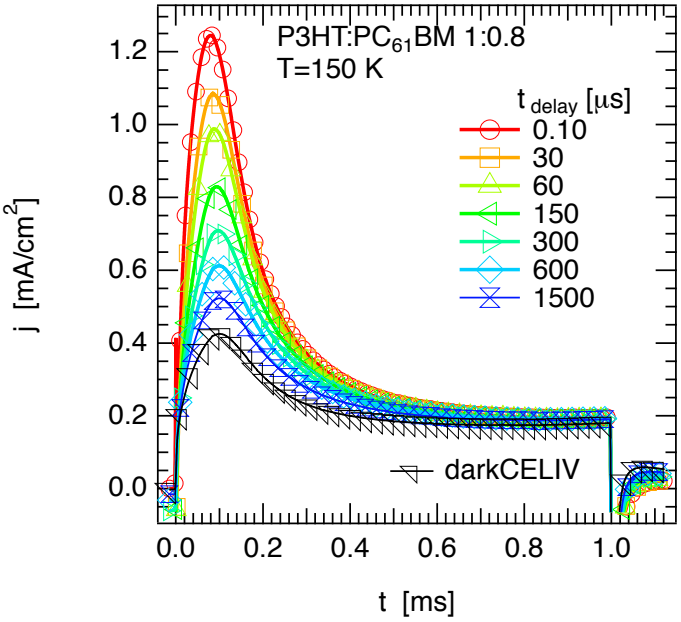

Figure 8.2: Photo-CELIV transient of an annealed P3HT:PC$_{61}$BM 1:0.8 BHJ solar cell at $T = 150$ K; the delay time t_{delay} was varied in the range from 100 ns to 10 ms. An offset voltage of 0.76 V was applied to account for the internal electric field.

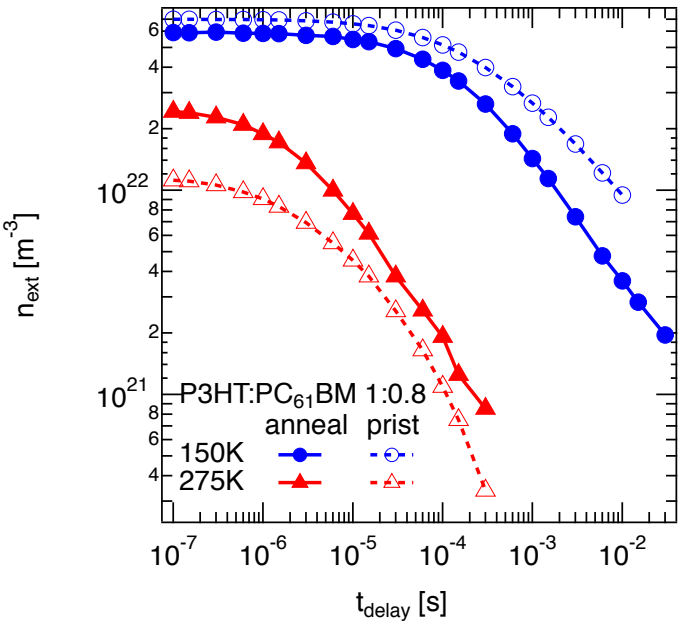

Figure 8.3: Extracted charge carrier density of P3HT:PCBM 1:0.8 solar cell for $T = 150$ K and $T = 275$ K.

approaches to a constant plateau for short delay times ($t_{delay} < 1$ μs) with the initial carrier concentration n_0 at $t_{delay} = 100$ ns and decreases thereafter continuously due to charge carrier recombination. A similar plateau can be observed in transient absorption measurement at early times. Thereby, the time at which the transient starts to decrease is attributed to the onset of non-geminate recombination [130, 131]. At low temperatures this onset is later as the recombination losses are diminished mainly due to low charge carrier mobilities. At high temperatures, however, the charge carriers being more mobile can meet their counterpart more easily, which leads to an increased charge carrier recombination according to Equation (4.12) [98, 132, 96] shifting the onset of non-geminate recombination to shorter times.

Alternatively, the charge carrier density is sometimes plotted versus the sum of the delay time t_{delay} and t_{max}, whereas the latter is the time at which the CELIV peak reaches its maximum value (see Figure 6.3). Especially at high temperatures, where the charge carrier recombination is increased, charge carriers may also recombine during the charge extraction process, which would have an impact on $n_{ext}(t)$. In Figure 8.4 both methods are compared, whereas the charge density extracted from a pristine P3HT:PC_{61}BM 1:0.8 BHJ solar cell is shown as a function of t_{delay} and of $t_{delay}+t_{max}$. It can be seen both data agree quite well. Thus, we can ignore the recombination of charge carriers for $0 < t < t_{max}$ (see Figure 6.3).

From the peak maximum of the photo-CELIV transient the charge carrier mobility can be determined (see Section 6.2). However, we note that the polarity of the latter cannot be distinguished in a CELIV experiment. Instead of plotting the charge carrier mobility μ versus the delay time t_{delay}, μ can also be shown as a function of the charge carrier concentration n_{ext} extracted from the bulk at each measured t_{delay}. In Figure 8.5 μ versus n_{ext} can be seen for pristine and annealed P3HT:PC_{61}BM and P3HT:bis-PC_{61}BM BHJ solar cells at $T = 150$ K. For the thermally treated P3HT:PC_{61}BM solar cell the charge carrier mobility is almost independent on the charge carrier concentration n_{ext}. However, for the thermally untreated P3HT:PC_{61}BM as well as both annealed and pristine P3HT:bis-PC_{61}BM BHJ solar cells a significant decrease of the charge carrier mobility with charge carrier concentration can be observed. For the blend composition P3HT:bis-PC_{61}BM we can generally assign a reduced mobility of the charge carriers, as can be seen in Figure 8.5.

To address the recombination processes responsible for the time dependent charge carrier concentration decay revealed by the photo-CELIV technique, the experimental data was fitted by solving the continuity equation (see Equation (4.2)). Different recombination processes were taken into account. From Figure 8.6 a reduced Langevin recombination can be addressed in accordance to previous findings [117, 133]. However, at large delay times t_{delay} the exper-

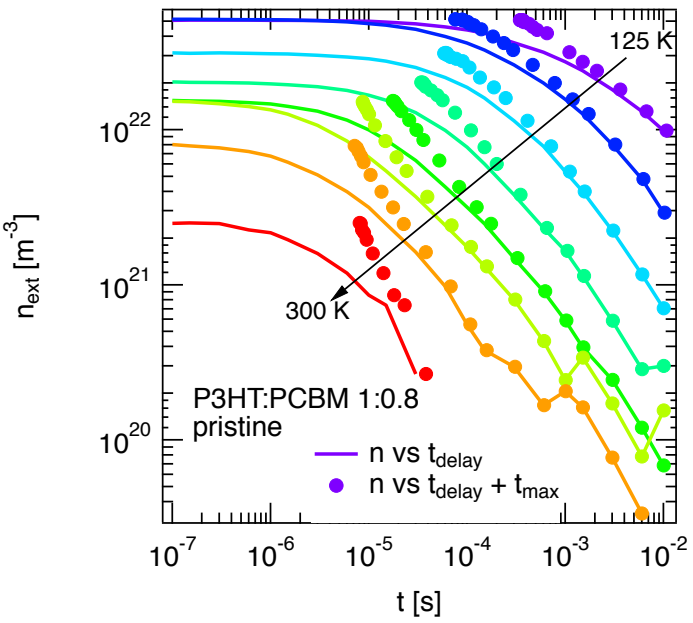

Figure 8.4: The charge carrier density n_{ext} as a function of the delay time t_{delay} (solid lines) compared to the density plotted versus the sum of t_{delay}+t_{max} (dots) for a pristine P3HT:PC$_{61}$BM 1:0.8.

imental data show an increasing deviation from the fit, when using a constant prefactor ζ in the latter. Thus, we used in analogy to Ref. [134] a more generalized equation $dn/dt = kn^{\lambda+1}$ assuming bimolecular recombination and the validity of $n = p$ with a general recombination coefficient k and the order of recombination $\lambda+1$. The obtained fit is qualitatively in good agreement with the experimental $n_{ext}(t)$ data. From the fit we can determine a charge carrier concentration decay order, corresponding to the recombination order, for an annealed P3HT:PC$_{61}$BM device at $T = 150$ K to be $\lambda + 1 = 2.65$ being consistent with previously published values deduced from complementary techniques [134, 130, 135]. Thereby, the carrier concentration decay order even increases up to 4.7 for pristine and to 3.6 for annealed P3HT:PC$_{61}$BM devices at $T = 125$ K. With increasing temperature the recombination order approaches two for both devices, however, never becoming exactly two (see Figure 8.7).

From the time dependent charge carrier density revealed from photo-CELIV measurements the recombination rate R_{exp} can be determined using the equation

$$\frac{dn}{dt} = G - R \approx \frac{dn_{ext}}{dt} = G - R_{exp} \quad , \tag{8.1}$$

whereas the generation rate $G = 0$ for $t_{delay} > 0$. In Figure 8.8(a) R_{exp} is shown

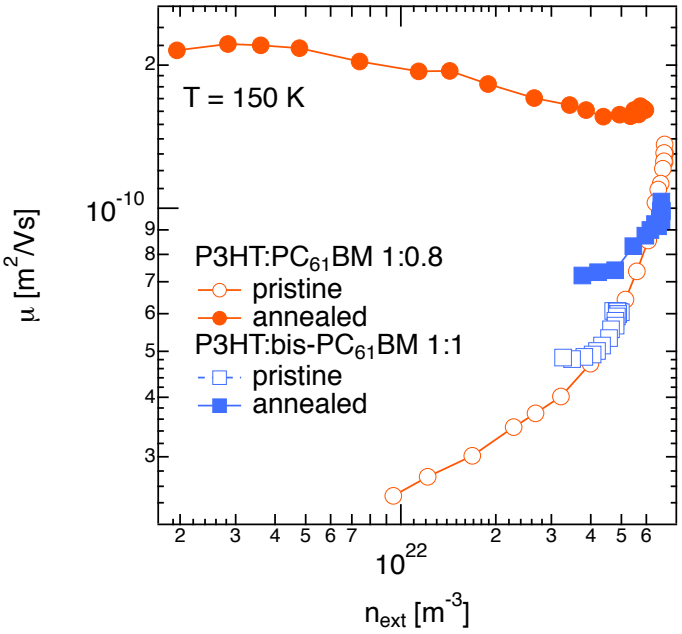

Figure 8.5: Charge charge carrier mobility μ of both pristine and annealed P3HT:PC_{61}BM 1:0.8 and P3HT:bis-PC_{61}BM 1:1 BHJ solar cell deduced from the corresponding CELIV transients at $T = 150$ K. Independent on the thermal treatment μ exhibit a significant dependence on the charge carrier concentration in P3HT:bis-PC_{61}BM devices.

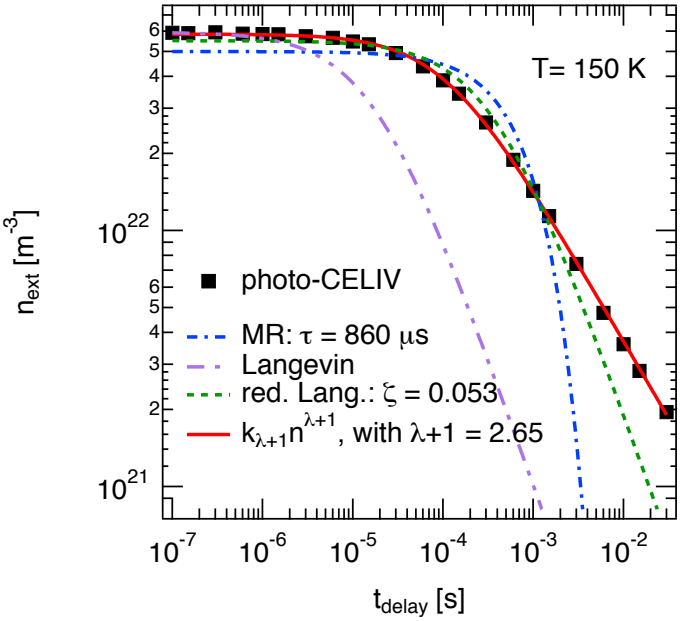

Figure 8.6: Photo-CELIV transient of an annealed P3HT:PC$_{61}$BM 1:0.8 BHJ solar cell at $T = 150$ K; the delay time t_{delay} was varied in the range from 100 ns to 10 ms. An offset voltage of 0.76 V was applied to account for the internal electric field. Four different types of recombination processes are fitted to the experimental data: (a) (blue dashed dotted line) first order process $R = n/\tau$ (b) (purple fine dashed) Langevin recombination: $R = \frac{q}{\varepsilon\varepsilon_0}(\mu_n + \mu_h)np$ (c) (green dashed) reduced Langevin recombination with an additional constant prefactor ζ (d) (red solid line) generalized equation $dn/dt = k_{\lambda+1}n^{\lambda+1}$ with the charge carrier concentration decay order (recombination order) $\lambda + 1$ and recombination rate coefficient $k_{\lambda+1}$.

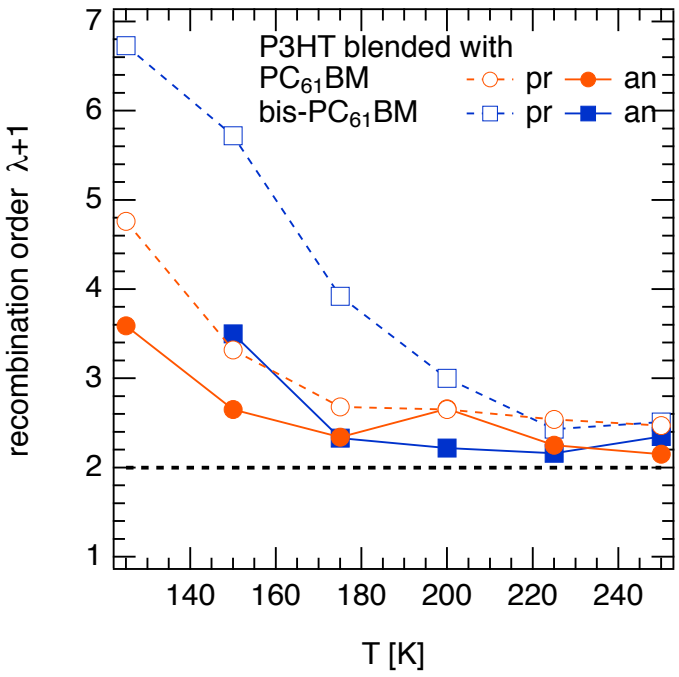

Figure 8.7: Charge carrier concentration decay order deduced from fitting the $n_{ext}(t)$ data (see Figure 8.6).

as a function of the carrier concentration n_{ext} at $T = 150$ K for the studied blend systems. The ratio ζ between the experimentally observed recombination rate R_{exp} and the rate described by Langevin R_L (Equation (4.12)) shown in Figure 8.8(b) is given by [117]

$$\zeta(n) = \frac{R_{exp}}{R_L} = \frac{k(n)}{\gamma_L} = \frac{k(n)}{\frac{q}{\varepsilon\varepsilon_0}\mu(n)} \quad . \tag{8.2}$$

As can be seen for P3HT:$PC_{61}BM$ devices the recombination rate is significantly lower and the deviation from the Langevin recombination rate R_L (Equation (4.12)) with $np \gg n_i^2$) is stronger for thermally untreated solar cells with decreasing charge carrier concentration. Even though the charge carrier mobility is different in pristine and annealed P3HT:$PC_{61}BM$ devices with a different charge carrier density dependence (see Figure 8.5), a quite similar deviation from Langevin recombination can be observed with the almost identical charge carrier concentration dependence. For BHJ solar cells with bis-$PC_{61}BM$ as acceptor material we observed the recombination rate similar to pristine P3HT:$PC_{61}BM$ BHJ solar cells, however with smaller difference between the annealed and pristine samples. Taking into account the charge carrier mobility we observe a larger deviation from Langevin recombination for both pristine and annealed P3HT:bis-$PC_{61}BM$ devices, as can be

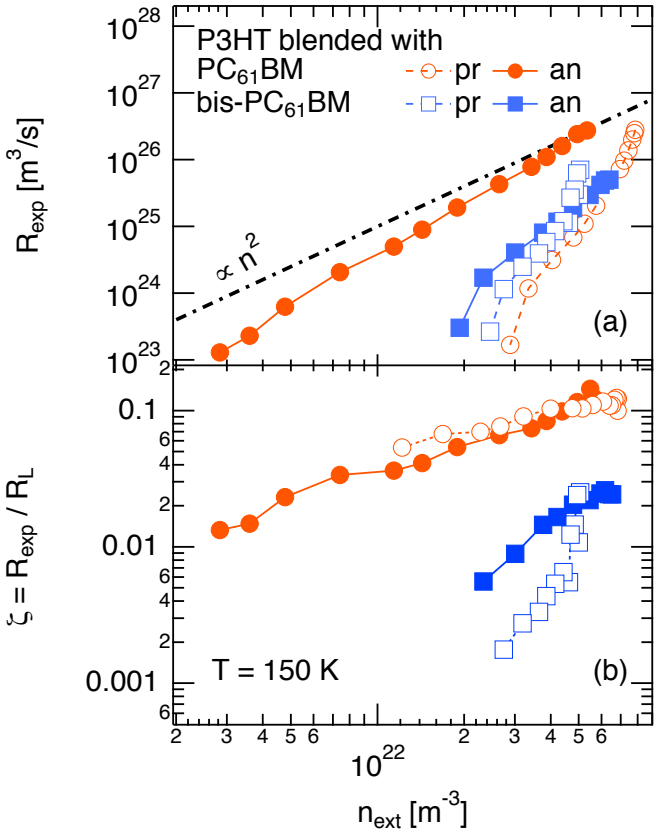

Figure 8.8: (a) The recombination rate R_{exp} as a function of the charge carrier density n_{ext} for P3HT:PC$_{61}$BM and P3HT:bis-PC$_{61}$BM BHJ solar cells. As a guide to the eye the recombination rate proportional to n^2 is added to the graph (dash dotted line). (b) The ratio between the experimentally observed recombination rate and the rate given by Langevin for P3HT blended with various acceptor materials.

seen in Figure 8.8(b).

8.4 Discussion

Before we discuss the physical origin of the experimental observations we want to stress the importance of the experimental parameters and their potential influence on the results if the limitations of the photo-CELIV technique are not considered adequately. For mobility calculations the time t_{max} at which the photo-CELIV peak reaches its maximum has to be determined. However, t_{max} may be affected by the RC time τ_{RC} of the circuit as was discussed in Section 6.2 (see Figure 6.5). τ_{RC} depends on the capacitance of the solar cell and thus on the charge carriers at the electrodes and within the bulk. For recombination studies using photo-CELIV the internal electric field V_{bi} of illuminated solar cells should be compensated to minimize the losses of photogenerated charge carriers due to charge extraction by V_{bi}. Furthermore, at V_{bi} a decent amount of charge carriers is thermally injected into the bulk under dark conditions, which can interact with photogenerated carriers. Furthermore, the injection of charge carriers into the bulk leads to an increase in the capacitance of the overall circuit and hence increases τ_{RC}, which limits the time resolution of the measurement. In this case, the charge carrier mobility is underestimated due to a RC shifted t_{max} position, as can be seen in Figure 8.9 ($t_{tr} < \tau_{RC}$). Consequently, the mobility calculated from the photo-CELIV transient at $V_{off} = V_{bi}$ of $\mu = 3.6 \times 10^{-9}$ m^2/Vs is more than one order of magnitude smaller compared to the mobility at $V_{off} = 0$ V being $\mu = 6 \times 10^{-8}$ m^2/Vs.

At low temperatures a reduced charge carrier injection as well as the reduced charge carrier mobility lead to more reliable photo-CELIV studies even at $V_{off} = V_{bi}$. Therefore, we focused our interpretation of the charge carrier mobility only to the low temperature regime ($T < 200$ K).

At $T = 150$ K the charge carrier mobility as a function of the charge carrier concentration revealed a drop of almost one order of magnitude over the measured time range for pristine P3HT:PC$_{61}$BM BHJ devices. In contrast, the annealed devices showed no dependency on the carrier concentration n_{ext}. However, for P3HT:bis-PC$_{61}$BM BHJ devices n_{ext} has a strong influence on μ for both annealed and pristine devices (see Figure 8.5).

The time or charge carrier concentration dependence of the charge carrier mobility is widely discussed in literature [79, 108, 107]. Mozer *et al.* found a time dependent $\mu(t)$ in MDMO-PPV:PC$_{61}$BM 1:4 BHJ solar cells using the technique of photo-CELIV. They assigned the time dependence to a relaxation process of charge carriers after photoexcitation to deep tail states

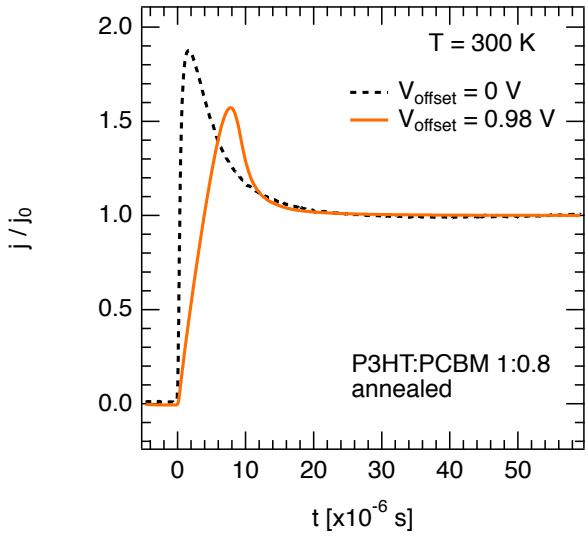

Figure 8.9: Photo-CELIV transients for two different offset voltages V_{offset} = 0 V and V_{offset} = 0.98 V being applied in forward direction of the solar cells; For comparison the transients are normalized to the capacitive current step j_0. In case of an applied offset voltage the transient is affected by the increased capacitance due to injected charge carriers (compare to Figure 6.5).

in a Gaussian density of states distribution, assuming the Gaussian disorder model (GDM) [108]. Furthermore, a carrier concentration dependent $\mu(n)$ can be obtained in the mean medium approximation (MMA), whereas the dependency increases with disorder [136, 86]. Recently, Bange *et al.* pointed out that a time dependent charge carrier mobility observed in the photo-CELIV technique is related to bimolecular recombination taking place during charge extraction, which was neglected in previous analysis of the current transients. They showed in numerical simulations that taking the Langevin recombination mechanism into account the maximum position of the current transient t_{max} is shifted to longer times resulting in a lower charge carrier mobility [107]. Considering our experimental results we can exclude that the recombination led to a time dependent mobility as suggested by Bange *et al.* as the recombination is comparable or even lower in the thermally untreated BHJ solar cells at low temperatures (see Figure 8.3). Moreover, for annealed P3HT:PC$_{61}$BM devices a constant charge carrier mobility was revealed from photo-CELIV experiments.

Instead, especially in thermally untreated P3HT:PC$_{61}$BM BHJ solar cells deep tail states of the Gaussian density of states distribution (GDOS) can be expected due to a broader distribution of site energies [83, 86, 136]. This will lead to a trap limited charge transport especially at low temperatures. Charge

carrier will undergo multiple trapping and release processes during their hopping transport, especially at low carrier concentrations (see Figure 3.4). However, at high enough carrier concentrations those states will be filled resulting in an increase in the charge carrier mobility. Indeed, this will lead to a concentration dependent charge carrier mobility as observed in the pristine P3HT:$PC_{61}BM$ BHJ solar cells and found in MDMO-PPV:$PC_{61}BM$ blend system [108]. In P3HT:bis-$PC_{61}BM$ BHJ solar cells the broader DOS due to enhanced energetic disorder [67, 129] results in a trap affected charge transport in both pristine and annealed devices.

The event of charge trapping does not only affect the transport regarding the charge carrier mobility, but also influences the number of charge carriers actually participating in the dynamics and hence in recombination processes. According to Equation (4.12) the recombination described by the Langevin model is proportional to the charge carrier mobility. Recently, it was reported that a carrier concentration dependent charge mobility may explain the deviation of the recombination order from two and thus from Langevin [137]. However, by looking at the ratio $\zeta(n)$ (Equation (8.2)) we point out that the deviation from Langevin in P3HT:$PC_{61}BM$ solar cells can only partly be explained by a $\mu(n)$ (compare Figure 8.5 and Figure 8.8(b)). A residual dependence on the charge carrier concentration of ζ can be observed, which even increases if bis-$PC_{61}BM$ is used as the acceptor material (Figure 8.8(b)). The latter can be attributed again to the more broadened GDOS and thus larger energetic disorder parameter σ. Consequently, more deep tail states are present in bis-$PC_{61}BM$ related BHJ solar cells, which affect the charge transport more strongly compared to the one in P3HT:$PC_{61}BM$ with less disorder. Thereby, already P3HT:$PC_{61}BM$ BHJ solar cells exhibit a deviation from Langevin recombination mechanism (see Figure 8.8(b)).

In the following, we will explain how such a deviation from the Langevin model in dependence on the charge carrier concentration can be addressed to the energetic disorder in the blend system. In the Langevin model it is assumed that all charge carriers are mobile and thus can find a counterpart for recombination at every time (see Section 4.2), which is, however, not completely true for organic BHJ solar cells. Besides the free mobile charge carriers we have to take into account also trapped charges. Thus the carrier concentration for electrons (holes) can be written as $n = n_c + n_t$ ($p = p_c + p_t$), where n_c (p_c) is the concentration of free mobile electrons (holes) and n_t (p_t) the concentration of trapped electrons (holes). For the dynamics in organic bulk heterojunction solar cells, however, free as well as trapped charge carriers $n = n_c + n_t$ ($p = p_c + p_t$) have to be considered. Equation (4.12) can thus be

written as

$$R = \frac{q}{\varepsilon\varepsilon_0} \underbrace{\mu(n)}_{\propto n^{\delta}} \underbrace{(n_c \cdot p_c + n_c \cdot p_t + p_c \cdot n_t + n_t \cdot p_t)}_{\propto n^{\lambda+1-\delta}} \quad , \tag{8.3}$$

It is obvious that in addition to the charge carrier mobility $\mu(n)$ the second factor in brackets in Equation (8.3) leads to a charge carrier concentration dependence ($n^{\lambda+1-\delta}$). Especially the second factor can be related to a dynamical process of trapping and release of charge carriers. Thus, trapped charge carriers, if released after a dwell time, can participate, even though delayed, in the dynamics in BHJ solar cells affecting $n_{ext}(t)$.

Looking at the initial charge carrier concentration n_0, we observe a lower n_0 in the photo-CELIV experiment for high temperatures, whereas for pristine devices the decrease in n_0 with increasing temperature is generally more pronounced (see Figure 8.3). This might indicate a loss mechanism, which is faster than the here studied time scales ($t < 100$ ns). Marsh *et al.* [138] used Monte Carlo simulation to model the charge separation efficiency in organic BHJ solar cells. They assigned a poor performance of BHJ solar cells to those cells, which exhibit heterojunctions being randomly aligned with respect to the electric field. This leads to an enhanced geminate recombination [138]. The dynamics for geminate recombination, however, occur on sub-microsecond time scales [47] and hence faster than the time scales measured by photo-CELIV. Thus, the conclusions made by Marsh *et al.* may support our results on the lowered n_0 observed in pristine devices exhibiting well intermixed, and more randomly distributed donor–acceptor phases in the bulk. In addition, the recombination of charge carriers will change the flat band conditions of the solar cell, which results in a sweep out of some of the photogenerated charges, in addition to recombination. This effect is proportional to the charge carrier mobility and therefore stronger at higher temperatures. However, further experiments on time scales faster than 100 ns such as transient absorption are needed to give a more clear answer to this question.

In Figure 8.10 the time dependent charge densities for P3HT:PC$_{61}$BM and P3HT:bis-PC$_{61}$BM are compared for both pristine and annealed devices at $T = 200$ K. The initial charge carrier density n_0 at $T = 200$ K is similar for all blend compositions pristine and annealed. If we compare e.g. both pristine devices, P3HT:PC$_{61}$BM and P3HT:bis-PC$_{61}$BM, which exhibit similar recombination orders (see Figure 8.7), we see a significantly later onset of non-geminate recombination for P3HT:bis-PC$_{61}$BM. We attribute this to the increased energetic disorder in the P3HT:bis-PC$_{61}$BM blend composition, which is also reflected by the experimentally observed reduced charge carrier mobility. As has been reported by Nelson [139] a tail of deep states in interpenetrating bulk heterojunction blend systems serves to delay recombination

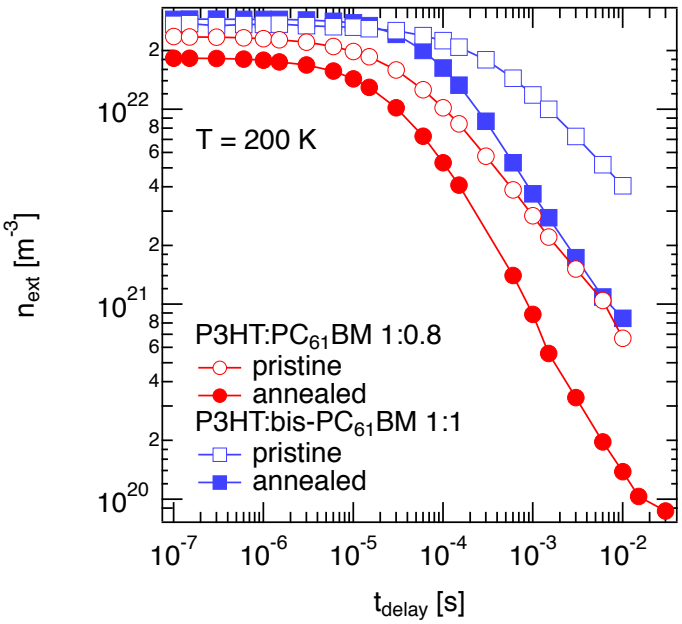

Figure 8.10: Charge carrier density for P3HT:PC_{61}BM 1:0.8 and P3HT:bis-PC_{61}BM 1:1 pristine and annealed BHJ solar cells as a function of time for $T = 200$ K. For P3HT:bis-PC_{61}BM the onset of non-geminate recombination—time at which the charge density starts to decay—is shifted to later times.

of charge carriers, as charge carriers are more impeded in finding each other at the donor–acceptor heterojunction interface. Thereby, the release of polarons from traps is the key process, which determines the recombination times in organic solar cells [139]. This would explain also the increasing recombination order with decreasing temperature, as the process of charge trapping plays a more important role in the dynamics with an increased concentration of trapped charge carriers at low temperatures. To summarize, energetic disorder will not only cause a reduced charge transport, but also lead to delay in charge carrier recombination dynamics.

8.5 Conclusion

We studied the charge transport and recombination dynamics in BHJ solar cells made from P3HT blended with PC_{61}BM and bis-PC_{61}BM as acceptor materials by the photo-CELIV technique. Thereby, thermally treated and untreated devices were compared. A concentration dependent charge carrier mobility was observed in pristine P3HT:PC_{61}BM BHJ solar cells, which we assigned to charge carriers filling up deep states of the GDOS. In contrast, annealed P3HT:PC_{61}BM devices showed no dependence on the carrier concen-

tration at $T = 150$ K. Besides $\mu(n)$, the trapping of charge carriers led also to a concentration dependent Langevin prefactor $\zeta(n)$. As a result, recombination orders above two can be observed in BHJ solar cells, even though the dynamics are considered to be bimolecular. Replacing $PC_{61}BM$ by bis-$PC_{61}BM$ as acceptor material led to a carrier concentration dependent mobility in both pristine and annealed devices with an even stronger deviation from Langevin recombination. We attributed this to a strong impact of charge trapping due to an increased energetic disorder in P3HT:bis-$PC_{61}BM$, which led to a reduced charge carrier mobility and a delay in recombination.

Chapter 9

Influence of Phase Segregation on the Charge Carrier Mobility and Lifetime in Organic Bulk Heterojunction Solar Cells

In the previous chapter, the results on the transport and recombination studies in P3HT:$PC_{61}BM$ and P3HT:bis-$PC_{61}BM$ BHJ solar cells were presented. Bimolecular recombination dynamics were found in the studied organic solar cells with a recombination coefficient being more strongly dependent on the carrier concentration in disordered blend systems. Furthermore, the experimentally observed charge carrier concentration decay order was found to be affected by the energetic disorder of the bulk. Here, in this chapter we will discuss how the degree of phase segregation between the donor and the acceptor will influence the charge transport and recombination in a bulk heterojunction solar cell.

Part of the results discussed in this chapter is published in Paper 8.

9.1 Introduction

The interpenetrating network of donor and acceptor phase is a key issue for further increasing the performance of polymer–fullerene bulk heterojunction solar cells, as it affects the exciton dissociation, charge transport and recombination [9]. Whereas a fine phase intermixing on the sub–nm scale is believed to be beneficial for efficient photogeneration, the charge transport is strongly related to the percolation pathways formed within the bulk of the solar cell. A crucial parameter having a great impact on the morphology of a bulk heterojunction solar cell is the donor–acceptor ratio. For many conjugated polymers, e.g. poly(p-phenylene vinylene) (PPV) [15], a fullerene content of 67 wt.-% to 80 wt.-% was found to be best for the performance of those solar cells. Only a few polymer:fullerene systems have their optimum blend ratio at 1:1, e.g. P3HT:$PC_{61}BM$ [140]. Recently, it was reported that depending on the chain length and denseness of the polymer side chains, as well as the size of

the fullerene, intercalation of the fullerenes in between the side chains can occur [141, 142]. Mayer et al. found an optimum polymer:fullerene blend ratio of 1:3-1:4 in the blend system consisting of poly(2,5-bis(3-tetradecyl thiophen-2-yl) thieno[3,2-b]thiophene) (pBTTT): phenyl-C_{71}-butyric acid methyl ester ($PC_{71}BM$), as an excess of $PC_{61}BM$ molecules was necessary to create phase segregation. In MDMO-PPV:$PC_{61}BM$ blend system the same optimum blend ratio of 1:3–1:4 was assigned to a nanoscale phase segregation with pure $PC_{61}BM$ domains surrounded by a matrix of polymer containing up to 50 wt.-% of fullerene [143]. Following an efficient charge generation, charge transport and recombination dynamics in blend systems are intuitively expected to be affected by the phase segregation and the dimensions of domain sizes, which will be addressed in detail in this chapter.

9.2 Experiment

BHJ solar cells were prepared as described in Chapter 5. Without further annealing the active blend layer Ca (3 nm)/Al (100 nm) were evaporated thermally on top. $PC_{61}BM$ was purchased from Solenne, poly(2,5-bis(3-dodecyl thiophen-2-yl) thieno[2,3-b]thiophene) (pBTCT-C_{12}) was synthesized according to the published procedure in Ref. [144]. All materials were used without further purification.

Photo-CELIV measurements were performed at different temperatures ranging from 175 K to 300 K in steps of 25 K. The experimental technique is explained in detail in Section 6.2. In contrast to the results presented in Chapter 8, temperatures up to 300 K could be measured for the here studied blend composition as the RC constant did not limit the transients. This was mainly due to the device thicknesses of up to 200 nm and especially due to rather small extraction peak heights measured in 1:1 and 1:4 pBTCT-C_{12}:$PC_{61}BM$ blend ratios compared to those measured for P3HT:$PC_{61}BM$ and P3HT:bis-$PC_{61}BM$. The delay time between the laser excitation and the extraction voltage pulse was varied from 100 ns to 10 ms. We used the second harmonic of a Nd:YAG laser ($\lambda = 532$ nm, < 80 ps pulse duration) for laser excitation. For calculating the charge carrier mobility the parametric equation according to Equation (6.4) was used.

Furthermore, the decay of charge carriers was studied by transient microwave conductivity. By using this technique both mobile holes and electrons contribute to the measured change in microwave conductance (ΔG). The microscopic charge carrier mobilities were deduced from the TRMC transients by equation

$$\varphi \Sigma \mu = \frac{\Delta G_{MAX}}{\beta e I_0 F_A} \quad . \tag{9.1}$$

φ is the quantum efficiency for charge generation and $\Sigma\mu$ is the sum of the mobilities of the positive and negative charge carrier. β denotes the ratio between the broad and narrow inner dimension of the waveguide, e is the elementary charge, J_0 the incident laser fluence and F_A is the fractions of photons absorbed by the sample. The laser fluence in the TRMC experiment was 135 μJ/cm^2/pulse. As described in more detail previously [145, 146, 147], if φ is undetermined, the value of $\varphi\Sigma\mu$ is a lower limit of the local charge carrier mobility. Samples for TRMC measurements were prepared from the same solution as the solar cells. A powerful technique to study the crystallinity of a material is to measure X-ray diffraction (XRD). As pBTCT-C_{12} is a polymer showing high crystallinity, XRD can be used to study the molecular packing, i.e. the stacking of the polymer backbones.

9.3 Results

Figure 9.1 shows the results of XRD measurements on as spun pBTCT-C_{12} films and those blended with $PC_{61}BM$ in a 1:1 and 1:4 weight ratio. No additional annealing was applied. For the pure pBTCT-C_{12} film a diffraction peak at 4.3° is observed, corresponding to a lamellar spacing of 2.0 nm, i.e. the distance between two neighboring sheet-like structures consisting of π-stacked polymers. Upon addition of $PC_{61}BM$, the X-ray peak was shifted towards smaller angles, corresponding to an increase in the lamellar packing distance to 2.8 nm, whereas no further shift was observed from the 1:1 to the 1:4 weight ratio.

By measuring the wavelength dependent photocurrent the external quantum efficiency (EQE) can be determined, which is defined as the ratio between the number of extracted electron–hole pairs and the number of photons absorbed by the blend system. In Figure 9.2 the EQE spectra on the left axis are shown together with the absorption spectra as a function of the incident wavelength for pBTCT-C_{12}:$PC_{61}BM$ 1:1 and 1:4 blend ratio. $PC_{61}BM$ molecules absorb mainly in the UV region at a maximum of around 325 nm (see Figure 2.10), whereas the polymer pBTCT-C_{12} exhibit a maximum absorption at 460 nm. It can be seen that light with a wavelength longer than 550 nm is hardly absorbed by the studied polymer:fullerene blend system. As a consequence, the generation of a photocurrent is limited to a rather small range of the sun spectrum.Thus, looking at the illuminated J–V characteristics of the two studied solar cells, it is not surprising that the obtained PCE is rather low. Comparing both ratios, the efficiency of a pBTCT-C_{12}:$PC_{61}BM$ 1:4 BHJ solar cells is 0.5%, which is almost threefold higher compared to the 1:1 blend ratio with a PCE of 0.15%. This is mainly due to a reduced short circuit current

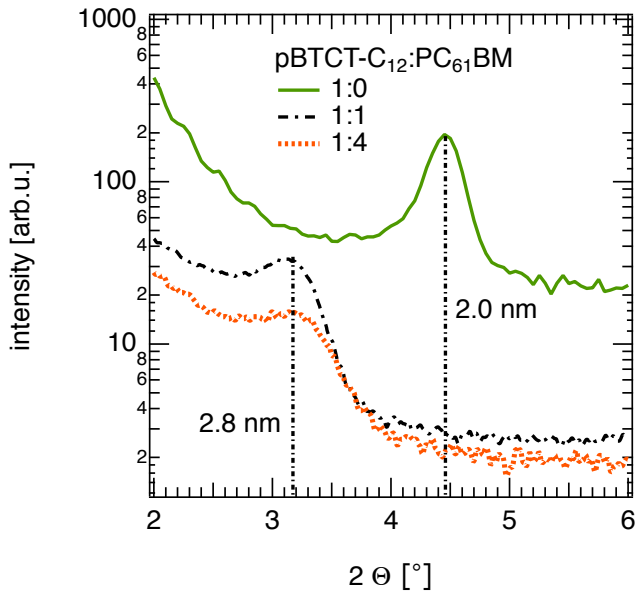

Figure 9.1: X-ray diffraction measurements on pure a pBTCT-C_{12} film and blended with $PC_{61}BM$ in a 1:1 and 1:4 ratio. The X-ray peak is shifting from 4.45° in the pristine pBTCT-C_{12} film to 3.17° in the blend corresponding to a lattice distance of 2.0 nm and 2.8 nm, respectively.

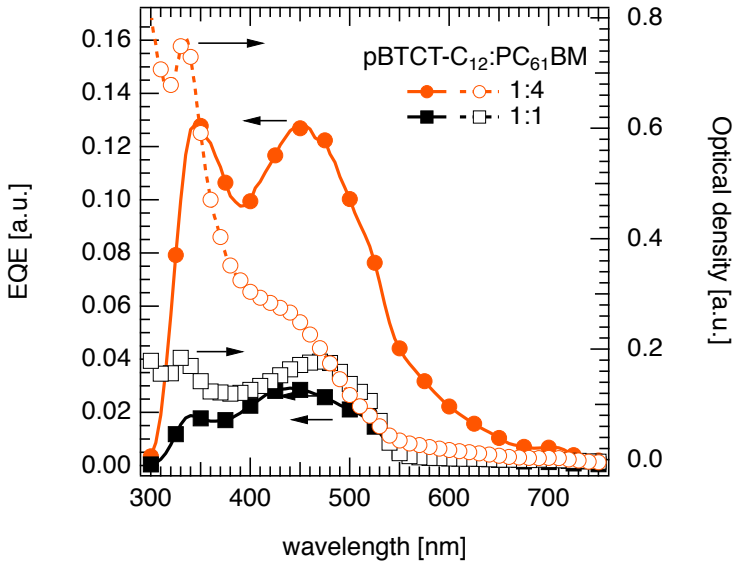

Figure 9.2: (left axis) External quantum efficiency (EQE) of pBTCT-C_{12}:$PC_{61}BM$ 1:1 and 1:4 as a function of the wavelength (solid lines); (right axis) wavelength dependent optical density of the studied blend systems (dashed lines).

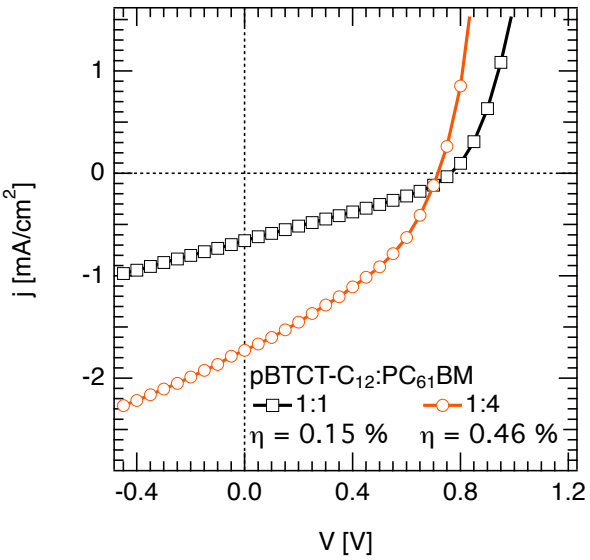

Figure 9.3: J–V characteristics of pBTCT-C_{12}:PC_{61}BM 1:1 and 1:4 bulk heterojunction solar cells illuminated under AM1.5G solar simulator.

density (see Figure 9.3). Obviously, the charge carriers can be extracted more efficiently in case of pBTCT-C_{12}:PC_{61}BM 1:4 compared to the 1:1 ratio. To find an answer for the reduced j_{sc} and hence PCE in pBTCT-C_{12}:PC_{61}BM 1:1 solar cells the charge dynamics are investigated for both blend ratios.

In order to study the macroscopic charge transport and recombination dynamics in the two blend ratios, we performed photo-CELIV measurements at temperatures ranging from $T = 300$ K to $T = 175$ K. In Figure 9.4 the current transients from pBTCT-C_{12}:PC_{61}BM 1:1 and 1:4 are shown at $T = 250$ K, respectively. For both pBTCT-C_{12}:PC_{61}BM 1:1 and 1:4 devices charge carriers can be extracted from the bulk after laser excitation. However, in case of the 1:1 blend ratio less charge carriers can be extracted by the voltage pulse (see Figure 9.4(a)), which agrees quite well with the reduced j_{sc} obtained in the 1:1 ratio.

In Figure 9.5 the time dependent charge carrier concentration $n_{ext}(t)$ at $T = 200$ K and $T = 275$ K for pBTCT-C_{12}:PC_{61}BM 1:1 and 1:4 are compared. For both ratios a bimolecular recombination process can be observed, but with different order of the carrier concentration decay. At $T = 275$ K the carrier concentration decay is faster and more pronounced compared to $T = 200$ K for 1:1 and 1:4 blend device, which can be seen in a stronger decrease of the carrier concentration at large delay times.

Using again the generalized continuity equation $dn/dt = kn^{\lambda+1}$ the experimental data can be fitted in analogy to Chapter 8 (see Figure 8.6). From the fits shown in Figure 9.5 a charge carrier concentration decay order of

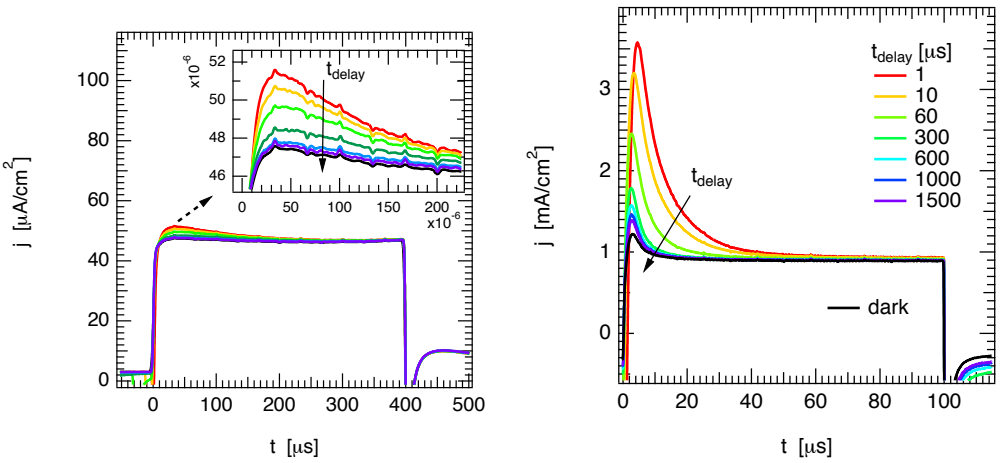

(a) pBTCT-C_{12}:$PC_{61}BM$ 1:1 (b) pBTCT-C_{12}:$PC_{61}BM$ 1:4

Figure 9.4: Photo-CELIV transients at $T = 250$ K for a pBTCT-C_{12}:$PC_{61}BM$ BHJ solar cell with a ratio of (a) 1:1 and (b) 1:4. CELIV parameters: $V_p = -4$ V, $V_{off} = 0.94$ V.

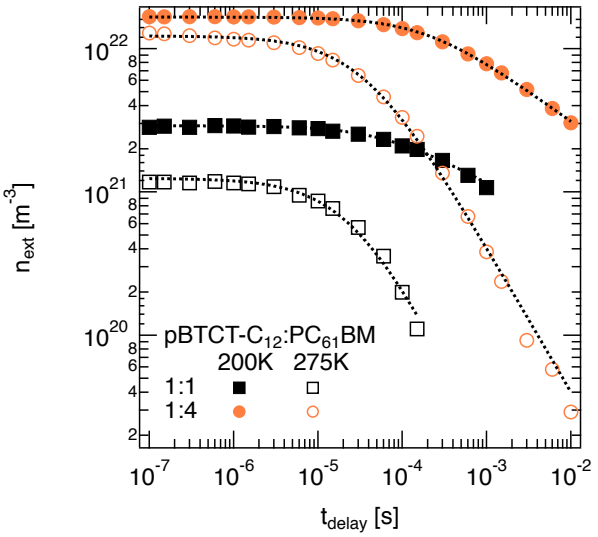

Figure 9.5: Extracted charge carrier density deduced from the photo-CELIV experiment at $T = 200$ K and $T = 275$ K. The initial charge carrier concentration n_0 (at $t_{\text{delay}} = 100$ ns) is about an order of magnitude less for the 1:1 ratio compared to the 1:4 device. For $t_{\text{delay}} > 100$ ns a bimolecular recombination with differing order can be observed for both ratios.

$\lambda + 1 = 4.1$ for 1:1 pBTCT-C_{12}:$PC_{61}BM$ at $T = 200$ K can be obtained, whereas at $T = 275$ K the order decreases to $\lambda + 1 = 1.8$. For the 1:4 blend device, $\lambda + 1$ decreases from 3.3 at $T = 200$ K to $\lambda + 1 = 2.0$ at $T = 275$ K. Considering the initial concentration of extracted charge carriers n_0 from the photo-CELIV measurements determined at a delay time of 150 ns, we observe an order of magnitude difference between the studied blend ratios (see Figure 9.5), the reason of which will be discussed later. For pBTCT-C_{12}:$PC_{61}BM$ 1:4 n_0 is 9.4×10^{21} m^{-3} at $T = 300$ K, whereas for the 1:1 ratio the initial carrier concentration is decreased to a value of 9.6×10^{20} m^{-3}.

The average charge carrier mobility μ deduced from photo-CELIV measurements at a fixed delay time of 60 μs is shown in Figure 9.7(a). In the 1:4 blend ratio μ is about an order of magnitude higher as compared to the one in the 1:1 ratio over the entire studied temperature range with $\mu = 4.8 \times 10^{-4}$ cm^2/Vs for 1:4 and $\mu = 4.5 \times 10^{-5}$ cm^2/Vs for 1:1 pBTCT-C_{12}:$PC_{61}BM$ BHJ solar cells at $T = 300$ K, respectively. As already mentioned above, the current transients were not limited by RC not even for temperatures up to 300 K. Furthermore, we note that no charge carriers could be extracted in 1:1 devices below $T = 175$ K.

TRMC measurements were performed to investigate the local charge transport in pBTCT-C_{12}:$PC_{61}BM$ 1:1 and 1:4 samples. TRMC signals of both samples show a fast initial rise due to the nanosecond laser pulse until the signal decays again. For the 1:4 blend the maximum photoconductivity ΔG_{MAX} at $T = 300$ K is more than one order of magnitude higher than that of the 1:1 blend (see Figure 9.6), which is in good agreement with the experimentally observed order of magnitude difference in the photo-CELIV signal for 1:1 and 1:4 devices. Variations of the photoconductivity on a similar scale depending on the relative $PC_{61}BM$ concentration were observed previously for $PC_{61}BM$:poly(phenyl vinylene) derivatives [148]. Generally, the decrease of the photoconductivity after ΔG_{MAX} is due to charge recombination and due to immobilization caused by trapping of charge carriers. Note that due to the absence of electrodes no charges are collected. In the inset of Figure 9.6 the product of the quantum efficiency for charge generation φ and the sum of the mobilities of the positive and negative charge carrier $\Sigma\mu$ is shown for the 1:1 and 1:4 ratios for $T = 200$ K. For the TRMC transients we used the same fitting routine as for the photo-CELIV transients. For both ratios similar recombination orders can be obtained with $\lambda + 1 = 2.8$ in the 1:4 and $\lambda + 1 = 3.1$ in the 1:1 ratio.

In Figure 9.7(b) the product $\varphi\Sigma\mu$ is plotted as a function of $1/T$ for both studied blend ratios. Clearly, two different contributions are observed for the pBTCT-C_{12}:$PC_{61}BM$ 1:4 sample. Below $T = 200$ K a small activation energy of $E_A = 19$ meV can be obtained, whereas for temperatures above 200 K it

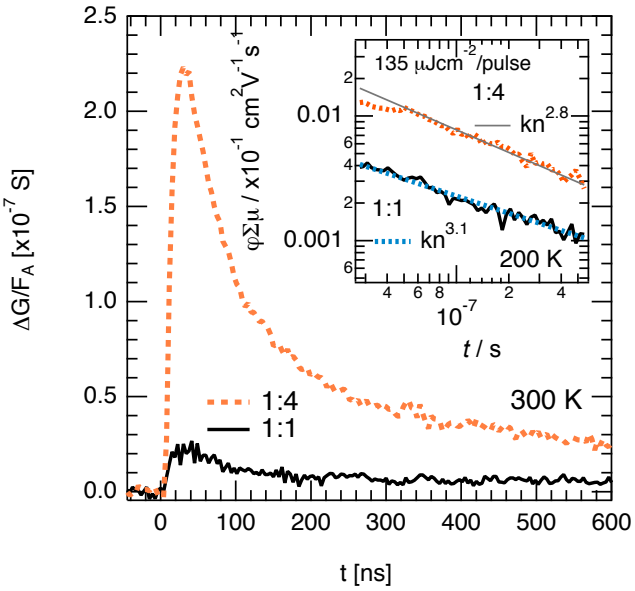

Figure 9.6: Photoconductance transients for the 1:1 (solid line) and 1:4 (dashed line) weight ratios of pBTCT-C_{12}:$PC_{61}BM$ blends photoexcited at 532 nm and a fluence of 1.4×10^{14} photons/cm^{2}pulse at $T = 300$ K. TRMC signals were normalised to the optical attenuation of the film. The inset shows the transients at $T = 200$ K fitted by the generalized continuity equation. The laser intensity was adjusted to be 135 μJ/cm^2/pulse.

becomes larger, i.e. $E_A = 52$ meV. In contrast, only one activation energy of approximately $E_A = 13$ meV can be seen in the 1:1 blend ratio. At $T = 300$ K the product $\varphi\Sigma\mu$ for the 1:1 weight ratio is 6×10^{-4} cm^2/Vs, whereas for the 1:4 blend ratio a value of 3.2×10^{-3} cm^2/Vs can be determined.

The recombination order deduced from the fit (see also Chapter 8) of the photo-CELIV and TRMC transients for pBTCT-C_{12}:PC_{61}BM 1:1 and 1:4 BHJ solar cells is shown in Figure 9.8 as a function of temperature. From both techniques an increasing recombination order with decreasing temperature can be determined for both studied blend ratios. In the 1:4 device a charge carrier concentration decay order of $\lambda + 1 = 1.9$ was deduced from TRMC and $\lambda + 1 = 1.8$ from photo-CELIV at $T = 300$ K increasing to around 3.4 and 4.6 at $T = 175$ K, respectively. Similar decay orders were observed in 1:1 blend devices with an increase from 2.1 to 4.9 obtained from the photo-CELIV experiments and 2.3 to 3.1 from corresponding TRMC transients. We note that slightly higher decay orders are revealed from photo-CELIV measurements at low temperatures, the origin of which will be discussed. For comparison, the data of an annealed P3HT:PC_{61}BM 1:0.8 device is also shown. There, the experimentally determined recombination order increases only slightly from 2.1 to 2.2 in the studied temperature range from $T = 300$ K to $T = 175$ K, respectively.

9.4 Discussion

In XRD measurements a lamellar spacing of 2.0 nm can be found in a pure pBTCT-C_{12} film. This is slightly larger than the 1.84 nm spacing peak observed for a thermally annealed film, but is nonetheless shorter than the length of two dodecyl chains placed end-to-end, which is indicative of some interdigitation of the side chains of adjacent polymer backbones [149]. For both pBTCT-C_{12}:PC_{61}BM blend ratios a clear shift of the XRD peak is observed pointing at an increase of the lamellar distance of 0.8 nm due to incorporation of methanofullerenes in the studied blend system.

The observation of only one X-ray peak and the absence of further shifting upon addition of more PC_{61}BM indicates the occurrence of intercalation [141] and its saturation at a PC_{61}BM concentration of 50%. For both weight ratios 1:1 and 1:4 an increase in the molecular stacking of 0.8 nm can be calculated. Similar to PPV:PC_{61}BM blend systems [143] it was suggested for pBTTT:PC_{71}BM devices—chemically related to the blend system studied in this work—that the addition of more than 50 wt.% of fullerene lead to phase segregation with PC_{71}BM domains growing in proportion to an increasing amount of fullerene [141]. Thus, although residual PC_{61}BM molecules in

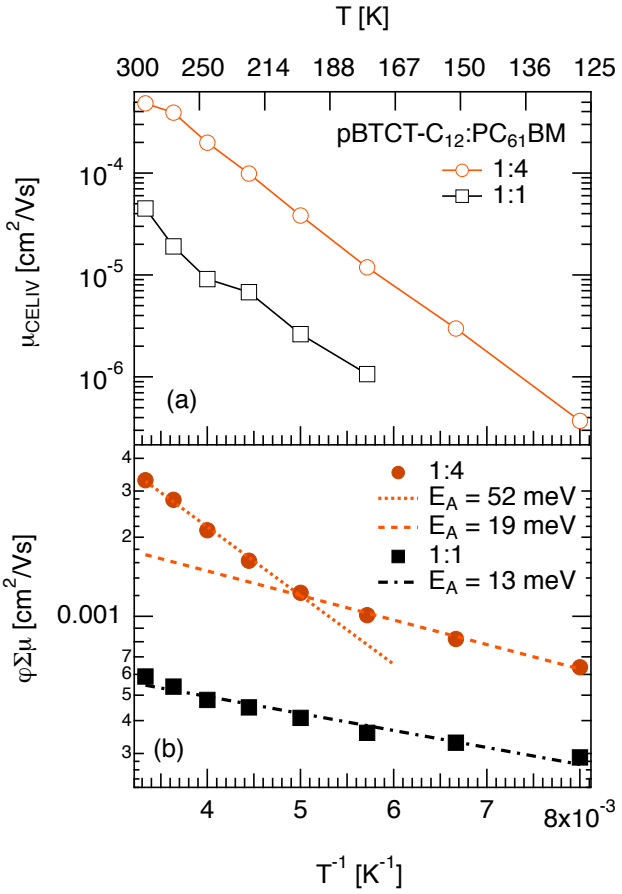

Figure 9.7: (a) Average bulk charge carrier mobility deduced from the photo-CELIV transients at a fixed delay time of 60 μs and (b) $\varphi\Sigma\mu$ deduced from TRMC experiment is plotted against $1/T$ for pBTCT-C_{12}:$PC_{61}BM$ 1:1 and 1:4. From TRMC two activation energies can be observed in the 1:4 blend ratio—52 meV for $T > 200$ K and 19 meV for $T < 200$ K—, whereas in the 1:1 ratio only one activation energy of 13 meV over the whole temperature range is detected.

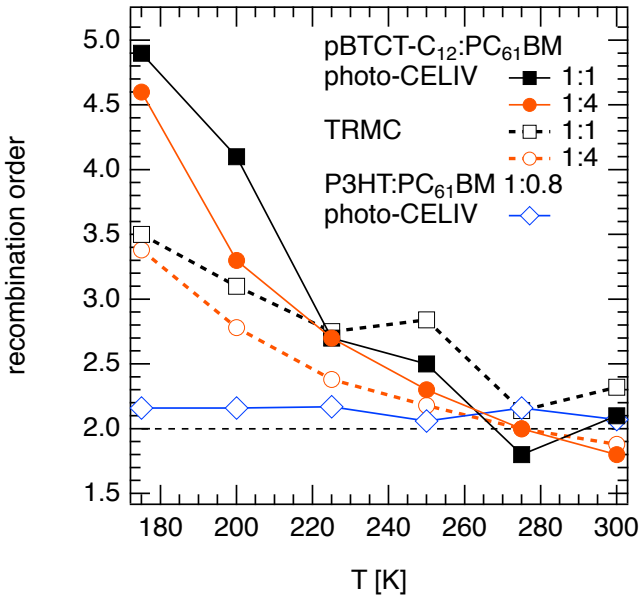

Figure 9.8: Recombination order shown as a function of temperature deduced from fitting the $n_{ext}(t)$ data of the photo-CELIV and $\varphi\Sigma\mu$ data of the TRMC transients for pBTCT-C_{12}:PC_{61}BM 1:1 and 1:4. For comparison the blend system P3HT:PC_{61}BM is also shown (data from Figure 8.7).

the 1:4 blends are not contributing to a further increase of the lamellar distance, the changed phase segregation does affect the transport properties and recombination dynamics in a BHJ solar cell, which was already suggested previously [56, 150, 151] and will be discussed in the following.

In the 1:4 blend device a higher charge carrier mobility in the bulk (photo-CELIV) as well as detected locally (TRMC) is observed experimentally. From temperature dependent TRMC measurements the contribution of charge carriers to the photoconductance can be deduced by determining the activation energy from an Arrhenius plot. In pBTCT-C_{12}:PC_{61}BM 1:4 two different activation energies could be assigned (see Figure 9.7) with a transition temperature of $T = 200$ K. Similar results were reported previously in different polymer:PC_{61}BM blend systems, e.g. P3HT:PC_{61}BM [152]. There, the activation energy for $T > 200$ K was assigned to the contribution of electrons in PC_{61}BM, whereas at low temperatures the hole mobility in the polymer dominates the product $\varphi\Sigma\mu$. If we project these findings to the here studied pBTCT-C_{12}:PC_{61}BM solar cells, above $T = 200$ K we observe only an electron mobility in the 1:4 blends. In contrast, in the 1:1 blend ratio holes on pBTCT-C_{12} dominate $\varphi\Sigma\mu$ over the entire studied temperature range. From photo-CELIV measurements the polarity of the extracted charge carriers can not been distinguished (see Section 6.2). However, we can conclude that in the

1:4 blend ratio extensive phase segregation leads to an efficient charge transport, whereas both charge carriers contribute to the transport. In contrast, a reduced charge carrier mobility is observed in the 1:1 pBTCT-C_{12}:$PC_{61}BM$ BHJ solar cell, which can be assigned to the fine donor–acceptor intermixing with less percolation paths for the polarons to the corresponding electrodes.

Furthermore, from J–V characteristics of the two blend ratios we find in the best solar cells a 2.6 times higher short circuit current density under AM1.5G illumination in the 1:4 blend ratio compared to the 1:1 ratio (see Figure 9.3).

The initial charge carrier concentration n_0 experimentally found within (TRMC experiment, Figure 9.6) and extracted from (photo-CELIV, Figure 9.5) the device for both pBTCT-C_{12}:$PC_{61}BM$ blend ratios was about an order of magnitude lower at 150 ns in the 1:1 device as compared to 1:4 with both techniques. This was despite the higher polymer content and thus larger absorption coefficient at 532 nm in the former. We note that the TRMC signal was corrected for the optical attenuation (see Equation 9.1). The photoluminescence in intercalated bulk systems is quenched very efficiently [153, 154], indicating that almost every photogenerated singlet exciton is separated at a donor–acceptor interface. However, fine phase intermixing and disorganized percolation paths in pBTCT-C_{12}:$PC_{61}BM$ 1:1 blends may lead to a less efficient separation of photogenerated polaron pairs as compared to the 1:4 ratio. Thus, we assign the reduced charge carrier extraction in the 1:1 device at $t = 150$ ns to an enhanced geminate recombination—occurring on shorter time scales—due to lower delocalization of the charge carriers caused by a lack of percolation paths. The process of geminate recombination would also explain the experimentally observed reduction in j_{sc} in the 1:1 ratio (see Figure 9.3). Similar was suggested by Monte Carlo simulations as an impeded charge carrier motion during the initial separation process due to randomly aligned, well intermixed donor–acceptor heterointerfaces leads to enhanced geminate recombination [138]. In the previous chapter, a difference in n_0 was found for P3HT:$PC_{61}BM$ BHJ solar cells especially at high temperatures with a lower n_0 for pristine devices. This agrees quite well with the results obtained for pBTCT-C_{12}:$PC_{61}BM$ 1:1 BHJ solar cells with the fine phase intermixed bulk structure. However, as already stated in Chapter 8 complementary experimental techniques, such as transient absorption, would be helpful to get a more complete picture of the polaron dynamics, especially in the sub-ns time scale. In the following, the charge carrier concentration decay after 150 ns will be discussed in view of polaron recombination.

The recombination of charges in low mobility materials is usually described by the bimolecular Langevin process (see Section 4.2) [98, 11]. This mechanism shows a charge carrier concentration decay of second order if electron

and hole concentrations are similar. In the previous chapter, an increased recombination order in P3HT:$PC_{61}BM$ BHJ solar cells at low temperatures was attributed to a charge transport, in which multiple trapping and release processes affect the experimentally observed $n_{ext}(t)$. In the following, we will show how recombination orders of larger and smaller than two can be also linked to the morphology found in the pBTCT-C_{12}:$PC_{61}BM$ devices under investigation. We will see that the influence of charge trapping again plays a crucial role in this respect.

In Figure 9.9 different scenarios of recombination processes are illustrated, whereas the impact of charge trapping—spatially and/or energetically—is taken into account. In typical donor–acceptor blends the transport of electrons is restricted to the acceptor and the hole transport to the donor domain. Consequently, the recombination of electrons and holes can only occur at the heterointerface,[155] which explains in part the overestimation of recombination rates by applying the Langevin model [33]. In addition to reducing the overall recombination probability, it is important to note that the occurrence of non geminate recombination requires mobile electrons and holes, p_c and n_c respectively, to meet at the heterointerface (Figure 9.9(a)). However, charge carriers may also be trapped during the hopping transport, whereas we distinguish between spatially $n_{t,s}$ and energetically $n_{t,e}$ trapped carriers. The former is related to charge carriers being confined in a material phase as illustrated in Figure 9.9(b). In contrast to energetically trapped charges, they are locally mobile and can thus recombine at the heterointerface with an oppositely charged carrier, but cannot be extracted at the contacts. We point out that photogenerated polaron pairs with at least one spatially confined charge carrier are not considered in the polaron dynamics, as they recombine geminately before dissociation, as already explained above. Energetically trapped charges—which are immobile—can only participate in the recombination process if (i) they are close enough to the donor–acceptor interface (for instance due to donor–acceptor intermixing) (Figure 9.9(c)), or (ii) if they are emitted after a certain dwell time, thus being mobile once again ($n_{t,e} \rightarrow n_c$, see Figure 9.9(d)). For (ii), the emission rate e_t of charges from traps depends crucially on the energetic distribution of the density of trap states. In the hopping systems under consideration, even the intrinsic density of states below the transport energy level (see Figure 3.3 and Figure 3.4)—the tail of an exponential or a GDOS distriubtion—can act as traps [92]. If we consider the continuity equation of free holes p_c, which can be extracted, we find (see Equation (8.3))

$$dp_c/dt = -kp_cn_c - k'p_cn_t \quad . \tag{9.2}$$

Again, n_c and n_t are the free and trapped electrons, respectively, and k and k'

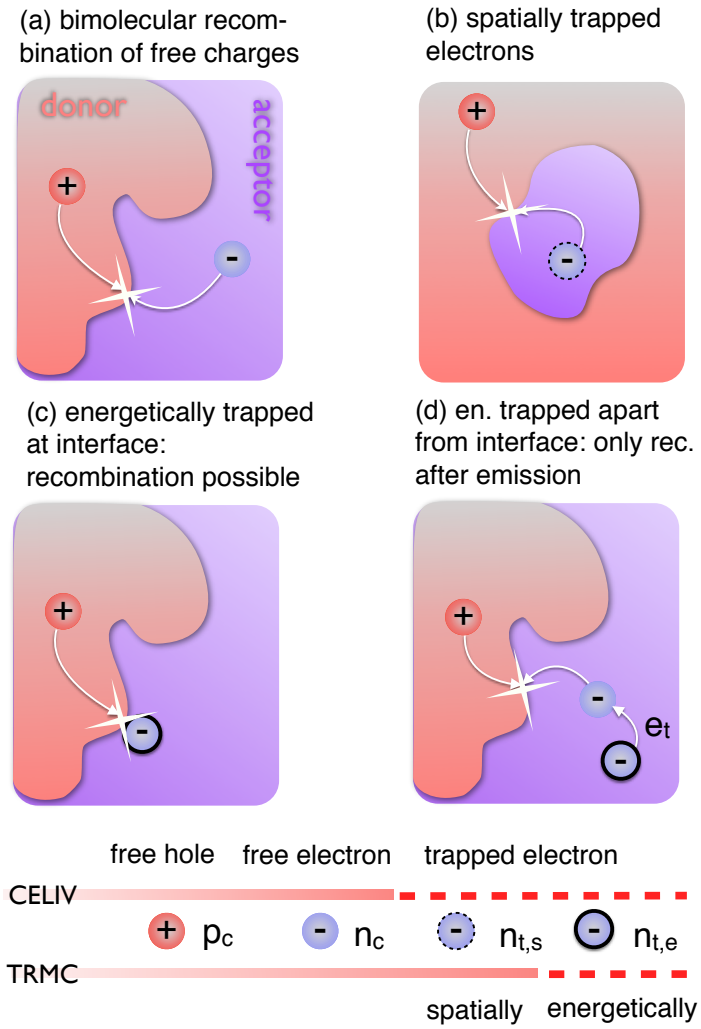

Figure 9.9: Schematic overview of the possible recombination processes, which may take place in a phase segregated bulk heterojunction solar cell: (a) bimolecular recombination of free mobile charge carriers p_c and n_c at the heterointerface, (b) spatially confined charge carriers $n_{t,s}$ can only recombine at the heterointerface but not extracted due to the lack of percolation paths. Energetically trapped charge carriers $n_{t,e}$ can only recombine (c) if they are close to the heterointerface (d) or if emitted after a dwell time being mobile again and thus being able to reach the heterointerface. However, recombination can only take place if the oppositely charged carrier has not already been recombined or extracted. The processes are also applicable to trapped holes instead of electrons. Using the extraction technique (photo-CELIV) only free mobile charge carriers (n_c, p_c) can be extracted, which includes charges emitted from trap states during the measurement time (a fraction of $n_{t,s}$ and $n_{t,e}$). With TRMC all locally mobile charge carriers can be detected (n_c, p_c, $n_{t,s}$) taking into account also charges being released from energetic trap states during the experiment ($n_{t,e}$).

are the relevant recombination prefactors. If $n_t \gg n_c, p_c$, the recombination dynamics become $dp_c/dt \approx -k' p_c n_t = p_c/\tau$, where $\tau = 1/k' n_t \approx const$—a first order process. Depending on the magnitude of n_t as compared to the mobile charge carriers, recombination orders between one and two would be observed.

In the studied pBTCT-C_{12}:PC_{61}BM blend system a recombination order far above two is observed at low temperatures by photo-CELIV and TRMC for both blend ratios (Figure 9.8) approaching close to or even decrease below two at $T = 300$ K. In 1:4 blends, the excess amount of fullerenes leads to the formation of acceptor rich domains, which allows a faster delocalisation on short time scales—improving the photogeneration yield [12]—and to percolation paths for the electrons, favouring the charge extraction process as compared to the 1:1 blend. Due to fine intermixing in the 1:1 ratio electrons will be mostly trapped—if not energetically, then spatially due to the lack of percolation paths on isolated fullerenes close to the polymer backbones. A large amount of polaron pairs will recombine before dissociation, as indicated by the initial signal magnitude for both, TRMC (Figure 9.6) and photo-CELIV (Figure 9.5) measurements being lower than for the 1:4 ratio. However, some of the charge carriers might find percolation paths to be extracted, or recombine as mobile carriers similar to those in the 1:4 device. With less thermal energy available the charge carriers will relax down to deep tail states of the DOS and thus being immobile if not being released again. As emission is thermally activated, the release of trapped charges takes much longer at low temperatures. Only after emission from the continuous distribution of trap states, the now mobile charges can either be extracted by the linear voltage pulse or recombine. The latter process becomes less probable the later the emission occurs: the recombination partners of opposite charge may already be recombined. This leads to a reduced charge carrier concentration decay similar to what was observed in the P3HT:PC_{61}BM blend system (see Chapter 8). Therefore, the observed high recombination order at low temperatures can be assigned to a delayed release of trapped charges not actively participating in the recombination process [156, 157, 135], as was already concluded in the previous chapter. With increasing temperature energetic trapping is more unlikely. However, the spatial restrictions in the bulk structure will affect the charge dynamics more dominantly. The recombination order decreases even slightly below two in both studied ratios, which we attribute to an imbalanced relation between free mobile electrons and holes due to spatial trapping in the fine intermixed phase.

Even though the two complementary techniques photo-CELIV and TRMC rely on different measurement principles, the results fit qualitatively together. In case of TRMC, all mobile charge carriers contribute to the measurement

signal, including also spatially restricted charge carriers $n_{t,s}$. Photo-CELIV is only sensitive to charge carriers, which can be extracted by the voltage pulse. This includes also charge carriers being energetically trapped in deep states during the delay time not participating in the recombination processes, but can be extracted by the voltage pulse. Thus a higher recombination order is deduced from the photo-CELIV experiment.

9.5 Conclusion

The transport and recombination dynamics in pBTCT-C_{12}:$PC_{61}BM$ bulk heterojunction solar cells were investigated by the combination of the two complementary techniques of photo-CELIV and TRMC for the first time probing different length scales. X-ray diffraction measurements indicate that structural changes occurred in the studied blend structure for a 1:1 and 1:4 weight ratio, where $PC_{61}BM$ molecules probably intercalate into the available space of two neighboring polymer side chain stacks. The order of magnitude less concentration of initially extracted polarons 1:1 ratio was attributed to an enhanced geminate recombination due to fine donor–acceptor intermixing. Furthermore, the lack of percolation pathways for electrons in the 1:1 ratio results in a low local charge carrier mobility decreasing the polaron pair dissociation probability significantly, whereas the latter causes j_{sc} to decrease. In contrast, in the 1:4 ratio extensive phase segregation lead to an efficient charge generation as the polarons can easily hop away from the heterointerface. The polaron recombination dynamics studied by TRMC and photo-CELIV are bimolecular with a recombination order above two for both studied ratios, which we attribute again to trapped charges not actively participating in the dynamics.

Chapter 10

Impact of Oxygen on the Performance of P3HT:PC_{61}BM Solar Cells

From the previous chapters we can conclude that the polaron dynamics—charge transport and recombination—in bulk heterojunction solar cells are strongly affected by the morphology and the energetic disorder of the blend system. In this chapter, P3HT:PC_{61}BM will be exposed to synthetic air, which will induce defect states in the GDOS. The results on the charge transport and, moreover, the charge carrier recombination in P3HT:PC_{61}BM BHJ solar cells exposed to synthetic air in the dark are presented. The technique of CELIV is used to study the intrinsic properties of the blend composition and photo-CELIV to get an insight in the lifetime and mobility of photogenerated charge carriers.

Part of the results discussed in this chapter is published in Paper 7.

10.1 Introduction

The PCE of organic solar cells experiences a consistent increase during the last decade and recently reached 8% for a single junction polymer fullerene solar cell [4]. The resistance of organic solar cells against degradation deserves, however, further attention. Exposure to synthetic air in the dark exhibits a decrease of the short circuit current with exposure time in P3HT:PCBM BHJ solar cells [158, 159, 160]. It was previously shown that oxygen induces trap states in the polymer, which results in a strong decrease of the charge carrier mobility [161]. So far, the role of charge trapping on the recombination dynamics and thus the performance of organic solar cells is not fully understood. If the solar cell is illuminated simultaneously during exposure to synthetic air, the degradation process accelerates [159, 158].

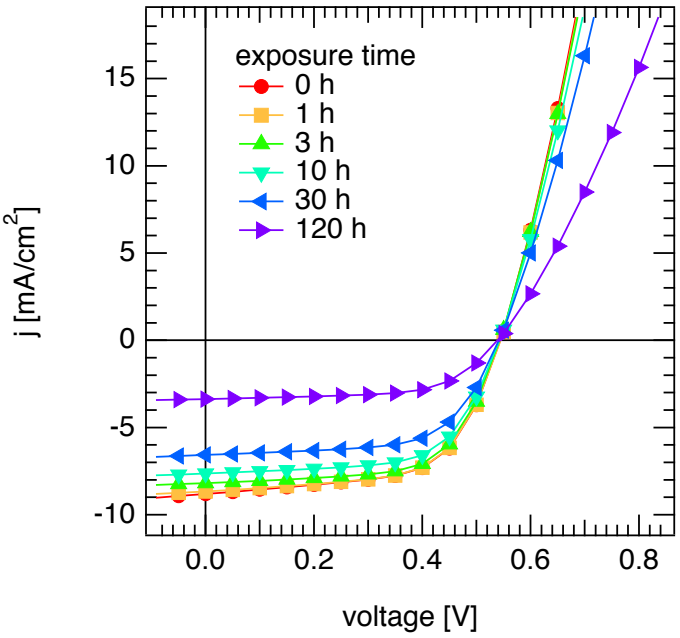

Figure 10.1: Illuminated J–V characteristics of P3HT:$PC_{61}BM$ 1:0.8 BHJ solar cell for different exposure times to synthetic air in the dark . With increasing oxygen exposure time j_{sc} decreases, whereas FF and V_{oc} remain rather constant.

10.2 Experimental

Bulk heterojunction solar cells were prepared according to the procedure described in Chapter 5. The solar cells were characterized in the glove box system by an Oriel 1160 AM1.5G solar simulator showing a PCE of approximately 3.5%. The samples were transferred into a optical cryostat (see Chapter 6) and exposed to synthetic air for defined duration without simultaneous illumination. After a maximum time of 120 hours of exposure to synthetic air in dark, the PCE of the solar cells dropped by more than 70% mainly due to a reduced short circuit current density with otherwise rather constant open-circuit voltage and fill factor (see Figure 10.1) During (photo)-CELIV and I–V measurements, the sample chamber of the cryostat is filled with helium as inert contact gas. For degradation studies, the helium is replaced by synthetic air (80% N_2, 20% O_2, $<$ 1 ppm H_2O) for various exposure times. We use the second harmonic of a Nd:YAG laser ($\lambda = 532$ nm, $<$ 80 ps pulse duration) in the photo-CELIV experiment to generate charge carriers within in the device. Thereby, the solar cell parameters are checked after the illuminated measurements to ensure no further degradation by the light exposure. The mobility is calculated according to Equation 6.4.

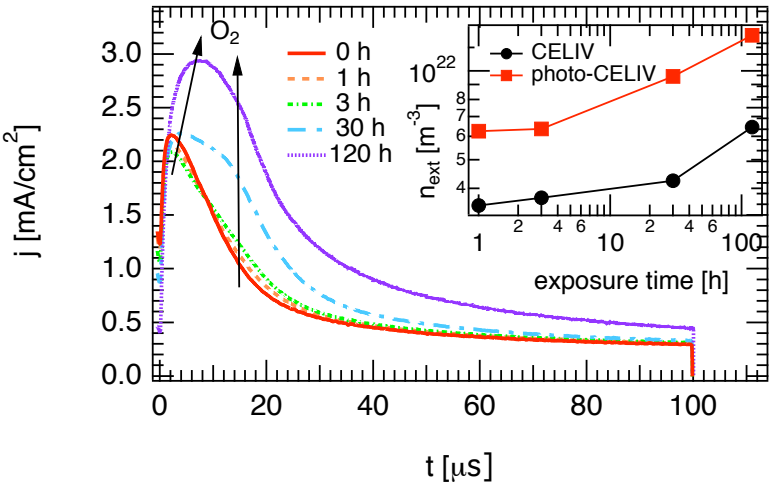

Figure 10.2: Photo-CELIV measurements of oxygen exposed P3HT:$PC_{61}BM$ 1:0.8 solar cell performed at $T = 300$ K with an offset voltage of $V_{off} = 0.3$ and a maximum extraction voltage $V_p = -2$ V. A shoulder arises at 20 μs as an indication of an additional extraction peak related to a lower charge carrier mobility. Inset: Extracted photogenerated charge carrier concentration and the equilibrium carrier concentration deduced from CELIV as a function of oxygen exposure time.

10.3 Results and Discussion

In Figure 10.2 photo-CELIV transients are shown for different exposure times to synthetic air. It can be clearly seen that the intensity of the extraction peak strongly increases with exposure time. By subtracting the dark current transient and integrating the resulting transient the carrier concentration n_{ext} of photogenerated charges deduced from the photo-CELIV experiment can be determined, which is shown in the inset to Fig. 10.2 (squares). The intrinsic charge carrier concentration from dark CELIV is also added to the the inset (circles). The increase in equilibrium charge carrier concentration in CELIV measurements upon degradation was assigned to be due to oxygen doping [158]. After 120 hours of oxygen exposure the current transient does not reach the saturation current level j_0 after 100 μs as in the non-exposed solar cell. Thus, not all charge carriers were extracted within the measurement time of 100 μs, which is an indication for charge carriers being trapped in the device causing an increased capacitance. Note that the same experimental conditions were used for all photo-CELIV measurements shown in Figure 10.2. The charge carrier mobility decreased by one order of magnitude from around 1.2×10^{-7} m^2/Vs to 1.2×10^{-8} m^2/Vs after 120 hours of

exposure to synthetic air. Furthermore, upon oxygen exposure a shoulder showed up in the photo-CELIV signal at around 20 μs indicating a second contribution to the extraction peak with a significantly reduced charge carrier mobility (Figure 10.2). A similar effect was reported recently in an oxygen exposed P3HT:$PC_{61}BM$ solar cell [162]. There, the first peak was assigned to electrons and the second peak to a hole mobility decreased by an order in magnitude from 10^{-8} to 10^{-9} m^2/Vs due to oxidation of the thiophene ring (backbone). We note, however, that the polarity of the extracted charge carriers cannot be discriminated in the CELIV experiment. Here, the shoulder appeared only in the photo-CELIV experiment, but not in the CELIV experiment without laser excitation. Thus, the second contribution to the extraction peak can be assigned to photogenerated charge carriers. Interestingly, up to 30 hours of exposure only the shoulder increased, whereas the first main extraction peak is almost constant or even slightly decreased in the first three hours. Thus, only those photogenerated charge carriers, which are extracted at a later time at a higher electric field, contribute mostly to the increase in the charge carrier concentration n_{ext} in the photo-CELIV experiment with exposure to synthetic air. This can be seen in the inset of Figure 10.2 as n_{ext} of photogenerated charge carriers increases more strongly with exposure time than the equilibrium charge carriers deduced from CELIV experiments, especially for times more than 3 hours. It was reported by Arkhipov et al. that doping increased the energetic disorder broadening the tail of the density of states distribution (DOS) [163]. From degradation studies performed on P3HT [161] and P3HT:PCBM [158] an enhanced density of deep traps as well as a reduced charge carrier mobility were revealed. Thus, the additional CELIV peak may arise from charge carriers being extracted from trap states at a higher field and thus with a delay compared to free mobile charge carriers.

Looking at the charge carrier mobility deduced from the first extraction peak at low temperatures, we observed a carrier concentration dependent charge carrier mobility in oxygen exposed BHJ solar cells increasing with exposure time (see Figure 10.3). In non-degraded solar cells, however, the mobility is almost unaffected by the charge density. This is again an indication, that the DOS is broadened due to the oxygen induced doping [163] having a strong impact on the charge transport within the bulk of the solar cells. At high carrier concentrations the deep states might be filled so that mobile charge carriers are not further trapped in those states. In Chapter 8 a carrier concentration dependent charge carrier mobility was found for P3HT:bis$PC_{61}BM$ BHJ solar cells being attributed to the broadened DOS and hence to an increased energetic disorder (see Figure 8.5).

To further study these oxygen induced trap states, the CELIV scheme was extended by using continuous white light background illumination during the

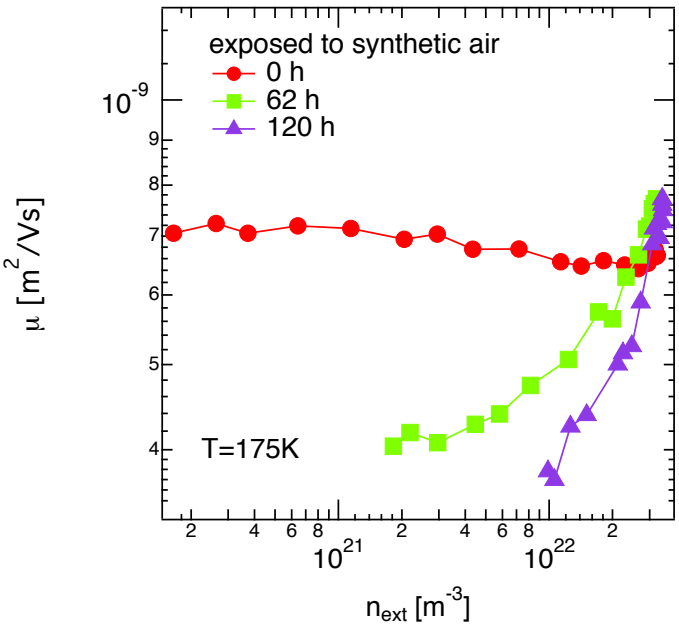

Figure 10.3: Charge carrier mobility μ revealed by photo-CELIV measurements on oxygen exposed P3HT:PC_{61}BM 1:0.8 BHJ solar cells as a function of the extracted charge density n_{ext} (compare to Figure 8.5).

whole experiment. We note that these background illumination conditions are even closer to the working regime of an organic bulk heterojunction solar cells compared to pulsed photo-CELIV experiments. In Figure 10.4 the CELIV signals with and without continuous LED background illumination are shown for a P3HT:PC_{61}BM BHJ solar cell exposed for 62 hours to synthetic air. As can be seen the saturation current j_0 is increased in the CELIV measurement with continuos background illumination. This is due to charge carriers being generated by the LED throughout the experiment and hence new "equilibrium" conditions are created. Furthermore, again a shoulder is visible in the illuminated CELIV transient performed on the oxygen exposed BHJ solar cell. By subtracting the dark current transient without LED background illumination (black dash dotted line in Figure 10.4) from the one with LED illumination the contribution of photogenerated charge carriers ($\Delta j = j_{\mathrm{LED}} - j_{\mathrm{dark}}$) to the current transient can be illustrated (green dashed line in Figure 10.4). Compared to the dark CELIV measurement the maximum charge extraction peak is shifted to larger times, which indicates that the photogenerated charge carriers exhibit a lower charge carrier mobility in contrast to the intrinsic charge carriers probed in the dark CELIV experiment. Charge carriers after being generated by the LED or the laser flash will thermalize down in energy and fill up deep states. If these charge carriers are extracted by the voltage pulse

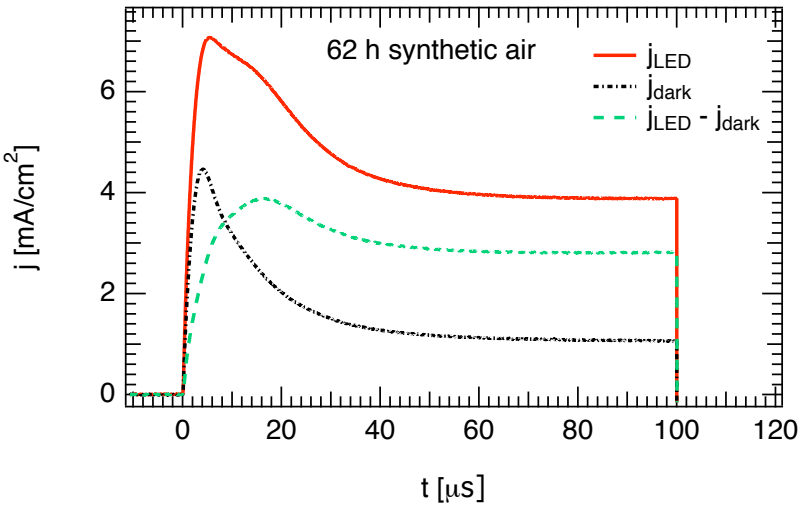

Figure 10.4: CELIV signals at T=300 K with (red solid) and without LED background illumination (dark dash dotted); the extraction voltage was kept at $V_{\mathrm{p}} = -2\mathrm{V}$ and the offset voltage at $V_{\mathrm{off}} = 0.5\mathrm{V}$; the green dashed line represents the difference $\Delta j = j_{LED} - j_{dark}$. In the CELIV transient with continuous background illumination an increased capacitance is observed due to additional generated charge carriers within the active layer.

in the CELIV experiment, they will have an impact on the extraction current at higher electric fields and thus show up at larger extraction times. In non-exposed P3HT:PC_{61}BM 1:0.8 BHJ solar cells such a second extraction peak due to photogenerated charge carriers could not be observed. This delayed release of charge carriers from deep trap states will have a significant impact on the recombination dynamics of oxygen exposed organic solar cells, which will be discussed in the following.

The time dependent extracted charge density n_{ext} is shown in Figure 10.5. It can be clearly seen that $n_{ext}(t)$ increases for $t_{delay} > 10^{-5}$ s with oxygen exposure time corresponding to a reduced charge carrier recombination. In Chapter 8 the delayed recombination in P3HT:bis-PC_{61}BM 1:1 was attributed to the enhanced energetic disorder caused by the fullerene bisadduct. Especially in the pristine device the charge carrier concentration decay order increased by a factor of two with decreasing temperature from $\lambda + 1 = 3$ at $T = 200$ K to $\lambda + 1 = 6.7$ at $T = 125$ K (see Figure 8.7). This agrees well with the results obtained here for the oxygen exposed solar cells. In this case, not the temperature is decreased, which lead to an impeded charge transport due to less thermal energy available for the hopping jumps and hence to an increased recombination order, but the GDOS is broadened due to oxygen induced tail states. Consequently, charge carriers get trapped in those deep

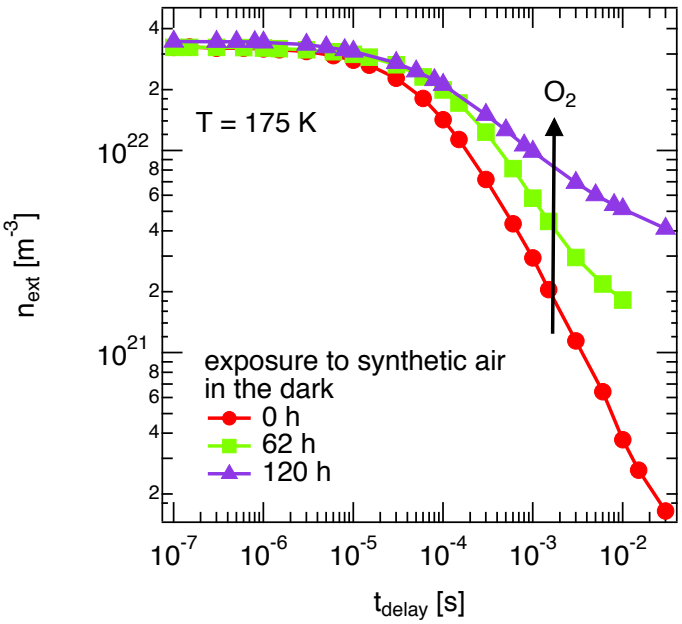

Figure 10.5: Charge carrier concentration $n_{ext}(t)$ deduced from photo-CELIV measurements at $T = 175$ K on P3HT:PC_{61}BM 1:0.8 BHJ solar cells exposed for 0, 62 and 120 hours to synthetic air in the dark. With increasing oxygen exposure the charge carrier concentration decay decreases.

states during their hopping transport and have to be released before they can recombine at the interface, which results in a delay in recombination [139] showing up in an increased recombination order (see Figure 10.5). In analogy to Chapter 8, we can determine the recombination rate R_{exp} from the time dependent charge carrier concentration n_{ext} using equation

$$\frac{dn}{dt} = G - R \approx \frac{dn_{ext}}{dt} = R_{exp} \quad , \tag{10.1}$$

whereas the generation $G = 0$ for $t > 0$ (compare to Equation (8.1)). Furthermore, the charge carrier mobility μ revealed by the experiment can be used to determine the recombination rate described by the Langevin theory (Section 4.2) [98]

$$R_L = \gamma \cdot n^2 \approx \frac{q}{\varepsilon\varepsilon_0}\mu \cdot n_{ext}^2 \quad , \tag{10.2}$$

with the Langevin recombination coefficient γ and the dielectric constant $\varepsilon\varepsilon_0$. In Figure 10.6 both, R_{exp} (Eq. (10.1)) and R_L (Eq. (10.2)), are shown in Figure 10.6 as a function of n_{ext} at $T = 175$ K. It can be seen that the recombination rate is reduced compared to the Langevin theory, as was already found previously [128, 117] and described extensively in the previous Chapters 8 and 9. When exposed to synthetic air the recombination rate decreases

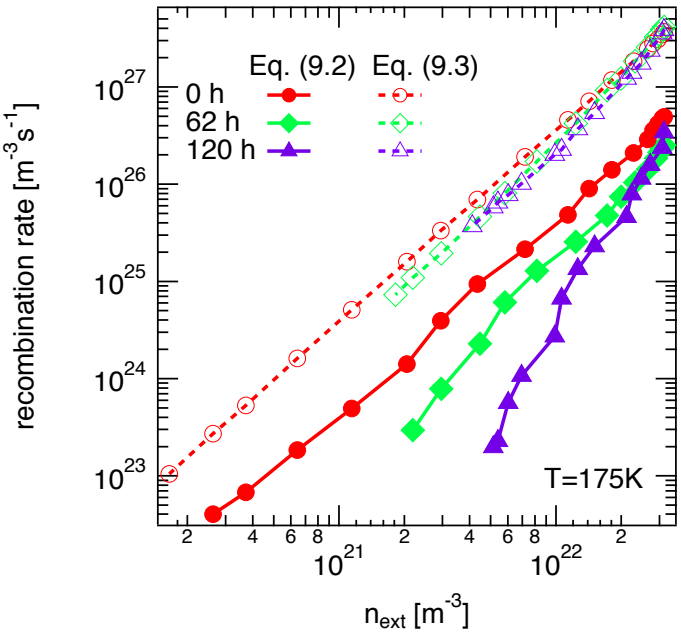

Figure 10.6: Recombination rate at T=175 K as a function of the extracted charge carrier concentration for 0, 62 and 120 hours exposure to synthetic air. The bimolecular Langevin recombination rates calculated from the charge carrier mobility deduced from photo-CELIV are also shown in the graph (dashed lines). With increasing oxygen exposure an increase in charge carrier concentration dependence of the recombination rate can be observed.

for a given n_{ext} with exposure time, which corresponds to a reduced charge carrier concentration decay (see Figure 10.5). Furthermore, the recombination rate shows an increased dependence on the charge carrier concentration with increasing exposure time deviating even more from Langevin type recombination behavior as can be seen in Figure 10.6. Similar to the results shown in Chapter 8 the increasing dependence of the recombination rate on the carrier concentration with oxygen exposure deviating more and more from Langevin can be assigned to the increased disorder, which is induced by the oxygen dopants. Thereby, the carrier concentration dependence of the recombination coefficient can neither be attributed to a $\mu(n)$ found in oxygen exposed bulk heterojunction solar cells.

The experimentally observed reduced recombination rate in oxygen exposed BHJ solar cells revealed by the time dependent photo-CELIV measurements can also be related to an increased effective charge carrier lifetime τ. In addition to photo-CELIV measurements, transient photovoltage (TPV) and transient photocurrent (TPC) experiments were performed on oxygen exposed P3HT:PC_{61}BM BHJ solar cells. Details to the measurement technique can be found in Ref. [135, 130, 134]. From measuring TPV and TPC the lifetime of photogenerated charge carriers can be determined. In analogy to the reduced recombination rate deduced from photo-CELIV, TPV/TPC revealed an increase of the charge carrier lifetime with exposure time.

Here, we point out again that the observed increased effective lifetime is assigned to the non-geminate recombination of charge carriers at open circuit conditions and cannot be used to explain the decrease in the short circuit current density. As was shown previously [158] a decrease in J_{sc} may explained by the doping of the active blend, which causes an increase in the charge density and hence leads to less band bending. We rule out contact degradation, as we did not observe characteristic s-shaped J–V curves for any oxygen exposure times, which would be an indication for a lowered charge extraction rate [164, 165, 166]. Furthermore, no change in V_{oc} was observed in oxygen exposed BHJ solar cells in the dark. Moreover, an increased geminate recombination or an insufficient polaron pair dissociation would decrease the J_{sc} in an organic BHJ solar cells. However, further investigations are needed, especially in sub-ns time scales, to address the charge losses at short circuit conditions.

10.4 Conclusion

The charge transport and the recombination dynamics in P3HT:PC_{61}BM BHJ solar cells exposed to synthetic air in the dark were investigated using the tech-

nique of CELIV and photo-CELIV. From the sets of experiments we observed an increased equilibrium charge carrier concentration due to oxygen doping of the active blend material as well as a reduced charge carrier mobility. Furthermore, from photo-CELIV measurements a reduced recombination probability could be found in oxygen exposed solar cells, whereas the recombination rate showed an increased dependence on the charge carrier concentration in those degraded BHJ solar cells. Both, the reduced recombination rate and the increased dependence on n_{ext} can be attributed to oxygen, which broadens the GDOS by inducing tail states.

Chapter 11

Transient Charge Extraction in Organic Solar Cells: OTRACE vs. photo-CELIV—A Comparative Study

In this chapter the novel method of charge extraction, which was introduced in Section 6.3, will be compared to the conventional photo-CELIV technique. Both techniques are applied to the material system consisting of the low-band gap polymer poly[[9-(1-octylnonyl)-9H-carbazole-2,7-diyl]-2,5-thiophenediyl-2,1,3-benzothiadiazole-4,7-diyl-2,5-thiophenediyl] (PCDTBT) (see Figure 2.9) blended with $PC_{71}BM$. Recently, an internal quantum efficiency of almost 100% was reported for PCDTBT:$PC_{71}BM$ 1:4 BHJ solar cells with a power conversion efficiency of up to 6.1% [167].

11.1 Introduction

As has been illustrated in the previous chapters, it is important to study both the mobility and lifetime of charge carriers. Using the technique of photo-CELIV (Section 6.2) the charge carrier mobility and lifetime can be determined simultaneously. The major drawbacks of this method are the high illumination intensities due to the use of a high intense laser flash and the absence of non-blocking contacts and thus charge carrier injection during the application of a constant offset voltage V_{off} in forward direction (see Section 6.2). The latter affects the RC time τ_{RC} of the measurement circuit significantly, which limits the resolution of the technique especially at high temperatures ($T > 200$ K), as was illustrated in Chapter 8. Using the modified OTRACE (open circuit corrected transient charge extraction) method, however, the charge dynamics in organic BHJ solar cells can be studied even at $T = 300$ K and low light intensities, which are close to solar cell operating conditions. Thus, the mobility and lifetime of charge carriers generated by 1 sun illumination intensity can be investigated.

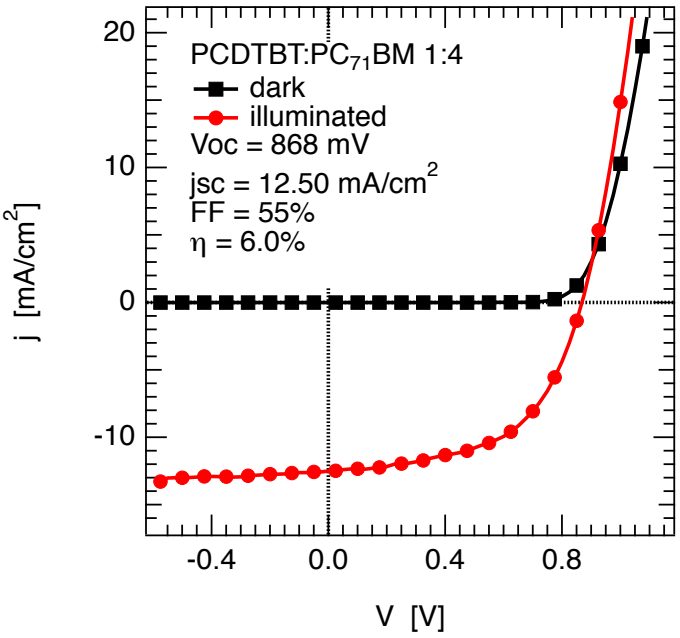

Figure 11.1: J–V characteristics of a PCDTBT:$PC_{71}BM$ 1:4 BHJ solar cell measured in the dark and under AM1.5G solar simulator.

11.2 Experimental

Organic BHJ solar cells are prepared according to Chapter 5. PCDTBT and $PC_{71}BM$ solved in chlorobenzene are mixed in a weight ratio of 1:4. The organic blend layer is thermally treated for 10 min at 50 °C before deposition of Ca/Al on top. The solar cells are characterized using a Oriel AM1.5G solar simulator. PCE values up to 6% could be achieved with the material blend system (see Figure 11.1). For OTRACE and photo-CELIV measurements the sample is transferred to the optical cryostat. For laser illumination (photo-CELIV) we use the second harmonic of a Nd:YAG laser ($\lambda = 532$ nm, 80 ps). In contrast, a pulsed white light LED generates charge carriers in the OTRACE technique. The V_{oc} transient needed to account for field compensation (see Section 6.3) in OTRACE is acquired by the oscilloscope using a high-impedance (1GΩ) load adapter to prevent current flow and is used as an input for the extraction voltage pulse being created by the function generator. For calculating the charge carrier mobility from both photo-CELIV and OTRACE measurements the Equation (6.5) is used.

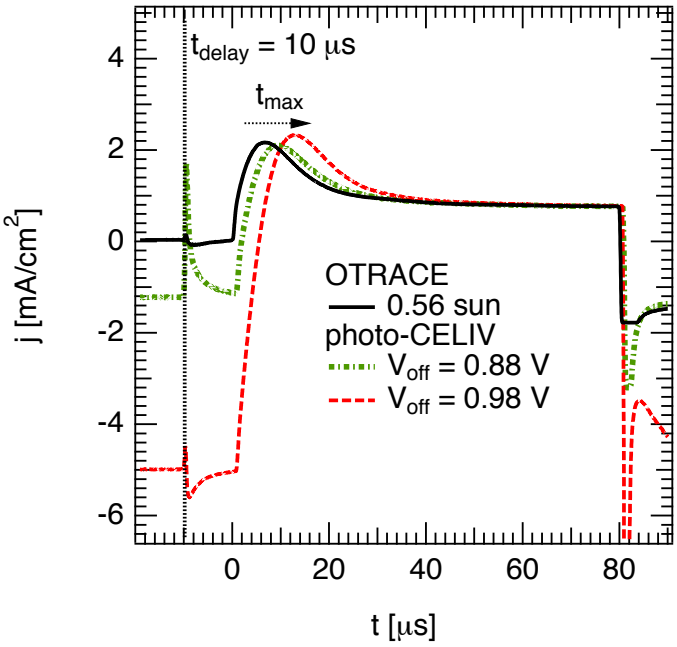

Figure 11.2: Current transients of PCDTBT:$PC_{71}BM$ 1:4 BHJ solar cells at $T = 300$ K from photo-CELIV (dashed line, dash dotted line) and the modified OTRACE technique (solid line). A fixed delay time of $t_{delay} = 10$ μs was used for all transients (see vertical dotted line). Clearly, no current is flowing in the OTRACE experiment for $t < t_{delay}$ and $0 \leq t \leq t_{delay}$ indicating no charge injection during LED illumination and no charge extraction after turning off the LED ($V = V_{oc} \rightarrow G = R$). In contrast, in the photo-CELIV experiment injected charge carriers lead to a forward current flow for $t < t_{delay}$, which increases with V_{off}

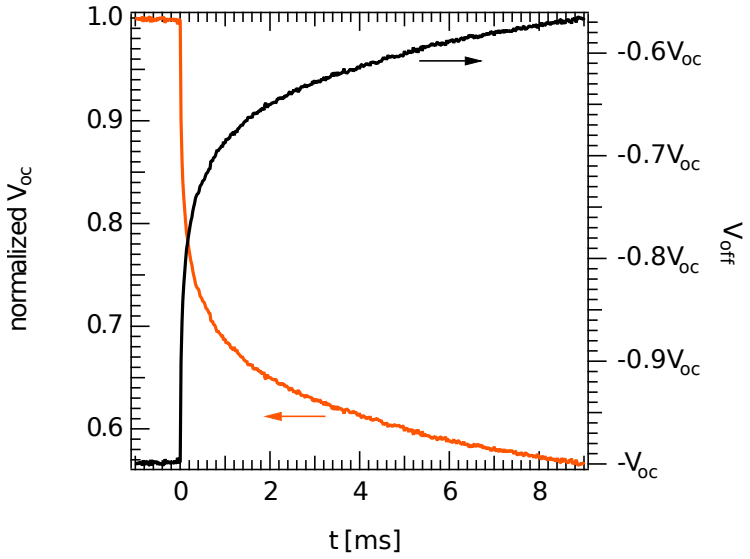

Figure 11.3: (Left axis) Normalized V_{oc} voltage transient for a PCDTBT:$PC_{71}BM$ 1:4 BHJ solar cells acquired at $T = 300$ K. The LED intensity was adjusted to be equivalent to one sun. (Right axis) Offset voltage V_{off}, which has to be created to compensate for the voltage loss due to charge carrier recombination, applied in forward direction (see Figure 6.7).

11.3 Results and Discussion

In Figure 11.2 the current transients of the conventional photo-CELIV technique are compared with those obtained by the modified OTRACE technique. Whereas in photo-CELIV the offset voltage is constant, a time dependent $V_{off}(t)$ was adapted from the V_{oc} transient in the OTRACE method (see Section 6.3). In Figure 11.3 an example for an offset voltage $V_{off}(t)$ (right axis) being created from the previously acquired V_{oc} voltage transient (left axis) is depicted for $T = 300$ K. The time range, in which the voltage transient is adapted, is determined by the delay time t_{delay} and will be varied in the time dependent OTRACE experiment (see Figure 6.7). The delay time in Figure 11.2 was chosen to be t_{delay}= 10 μs. It can be clearly seen from the transients that in case of the OTRACE method no current is flowing before charge extraction neither for $t \leq t_{delay}$ nor $0 \leq t \leq t_{delay}$. For $t \leq t_{delay}$ the LED generates charge carriers, which are hindered to leave the solar cells as $V = V_{oc}$ is applied to the sample. For $0 \leq t \leq t_{delay}$ the LED is switched off and polarons will undergo diffusion and recombination without charge extraction due to the absence of an electric driving force. Thereby, the changing flat band conditions due to charge recombination are accounted for by $V_{off}(t)$. Thus, during the t_{delay} the generation of polarons equals the recombination

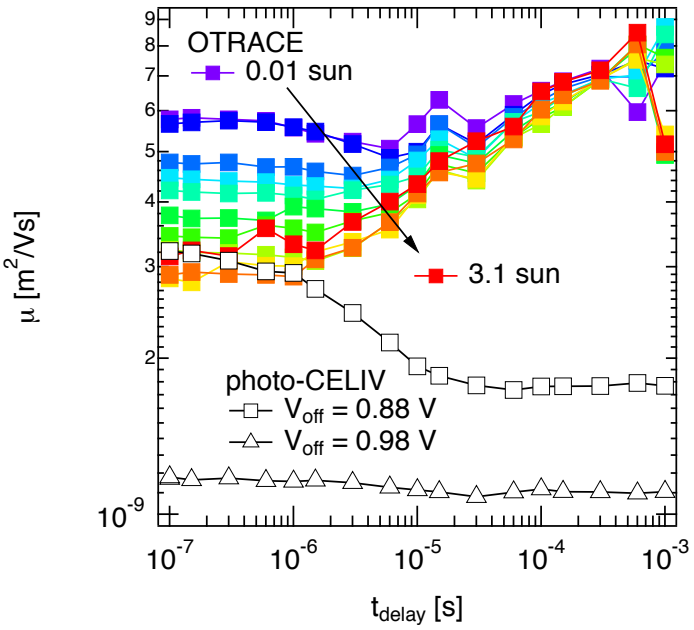

Figure 11.4: Charge carrier mobility determined from photo-CELIV and OTRACE transients on PCDTBT:$PC_{71}BM$ 1:4 BHJ solar cells measured at $T = 300$ K.

($G = R$). In contrast, in the conventional photo-CELIV experiment a constant offset voltage is applied to the solar cell with $V_{off} > V_{oc}$. It can be clearly seen from Figure 11.2) that in case of $V_{off} = 0.88$ V, which is close to V_{oc} (see Figure 11.1), photogenerated charge carriers still leave the device reflected by the delta shaped current flowing after the laser flash at $t_{delay} = 10$ μs. Furthermore, as the solar cell is only illuminated for a short time (80 ps) at $t = t_{delay}$ a constant offset bias superimposed to the extraction voltage pulse results in a current flow in forward direction for $t < t_{delay}$. In this case, charge carriers are injected into the bulk, which may interact with those generated by the laser. Moreover, the capacitance increases due to injected charge carriers and hence τ_{RC}. The latter affects the position of the peak t_{max} in the experiment as was already discussed in Section 6.2 and Chapter 8 (compare Figure 11.2 with Figure 6.5 and Figure 8.9). Consequently, t_{max} is shifted to longer times in the photo-CELIV transients compared to the OTRACE transient resulting in a reduced and hence underestimated charge carrier mobility (see Equation (6.5)). In Figure 11.4 μ determined from the transients of both techniques are shown as a function of t_{delay} at $T = 300$ K. As expected, the charge carrier mobility obtained by OTRACE is increased compared to the one obtained by photo-CELIV due to a smaller RC time. To avoid this underestimation of charge carrier mobility in photo-CELIV experiment, the

offset voltage needs to be lowered as shown in Figure 11.4. However, this implies that the charge carriers leave the device due to the residual internal field and hence the recombination dynamics cannot be determined simultaneously. Looking at the charge carrier mobilities deduced from illumination intensity dependent OTRACE transients a clear increase of μ can be observed with t_{delay} at high illumination intensities. As charge carrier injection is reduced in this technique the RC time is determined only by the device geometry. However, depending on the extraction peak height the transients and hence t_{max} can still be affected by the RC rise overlaying the peak (see Figure 6.5). With a low peak height this overlay can be minimized. Thus, we attribute the increase in charge carrier mobility with increasing t_{delay} to the decreasing CELIV peak height being less affected by RC. So to minimize the influence of τ_{RC} on the extraction experiment, low light intensities have to be used—like the 0.01 sun as shown in Figure 11.4—to ensure reliable charge carrier mobility values especially temperatures up to 300 K.

With the OTRACE technique it is now possible to study the mobility and lifetime of charge carriers in organic BHJ solar cells under operating conditions.

For PCDTBT:$PC_{71}BM$ 1:4 BHJ solar cells we found a shoulder in the OTRACE extraction peak at around 40 μs (see inset of Figure 11.5) for 0.01 sun illumination, which indicates a second contribution to the extraction current with a reduced charge carrier mobility. This might be an indication of an unbalanced charge transport of electrons and holes in the bulk or charge carriers being extracted from deeper states with the assistance of the electric field similar to what was observed in Chapter 10 (see Figure 10.2). Those deep states might originate from the acceptor material $PC_{71}BM$ and a possibly broader distributed DOS. Using the photo-CELIV technique this shoulder cannot be observed. The reason for that might be of different origins: The high laser intensity causes the first peak to overlap the shoulder. Furthermore, in photo-CELIV the first extraction peak is shifted to longer times due to RC, which again might cause the shoulder to be superimposed. Finally, in the OTRACE method charge carriers are generated by a relatively long LED light pulse (1 ms) so that deeper states can be filled more easily during the quasi steady-state conditions compared to the only very short laser flash (80 ps) in photo-CELIV.

In Figure 11.6 the time dependent charge carrier concentration extracted from the bulk are compared for both transient extraction methods. As can be seen, completely different recombination dynamics can be deduced from the two methods at $T = 300$ K. In case of the conventional photo-CELIV technique faster recombination times would be concluded from the data and hence much higher recombination rates. Furthermore, it can be seen from

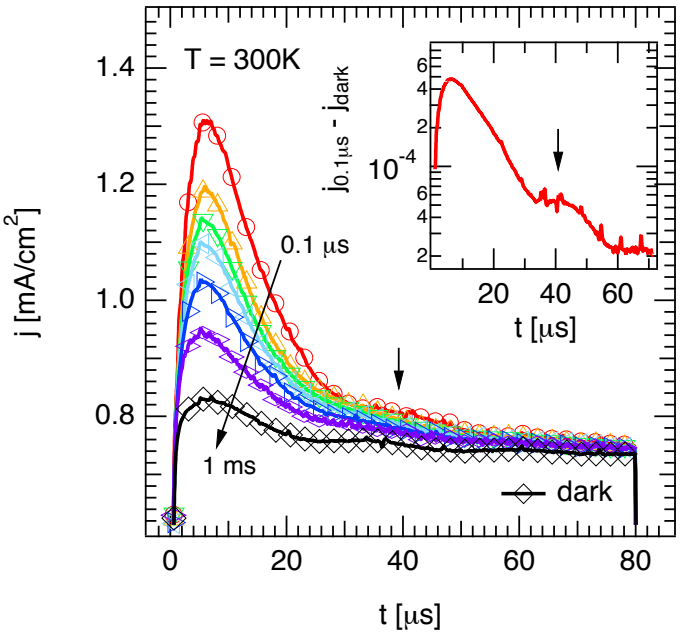

Figure 11.5: OTRACE current transients at $T = 300$ K for PCDTBT:$PC_{71}BM$ 1:4. The LED intensity was adjusted to be 0.01 sun and the extraction voltage was $V_p = 2$ V.

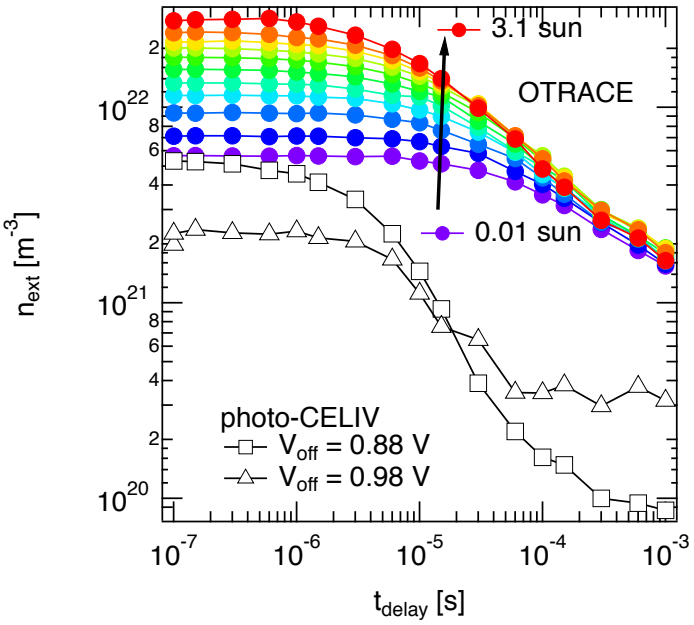

Figure 11.6: Charge carrier concentration n_{ext} as a function of the delay time t_{delay} deduced from photo-CELIV and OTRACE on PCDTBT:$PC_{71}BM$ 1:4 BHJ solar cells.

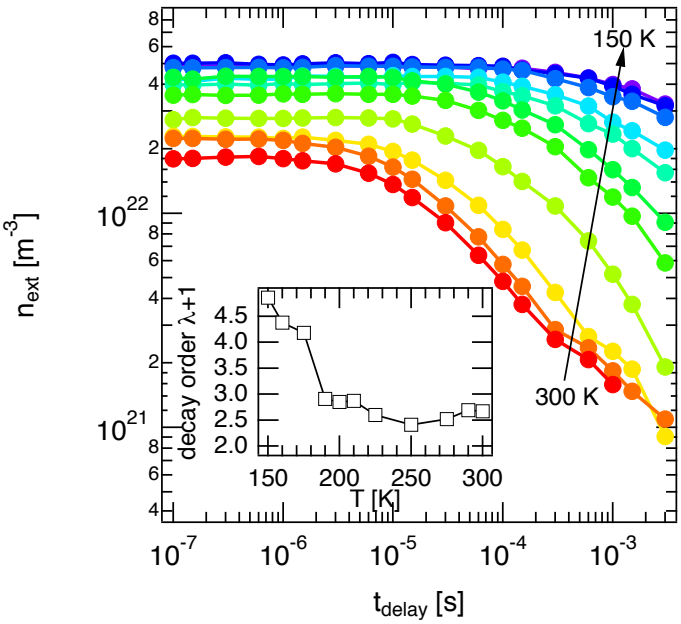

Figure 11.7: Charge carrier concentration n_{ext} obtained from temperature dependent OTRACE measurements on PCDTBT:$PC_{71}BM$ 1:4. Inset: The recombination order obtained from fitting the $n_{ext}(t)$ data according to Ref. [130, 135].

the illumination dependent OTRACE measurements that the onset of non-geminate recombination is generally shifted to longer times, when the charge density is lowered as already mentioned in Chapter 8. This is in good agreement with the results obtained from the complementary techniques such as transient absorption [131].

The temperature dependent $n_{ext}(t)$ data determined by OTRACE measurements on a PCDTBT:$PC_{71}BM$ 1:4 BHJ solar cell are shown in Figure 11.7. As also revealed for other organic blend compositions, such as P3HT:$PC_{61}BM$ or pBTCT:$PC_{61}BM$, the charge carrier recombination increases with increasing temperature mainly due to an increased charge carrier mobility. In the inset of Figure 11.7 the recombination order λ+1 is plotted as a function of the temperature T. As commonly observed for bulk heterojunction devices, the recombination order increases with decreasing temperature, which indicates that the charge transport is more dominated by charge trapping events at low temperatures due to less thermal energy being available for the hopping jumps (see also Chapter 8 and Chapter 9).

Finally, using the OTRACE technique at very low light intensities the energetic disorder can be estimated from the temperature dependent charge carrier mobility as the RC limitations are minimized. Considering the Gaus-

sian disorder model (GDM), as introduced in Section 3.2, the charge carrier mobility can be expressed according to Equation (3.5)

$$\mu \approx \exp\left\{-\left(\frac{2}{3}\frac{\sigma^*}{kT}\right)^2\right\} \quad , \tag{11.1}$$

whereas the field dependent term is neglected. In this case σ^* represents the effective width of the Gaussian density of states distribution (GDOS) and thus the effective energy disorder parameter for the charge transport in the studied blend system. From field dependent TOF measurements we generally find the disorder parameter to decrease when considering the zero field charge carrier mobility μ_0. Thus, the here obtained σ^* is an upper estimation for the disorder in the blend composition can be estimated. By fitting $\ln(\mu)$ versus $1/T^2$ σ^* can be obtained from the slope. Here, a cross section is made in the μ vs t_{delay} plot (Figure 11.8(a)) at $t_{delay} = 1$ ms to account for thermal relaxation of charge carriers at low temperatures and limitations by RC at high T. The extrapolated mobility values are plotted versus the $(1000/T)^2$ shown in Figure 11.8(b). Two different slopes can be obtained by fitting the experimental data, both of which can be attributed to an effective disorder parameter. For low temperatures the fit revealed $\sigma_2^* = 40$ meV, whereas for high temperatures $\sigma_1^* = 78$ meV with a transition temperature of around $T = 200$ K. The temperature dependent charge carrier mobility deduced from OTRACE measurements on the reference material system of P3HT:PC_{61}BM 1:0.8 is also shown in Figure 11.8(b). As can be seen, generally higher mobility values can be obtained for P3HT:PC_{61}BM 1:0.8 with an order of magnitude higher mobility at $T = 300$ K. Whereas the disorder parameter for P3HT:PC_{61}BM is smaller for $T > 180$ K with $\sigma_1^* = 58$ meV, it is quite similar for $T < 180$ K with $\sigma_2^* = 44$ meV.

The reason for the observed bend in the temperature dependent charge carrier mobility is not fully understood yet, however, is often observed in organic disordered systems [168]. One possible reason might be that additional states are available in the tail of the GDOS making it easier for the charge carriers to hop to a neighboring state, which leads to a increased charge carrier mobility compared to the one expected from the fit at high temperatures (σ_1^*). Those deep states might originate from a DOS shape deviating from the proposed GDOS, which may result from trap states overlapping with the intrinsic tail states. Furthermore, at low temperatures the charge transport might occur in terms of tunneling processes instead of thermally activated hopping steps. However, further investigations have to be done to address the origin of this experimental observation.

Finally, we note that the here presented novel OTRACE technique arose from the experience gained in this work. Thereby, it does by no means dimin-

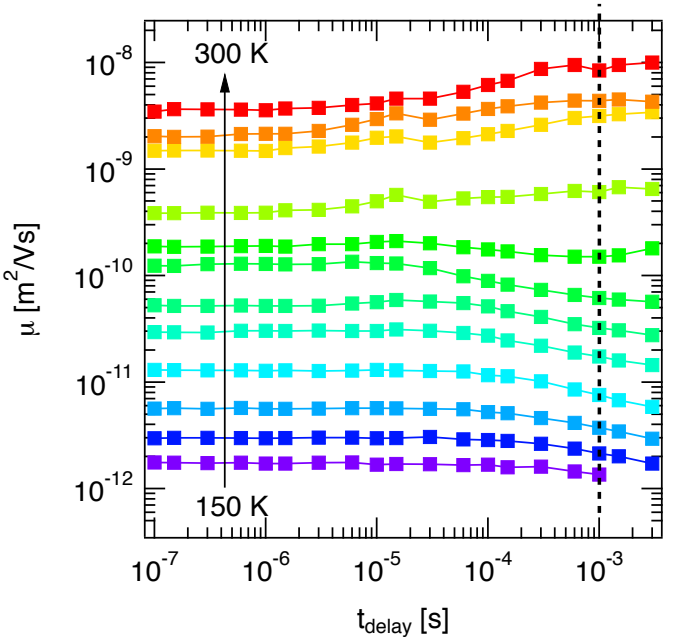

(a)

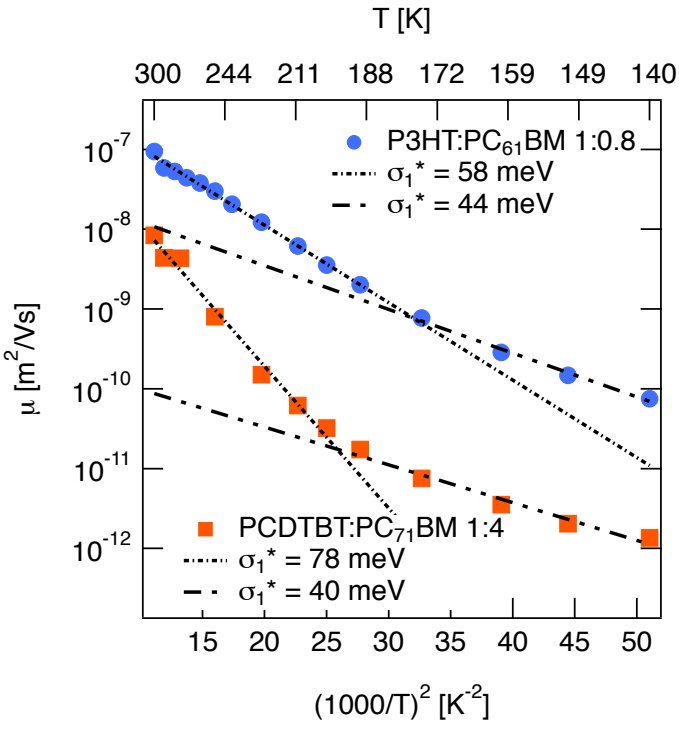

(b)

Figure 11.8: (a) Charge carrier mobility determined from delay time dependent OTRACE measurements on PCDTBT:PC_{71}BM 1:4 for temperatures ranging from 150 K to 300 K (closed squares). (b) Extrapolated mobility values for $t_{delay} = 1$ ms plotted versus $(1000/T)^2$. The charge carrier mobility from OTRACE measurements on P3HT:PC_{61}BM 1:0.8 is also shown for comparison (closed circles).

ish the correctness of the previously discussed and published photo-CELIV results.

11.4 Conclusion

The advanced measurement technique of OTRACE is a powerful tool to study the charge carrier dynamics in organic bulk heterojunction solar cells under operating conditions. It accounts for the drop in V_{oc} due to charge carrier recombination by adapting the V_{oc} transient for electric field compensation. Due to only minor charge injection from the contacts the RC time is minimized in the OTRACE technique and hence the time resolution is improved especially at room temperature. Applying the OTRACE technique to the blend composition of PCDTBT:PC_{71}BM1:4 we were able to resolve a shoulder in the extraction peak especially at low LED intensities. We attributed this shoulder to either an unbalanced charge transport of electrons and holes or to charge carriers being released from deep states with the aid of the external electric field. From temperature dependent measurements two slopes could be determined in the $\ln(\mu)$ vs $1/T^2$ plot indicating two different energy disorder parameters. Compared to the reference material system P3HT:PC_{61}BM a larger energetic disorder is found in PCDTBT:PC_{71}BM for temperatures above $T = 200$ K.

Chapter 12

Conclusions

Zusammenfassung

Ziel dieser Arbeit war es den Transport und die Rekombination von Ladungsträgern in organischen "bulk heterojunction" (Heterogemisch, BHJ) Solarzellen zu untersuchen. Dazu fand neben der transienten Photoleitfähigkeit (TOF) hauptsächlich die transiente Ladungsextraktionsmessmethode, genannt photo-CELIV, große Anwendung. Ein großer Vorteil dieser Messmethode ist, dass neben der Beweglichkeit der Ladungsträger auch die Konzentration derer simultan bestimmt werden kann. Im Vordergrund der Untersuchung standen dabei hauptsächlich organische Solarzellen mit dem Materialgemisch bestehend aus Poly-3-(Hexyl) Thiophen (P3HT) und [6,6]-Phenyl C_{61} Buttersäure Methylester ($PC_{61}BM$), das als Referenzsystem für neuartige Materialzusammensetzungen verwendet wurde.

Mit Hilfe der TOF Messmethode konnte für ein Gewichtsverhältnis von Donator zu Akzeptor von 1:1 ein ausgeglichener Ladungstransport von Elektronen und Löchern gefunden werden. Der Rekombination von Ladungsträgern in organischen BHJ Solarzellen wurde eine "bimolekularen" Dynamik, und folglich einem Prozess zweiter Ordnung zugeordnet. Allerdings weicht der experimentell bestimmte zeitliche Abfall der Ladungsträgerkonzentration oft von der Ordnung zwei ab. Diese Abweichung kann unterschiedliche Ursachen haben. Es konnte in dieser Arbeit gezeigt werden, dass der Prozess der Rekombination von lichterzeugten Ladungsträger sowohl von der räumlichen Unordnung, also der Morphologie, sowie von der energetischen Unordnung der aktiven Schicht stark beeinflusst wird. Bevor Ladungsträger zu den jeweiligen Elektroden transportiert werden können, müssen sie die Coulomb-Anziehungskraft ihres Partners überwinden. Dieser Trennungsprozess wird durch die Morphologie entscheidend geprägt. Im Materialgemisch pBTCT-C_{12}:$PC_{61}BM$ 1:1, das eine feine Durchmischung der Donator- und Akzeptorbereiche aufweist, wurde eine erhöhte "geminale" Rekombination gefunden. Dabei führt die feine Durchmischung dazu, dass nur wenig Perkolationspfade zu den Elektroden entstehen, so dass Ladungsträgerpaare (Polaronenpaare) an der Grenzfläche nur erschwert die Anziehungskraft überwinden können und rekombinieren. Der Ladungstransport in organischen BHJ Solarzellen ist

räumlich beschränkt. Elektronen werden typischerweise auf Fullerenmolekülen transportiert, wohingegen Löcher bevorzugt auf dem Polymer hüpfen. Eine Rekombination von Elektron und Loch kann generell nur an einer Donator–Akzeptor Grenzfläche stattfinden, wobei vor allem das Finden beider Ladungsträger die Rekombinatinonsdynamik mit entscheidend beeinflusst. Zu tiefen Temperaturen hin wird die Rekombinationsrate deutlich verlangsamt, was auf die reduzierte Beweglichkeit der Ladungsträger zurückzuführen ist. Des weiteren wird der Ladungstransport bei tiefen Temperaturen vor allem durch die geringe Anregungsenergie, die für die Hüpfprozesse benötigt wird, und den dadurch entstehenden vielen Einfang-Prozessen während des Transportes geprägt. Dies wiederum wirkt sich auf die Rekombinationsdynamik der Ladungsträger aus, indem eine erhöhte Rekombinationsordnung experimentell bestimmt wird. Dies wurde vor allem in thermisch unbehandelten Solarzellen verstärkt beobachtet. Diese Schlussfolgerungen wurden durch die Untersuchungen an P3HT:bis-$PC_{61}BM$ BHJ Solarzellen bekräftigt, die im Vergleich zum Referenzsystem P3HT:$PC_{61}BM$ eine größere energetische Unordnung aufweisen und damit auch mehr tiefe Zustände, die den Ladungstransport und die Rekombinationsdynamik deutlich verlangsamen. Eine ähnlich verminderte Rekombinationsdynamik wurde auch festgestellt nachdem P3HT:$PC_{61}BM$ BHJ Solarzellen synthetischer Luft ausgesetzt worden sind. Sauerstoff dotiert vornehmlich das Polymer der aktiven Schicht, wobei die Dotierung wiederum eine Verbreiterung der DOS verursacht. Die erhöhte Unordnung im System führt zu einem verringerten Ladungstransport und zu einer verlangsamten Rekombinationszeit. Dadurch ist auch die erhöhte Lebensdauer von Elektronen und Löchern zu erklären, die in degradierten Proben beobachtet wurde. In beiden Fällen, ob durch Sauerstoff induzierte energetische Unordnung oder aber durch Verringerung der thermischen Energie, konnte der verlangsamte Ladungstransport sowie verminderte Rekombinationsrate von Elektronen und Löcher auf einen Störstellen-limitierten Transport zurückgeführt werden. Dabei ist die Zeit, die zwei Ladungsträger benötigen um zu rekombinieren, stark davon abhängig, ob und wie schnell sie aus tiefen (Stör-)Stellen freigelassen werden.

Schließlich wurde die photo-CELIV Messmethode im Rahmen dieser Arbeit erweitert und verbessert. Die sogenannte OTRACE Messmethode nutzt auf der einen Seite die Vorteile des photo-CELIV Experiments gewährleistet, aber andererseits eine möglichst geringe RC Einschränkung sowie die Verwendung von niedrigen Lichtleistungen. Des weiteren wird in der erweiterten Messmethode der zeitliche Verlauf der Leerlaufspannung, die aufgrund der Rekombination von Ladungsträgern abfällt, berücksichtigt. Dies ermöglicht es zum ersten Mal, den Transport und die Rekombination von Ladungsträgern in organischen BHJ Solarzellen unter realen Betriebsbedingungen einer Solar-

zelle, also bei Raumtemperatur und mit niedrigen Lichtleistungen, simultan zu untersuchen.

Interessant wird es sein, die neue Messmethode zusammen mit komplementären Methoden wie der transienten Photospannung und des Photostromes anzuwenden. So lassen sich die Beweglichkeit und die Lebensdauer der Ladungsträger in organischen BHJ Solarzellen unter realen Arbeitsbedingungen effizient bestimmen. Des weiteren können zusätzliche Experimente, wie die transiente Absorption, dazu dienen gerade die Rekombinationsdynamik für Zeiten im sub-ns Bereich zu untersuchen, um so umfassendere Erkenntnisse über Rekombinationsverluste in organischen Solarzellen zu gewinnen.

Conclusions

The primary focus of this thesis was to investigate the charge transport and recombination dynamics in organic bulk heterojunction (BHJ) solar cells using the experimental techniques of transient photoconductivity (TOF) and charge carrier extraction by linearly increasing voltage (CELIV). The great advantage of the latter method is that the mobility and concentration of the photogenerated charge carriers can be determined simultaneously. In this work mainly the material blend composition of poly(3-hexylthiophene-2,5-diyl) (P3HT) and [6,6]-phenyl-C_{61}butyric acid methyl ester ($PC_{61}BM$) was studied and used as a reference material system for new donor–acceptor compositions.

Using the TOF experiment an ambipolar transport was found in P3HT:$PC_{61}BM$ devices with a balanced electron and hole mobility at a weight ratio of around 1:1. The polaron recombination dynamics in bulk heterojunction solar cells were assigned to be bimolecular, however, with a recombination order mostly deviating from two. This deviation can have different origins: The dynamics were found to be strongly dependent on the morphology, i.e. spatial disorder, as well as on the energetic disorder of the blend system. Before polarons can be transported to the electrodes they have to overcome the Coulomb attraction from their counterpart. The phase segregation plays an important role in this process. In pBTCT-C_{12}:$PC_{61}BM$ BHJ 1:1 solar cells consisting of fine intermixed phases an enhanced geminate recombination was observed due to the lack of percolated pathways impeding the process of polaron pair dissociation. In organic bulk heterojunction solar cells the transport of electrons is restricted to the acceptor and the hole transport to the donor phase. Generally, the non-geminate recombination is determined by the time, which is needed for the charge carriers to find each other at the heterointerface. During their transport, charge carrier may get trapped energetically or spatially in isolated phase domains influencing the recombination dynamics as was illustrated for the dynamics in pBTCT-C_{12}:$PC_{61}BM$ blends.

At low temperatures the recombination rate decreases mainly due to a reduced charge carrier mobility. Thereby, already deep tail states in the DOS may act as traps due to less thermal energy available for the hopping jumps, which impede the polaron hopping motion and hence lead to a charge transport, which is affected by multiple trapping and release (MTR) processes. Thus, the experimentally observed charge carrier concentration decay order in P3HT:$PC_{61}BM$ BHJ solar cells typically increased with decreasing temperature, which was found to be more pronounced for pristine devices. These conclusions are confirmed by the fact that the recombination dynamics are even

more delayed when P3HT:bis-$PC_{61}BM$ is considered, whereas bis-$PC_{61}BM$ exhibit typically broader DOS than $PC_{61}BM$ with an increased number of tail states. A similar reduction in the charge recombination dynamics was found as we exposed P3HT:$PC_{61}BM$ BHJ solar cells to synthetic air. The polymer is doped by the oxygen, which then leads to a broadening of the DOS. At a given temperature, the oxygen induced deep tail states led again to a reduced charge carrier mobility and increased the effective charge carrier lifetime with exposure time. Both, the increased order at low temperatures and the increase due to oxygen exposure can be explained by a trap-limited charge transport either by tail states of the DOS below the transport energy acting as trap states or due to oxygen induced traps broadening the DOS. Generally, the charge carrier recombination dynamics are highly affected by the release of energetically trapped charge carriers, which leads to a delay in recombination.

Finally, the commonly used technique of photo-CELIV was extended in this work. The OTRACE technique uses the advantages of photo-CELIV to determine the mobility and lifetime of charge carriers simultaneously, however, with minimized RC limitations and low light intensities. Furthermore, the extended method accounts for the transient decay of the open circuit voltage due to charge carrier recombination. For the first time it became possible to investigate the dynamics of organic solar cells under operating conditions, i. e. room temperature and low light intensities.

Using the new transient extraction method in combination with the complementary techniques of transient photovoltage and photocurrent will build a powerful experimental setup to determine the mobility and lifetime of charge carriers in organic solar cells very efficiently under operating conditions. Further studying the charge carrier dynamics by experimental techniques such as transient absorption at sub-ns time scales will result in a more comprehensive insight in the recombination losses in organic solar cells.

Bibliography

[1] Bundesministerium für Umwelt Naturschutz Reaktorsicherheit. Bekanntmachung über die Förderung von Forschung und Entwicklung im Bereich erneuerbarer Energien. Bundesanzeiger Nr. 179, September 2006.

[2] A. E. Becquerel. Mémoire sur les effets électriques produits sous l'influence des rayons solaires. *Comt. Rend. Acad. Sci.*, 9:561, 1839.

[3] D. M. Chapin, C. S. Fuller, and G. L. Pearson. A new silicon p-n junction photocell for converting solar radiation into electrical power. *J. Appl. Phys.*, 25:676, 1954.

[4] M. A. Green, K. Emery, Y. Hishikawa, and W. Warta. Solar cell efficiency tables (version 37). *Prog. Photovolt.*, 19:84, 2011.

[5] W. Shockley and H. J. Queisser. Detailed balance limit of efficiency of p-n junction solar cells. *J. Appl. Phys.*, 32:510, 1961.

[6] A. Goetzberger. Photovoltaic materials, history, status and outlook. *Materials Science and Engineering: R: Reports*, 40:1, 2003.

[7] R. Gaudiana. Third-generation photovoltaic technology - the potential for low-cost solar energy conversion. *J. Phys. Chem. Lett.*, 1:1288, 2010.

[8] C. J. Brabec, S. Gowrisanker, J. J. M. Halls, D. Laird, S. Jia, and S. P. Williams. Polymer–Fullerene Bulk-Heterojunction Solar Cells. *Adv. Mater.*, 2010.

[9] C. Deibel and V. Dyakonov. Polymer–fullerene bulk heterojunction solar cells. *Rep. Prog. Phys.*, 73:096401, 2010.

[10] G. A. Chamberlain. Organic Solar Cells: A Review. *Solar Cells*, 8:47, 1983.

[11] M. Pope and C. E. Swenberg. *Electronic Processes in Organic Crystals and Polymers*. Oxford University Press, USA, 2nd edition, 1999.

[12] C. Deibel, T. Strobel, and V. Dyakonov. Origin of the efficient polaron pair dissociation in polymer–fullerene blends. *Phys. Rev. Lett.*, 103:036402, 2009.

[13] C. W. Tang. Two-layer organic photovoltaic cell. *Appl. Phys. Lett.*, 48:183, 1986.

[14] G. Yu, J. Gao, J. C. Hummelen, F. Wudl, and A. J. Heeger. Polymer photovoltaic cells: enhanced efficiencies via a network of internal donor-acceptor heterojunctions. *Science*, 270:1789, 1995.

[15] S. E. Shaheen, C. J. Brabec, and N. S. Sariciftci. 2.5% efficient organic plastic solar cells. *Appl. Phys. Lett.*, 78:841, 2001.

[16] F. Padinger, R. S. Rittberger, and N. S. Sariciftci. Effects of postproduction treatment om plastic solar cells. *Adv. Funct. Mater.*, 13:85, 2003.

[17] J. Peet, J. Y. Kim, N. E. Coates, W. L. Ma, D. Moses, A. J. Heeger, and G. C. Bazan. Efficiency enhancement in low-bandgap polymer solar cells by processing with alkane dithiols. *Nat. Mater.*, 6:497, 2007.

[18] C. Deibel and V. Dyakonov. Sonnenstrom aus Plastik. *Physik Journal*, 7(5):50, 2008.

[19] L. W. Barbour, R. D. Pensack, M. Hegadorn, S. Arzhantsev, and J. B. Asbury. Excitation transport and charge separation in an organic photovoltaic material: Watching excitations diffuse to interfaces. *J. Phys. Chem. C*, 112:3926, 2008.

[20] E. Collini and G. D Scholes. Coherent intrachain energy migration in a conjugated polymer at room temperature. *Science*, 323:369, 2009.

[21] C. Deibel, D. Mack, J. Gorenflot, A. Schöll, S. Krause, F. Reinert, D. Rauh, and V. Dyakonov. Energy levels and exciton binding energy in the conjugated polymer poly(3-hexyl thiophene). *Phys. Rev. B*, 81:085202, 2010.

[22] T. R. Clarke and J. R. Durrant. Charge photogeneration in organic solar cells. *Chem. Rev.*, 110:6736, 2010.

[23] E. L. Frankevich, A. A. Lymarev, I. Sokolik, F. E. Karasz, S. Blumstengel, R. H. Baughman, and H. H. Hörhold. Polaron-pair generation in poly(phenylene vinylene). *Phys. Rev. B*, 46:9320, 1992.

[24] L. Onsager. Initial recombination of ions. *Phys. Rev.*, 54:554, 1938.

[25] C. L. Braun. Electric field assisted dissociation of charge transfer states as a mechanism of photocarrier production. *J. Chem. Phys.*, 80:4157, 1984.

[26] V. D. Mihailetchi, L. J. A. Koster, and P. W. M. Blom. Effect of metal electrodes on the performance of polymer:fullerene bulk heterojunction solar cells. *Appl. Phys. Lett.*, 85:970, 2004.

[27] L. J. A. Koster, V. D. Mihailetchi, R. Ramaker, and P. W. M. Blom. Light intensity dependence of open-circuit voltage of polymer:fullerene solar cells. *Appl. Phys. Lett.*, 86:123509, 2005.

[28] G. A. Buxton and N. Clarke. Predicting structure and property relations in polymeric photovoltaic devices. *Phys. Rev. B*, 74(085207), 2006.

[29] C. Deibel, A. Wagenpfahl, and V. Dyakonov. Influence of charge carrier mobility on the performance of organic solar cells. *Phys. Stat. Sol. (RRL)*, 2:175, 2008.

[30] R. J. O. M. Hoofman, M. P. de Haas, L.D.A. Siebbeles, and J. M. Warman. Highly mobile electrons and holes on isolated chains of the semiconducting polymer poly(phenylenevinylene). *Nature*, 392:54, 1998.

[31] T. J. Savenije, J. E. Kroeze, X. Yang, and J. Loos. The formation of crystalline p3ht fibrils upon annealing of a pcbm:p3ht bulk heterojunction. *Thin Solid Films*, 511:2, 2006.

[32] A. Devižis, A. Serbenta, K. Meerholz, D. Hertel, and V. Gulbinas. Ultrafast dynamics of carrier mobility in a conjugated polymer probed at molecular and microscopic length scales. *Phys. Rev. Lett.*, 103:027404, 2009.

[33] C. Deibel, A. Wagenpfahl, and V. Dyakonov. Origin of reduced polaron recombination in organic semiconductor devices. *Phys. Rev. B*, 80:075203, 2009.

[34] J. Subbiah, D. Y. Kim, M. Hartel, and Franky So. MoO_3/poly(9,9-dioctylfluorene-co-N-[4-(3-methylpropyl)]-diphenylamine) double-interlayer effect on polymer solar cells. *Appl. Phys. Lett.*, 96:063303, 2010.

[35] C. Yin, T. Kietzke, D. Neher, and H.-H. Hörhold. Photovoltaic properties and exciplex emission of polyphenylenevinylene-based blend solar cells. *Appl. Phys. Lett.*, 90:092117, 2007.

[36] M. D. Irwin, D. B. Buchholz, A. W. Hains, R. P. H. Chang, and T. J. Marks. p-type semiconducting nickel oxide as an efficiency-enhancing anode interfacial layer in polymer bulk-heterojunction solar cells. *P. Nat. Acad. Sci.*, 105:2783–2787, 2008.

[37] A. W. Hains, J. Liu, A. B. F. Martinson, M. D. Irwin, and T. J. Marks. Anode interfacial tuning via electron-blocking/hole- transport layers and indium tin oxide surface treatment in bulk-heterojunction organic photovoltaic cells. *Adv. Funct. Mater.*, 20:595, 2010.

[38] A. J. Mozer and N. S. Sariciftci. Negative electric field dependence of charge carrier drift mobility in conjugated, semiconducting polymers. *Chem. Phys. Lett.*, 389:438, 2004.

[39] S. R. Mohan, M. P. Singh, and M. P. Joshi. Negative field dependence of mobility in disordered organic thin films due to non-equilibrium charge transport. *Org. Electron.*, 11:1642, 2010.

[40] T. Strobel, C. Deibel, and V. Dyakonov. Role of Polaron Pair Diffusion and Surface Losses in Organic Semiconductor Devices. *Phys. Rev. Lett.*, 105:266602, 2010.

[41] S. Shoaee, T. M. Clarke, C. Huang, S. Barlow, S. R. Marder, M. Heeney, I. McCulloch, and J. R. Durrant. Acceptor energy level control of charge photogeneration in organic donor/acceptor blends. *J. Am. Chem. Soc.*, 132:12919, 2010.

[42] M. Jaiswal and R. Menon. Polymer electronic materials: a review of charge transport. *Polym. Int.*, 55:1371, 2006.

[43] A. A. Bakulin, D.S . Martyanov, D. Y. Paraschuk, M. S. Pshenichnikov, and P. H. M. van Loosdrecht. Ultrafast charge photogeneration dynamics in ground-state charge-transfer complexes based on conjugated polymers. *J. Phys. Chem. B*, 112:13730, 2008.

[44] V. Gulbinas, D. Hertel, A. Yartsev, and V. Sundström. Charge carrier photogeneration and recombination in ladder-type poly(paraphenylene): Interplay between impurities and external electric field. *Phys. Rev. B*, 76:235203, 2007.

[45] I.-W. Hwang, D. Moses, and A. J. Heeger. Photoinduced carrier generation in P3HT/PCBM bulk heterojunction materials. *J. Phys. Chem. C*, 112:4350–4354, 2008.

[46] S. De, T. Pascher, M. Maiti, K. G. Jespersen, T. Kesti, F. Zhang, O. Inganäsand A. Yartsev, and V. Sundström. Geminate charge recombination in alternating polyfluorene copolymer/fullerene blends. *J. Am. Chem. Soc.*, 129:8466, 2007.

[47] H. Ohkita, S. Cook, Y. Astuti, W. Duffy, S. Tierney, W. Zhang, M. Heeney, I. McCulloch, J. Nelson, D. D. C. Bradley, and J. R. Durrant. Charge carrier formation in polythiophene/fullerene blend films studied by transient absorption spectroscopy. *J. Am. Chem. Soc.*, 130:3030, 2008.

[48] J. Campbell Scott and George G. Malliaras. Charge injection and recombination at the metal-organic interface. *Chem. Phys. Lett.*, 299:115, 1999.

[49] J. Nelson, J. Kirkpatrick, and P. Ravirajan. Factors limiting the efficiency of molecular photovoltaic devices. *Phys. Rev. B*, 69:035337, 2004.

[50] C. Deibel, T. Strobel, and V. Dyakonov. Role of the charge transfer state in organic donor–acceptor solar cells. *Adv. Mater.*, 22:4097, 2010.

[51] C. J. Brabec, A. Cravino, D. Meissner, N. S. Sariciftci, T. Fromherz, M. T. Rispens, L. Sanchez, and J. C. Hummelen. Origin of the open circuit voltage of plastic solar cells. *Adv. Funct. Mater.*, 11:374, 2001.

[52] A. Gadisa, M. Svensson, M. R. Andersson, and O. Inganäs. Correlation between oxidation potential and open-circuit voltage of composite solar cells based on blends of polythiophenes/fullerene derivative. *Appl. Phys. Lett.*, 84:1609, 2004.

[53] C. M. Ramsdale, J. A. Barker, A. C. Arias, J. D. MacKenzie, R. H. Friend, and N. C. Greenham. The origin of the open-circuit voltage in polyfluorene-based photovoltaic devices. *J. Appl. Phys.*, 92:4266, 2002.

[54] M. C. Scharber, D. Mühlbacher, M. Koppe, P. Denk, C. Waldauf, A. J. Heeger, and C. J. Brabec. Design rules for donors in bulk-heterojunction solar cells — towards 10% energy-conversion efficiency. *Adv. Mater.*, 18:789, 2006.

[55] K. Vandewal, A. Gadisa, W. D. Oosterbaan, S. Bertho, F. Banishoeib, I. Van Severen, L. Lutsen, T. J. Cleij, D. Vanderzande, and J. V. Manca. The relation between open-circuit voltage and the onset of photocurrent generation by charge-transfer absorption in polymer:fullerene bulk heterojunction solar cells. *Adv. Funct. Mater.*, 18:2064, 2008.

[56] I. Riedel, E. von Hauff, J. Parisi, N. Martin, F. Giacalone, and V. Dyakonov. Diphenylmethanofullerenes: New and efficient acceptors in bulk-heterojunction solar cells. *Adv. Funct. Mater.*, 15:1979, 2005.

[57] R. B. Ross, C. M. Cardona, D. M. Guldi, S. G. Sankaranarayanan, M. O. Reese, N. Kopidakis, J. Peet, B. Walker, G. C. Bazan, E. Van Keuren, B. C. Holloway, and M. Drees. Endohedral fullerenes for organic photovoltaic devices. *Nat. Mater.*, 8:208, 2009.

[58] P. W. Atkins. *The elements of physical chemistry.* Oxford University Press, 1992.

[59] R. Hoffmann, C. Janiak, and C. Kollmar. A chemical approach to the orbitals of organic polymers. *Macromolecules*, 24:3725, 1991.

[60] A. J. Heeger. Nobel lecture: Semiconducting and metallic polymers: The fourth generation of polymeric materials. *Rev. Mod. Phys.*, 73:681–700, 2001.

[61] A. J. Heeger, S. Kivelson, J. R. Schrieffer, and W. P. Su. Solitons in conducting polymers. *Rev. Mod. Phys.*, 60:781–850, 1988.

[62] C. Brabec, U. Scherf, and V. Dyakonov. *Organic Photovoltaics.* Wiley VCH, Weinheim, Germany, 2008.

[63] B. Kraabel, D. Moses, and A. J. Heeger. Subpicosecond Photoinduced Electron Transfer in Semiconducting Polymer-C60 Composites. *Mol. Cryst. and Liq. Cryst.*, 256:733, 1994.

[64] T. Singh, N. Marjanovic, G. Matt, S. Guenes, N. S. Sariciftci, A. Montaigneramil, A. Andreev, H. Sitter, R. Schwodiauer, and S. Bauer. High-mobility n-channel organic field-effect transistors based on epitaxially grown C_{60} films. *Org. Electron.*, 6:105, 2005.

[65] P. Peumans, A. Yakimov, and S. R. Forrest. Small molecular weight organic thin-film photodetectors and solar cells. *J. Appl. Phys.*, 93:3693, 2003.

[66] M. Lenes, G.-J. A. H. Wetzelaer, F. B. Kooistra, S. C. Veenstra, J. C. Hummelen, and P. W. M. Blom. Fullerene bisadducts for enhanced open-circuit voltages and efficiencies in polymer solar cells. *Adv. Mater.*, 20:2116, 2008.

[67] M. Lenes, S. W. Shelton, A. B. Sieval, D. F. Kronholm, J. C. Hummelen, and P. W. M. Blom. Electron trapping in higher adduct fullerene-based solar cells. *Adv. Funct. Mater.*, 19:3002, 2009.

[68] P. W. Anderson. Absence of diffusion in certain random lattices. *Phys. Rev.*, 109:1492, 1958.

[69] Z. G. Yu, D. L. Smith, A. Saxena, R. L. Martin, and A. R. Bishop. Molecular geometry fluctuations and field-dependent mobility in conjugated polymers. *Phys. Rev. B*, 63:085202, 2001.

[70] J. Frenkel. On Pre-Breakdown Phenomena in Insulators and Electronic Semi-Conductors. *Phys. Rev.*, 54:647, 1938.

[71] R. A. Marcus. Electron transfer reactions in chemistry: Theory and experiment. *Rev. Mod. Phys.*, 65:599, 1993.

[72] R. A. Marcus. On the theory of oxidation-reduction reactions involving electron transfer. i. *J. Chem. Phys.*, 24:966, 1956.

[73] E. M. Conwell. Impurity band conduction in germanium and silicon. *Phys. Rev.*, 103(1):51, Jul 1956.

[74] N. F. Mott. On the transition to metallic conduction in semiconductors. *Can. J. Phys.*, 34:1356, 1956.

[75] A. Miller and E. Abrahams. Impurity conduction at low concentrations. *Phys. Rev.*, 120:745, 1960.

[76] G. Schönherr, R. Eiermann, H. Bässler, and M. Silver. Dispersive exciton transport in a hopping system with gaussian energy distribution. *Chem. Phys.*, 52:287, 1980.

[77] H. Bässler. Charge transport in disordered organic photoconductors — A Monte Carlo simulation study. *Phys. Stat. Sol. B*, 175:15, 1993.

[78] T. Offermans, P. A. van Hal, S. C. J. Meskers, M. M. Koetse, and R. A. J. Janssen. Exciplex dynamics in a blend of π-conjugated polymers with electron donating and accepting properties: MDMO-PPV and PCNEPV. *Phys. Rev. B*, 72(4):045213, 2005.

[79] W. F. Pasveer, J. Cottaar, C. Tanase, R. Coehoorn, P. A. Bobbert, P. W. M. Blom, D. M. de Leeuw, and M. A. J. Michels. Unified description of charge-carrier mobilities in disordered semiconducting polymers. *Phys. Rev. Lett.*, 94:206601, 2005.

[80] H. Houili, E. Tutis, I. Batistic, and L. Zuppiroli. Investigation of the charge transport through disordered organic molecular heterojunctions. *J. Appl. Phys.*, 100:033702, 2006.

[81] S. V. Novikov, D. H. Dunlap, V. M. Kenkre, P. E. Parris, and A. V. Vannikov. Essential role of correlations in governing charge transport in disordered organic materials. *Phys. Rev. Lett.*, 81:4472, 1998.

[82] R. Jankowiak, K. D. Rockwitz, and H. Bässler. Absorption spectroscopy of amorphous tetracene. *J. Phys. Chem.*, 87:552, 1983.

[83] N. Tessler, Y. Preezant, N. Rappaport, and Yohai Roichman. Charge transport in disordered organic materials and its relevance to thin-film devices: A tutorial review. *Adv. Mater.*, 21:2741, 2009.

[84] I. N. Hulea, H. B. Brom, A. J. Houtepen, D. Vanmaekelbergh, J. J. Kelly, and E. A. Meulenkamp. Wide energy-window view on the density of states and hole mobility in poly(*p*-phenylene vinylene). *Phys. Rev. Lett.*, 93:166601, 2004.

[85] O. Tal, Y. Rosenwaks, Y. Preezant, N. Tessler, C. K. Chan, and A. Kahn. Direct determination of the hole density of states in undoped and doped amorphous organic films with high lateral resolution. *Phys. Rev. Lett.*, 95:256405, 2005.

[86] Y. Roichman, Y. Preezant, and N. Tessler. Analysis and modeling of organic devices. *Phys. Stat. Sol. A*, 201:1246, 2004.

[87] V. I. Arkhipov, E. V. Emelianova, and H. Bässler. Equilibrium carrier mobility in disordered hopping systems. *Phil. Mag. B*, 81:985, 2001.

[88] O. Rubel, S. D. Baranovskii, P. Thomas, and S. Yamasaki. Concentration dependence of the hopping mobility in disordered organic solids. *Phys. Rev. B*, 69:014206, 2004.

[89] C. Tanase, E. J. Meijer, P. W. M. Blom, and D. M. de Leeuw. Unification of the hole transport in polymeric field-effect transistors and light-emitting diodes. *Phys. Rev. Lett.*, 91:216601, 2003.

[90] S. D. Baranovskii, H. Cordes, F. Hensel, and G. Leising. Charge-carrier transport in disordered organic solids. *Phys. Rev. B*, 62:7934, 2000.

[91] D. Monroe. Hopping in exponential band tails. *Phys. Rev. Lett.*, 54:146, 1985.

[92] V. I. Arkhipov, E. V. Emelianova, and G. J. Adriaenssens. Effective transport energy versus the energy of most probable jumps in disordered hopping systems. *Phys. Rev. B*, 64:125125, 2001.

[93] M. Grünewald and P. Thomas. A hopping model for activated charge transport in amorphous silicon. *Phys. Stat. Sol. B*, 94:125, 1979.

[94] A. R. Blythe and D. Bloor. *Electrical Properties of Polymers*. Cambridge University Press, 2005.

[95] N. F. Mott. Recombination: A survey. *Sol. Stat. Elec.*, 21:1275, 1978.

[96] L. J. A. Koster, E. C. P. Smits, V. D. Mihailetchi, and P. W. M. Blom. Device model for the operation of polymer/fullerene bulk heterojunction solar cells. *Phys. Rev. B*, 72:085205, 2005.

[97] T. Kirchartz, B. E. Pieters, J. Kirkpatrick, U. Rau, and J. Nelson. Recombination via tail states in polythiophene:fullerene solar cells. *Phys. Rev. B*, 83:115209, 2011.

[98] P. Langevin. Recombinaison et mobilites des ions dans les gaz. *Ann. Chim. Phys.*, 28:433, 1903.

[99] V. D. Mihailetchi, P. W. M. Blom, J. C. Hummelen, and M. T. Rispens. Cathode dependence of the open-circuit voltage of polymer:fullerene bulk heterojunction solar cells. *J. Appl. Phys.*, 94:6849, 2003.

[100] C. J. Brabec, A. Cravino, D. Meissner, N. S. Sariciftci, M. T. Rispens, L. Sanchez, J. C. Hummelen, and T. Fromherz. The influence of materials work function on the open circuit voltage of plastic solar cells. *Thin Solid Films*, 403-404:368, 2002.

[101] E. Ahlswede, J. Hanisch, and M. Powalla. Comparative study of the influence of LiF, NaF, and KF on the performance of polymer bulk heterojunction solar cells. *Appl. Phys. Lett.*, 90(163504), 2007.

[102] S. K. M. Jönsson, E. Carlegrim, F. Zhang, W. R. Salaneck, and M. Fahlman. Photoelectron spectroscopy of the contact between the cathode and the active layers in plastic solar cells: The role of lif. *Jpn. J. Appl. Phys.*, 44:3695, 2005.

[103] C. J. Brabec, S. E. Shaheen, C. Winder, N. S. Sariciftci, and P. Denk. Effect of LiF/metal electrodes on the perfomance of plastic solar cells. *Appl. Phys. Lett.*, 80:1288, 2002.

[104] H. Scher and E. W. Montroll. Anomalous transit-time dispersion in amorphous solids. *Phys. Rev. B*, 12:2455, 1975.

[105] A. D. Petravichyus, G. Juška, and R. V. Baubinas. Drift of Holes in High-Resistivity p-Type CdSe Crystal Plates. *Sov. Phys. Semicond.*, 9:1530, 1975.

[106] G. Juška, K. Arlauskas, M. Viliūnas, and J. Kočka. Extraction current transients: New method of study of charge transport in microcrystalline silicon. *Phys. Rev. Lett.*, 84:4946, 2000.

[107] S. Bange, M. Schubert, and D. Neher. Charge mobility determination by current extraction under linear increasing voltages: Case of nonequilibrium charges and field-dependent mobilities. *Phys. Rev. B*, 81:035209, 2010.

[108] A. J. Mozer, G. Dennler, N. S. Sariciftci, M. Westerling, A. Pivrikas, R. Österbacka, and G. Juška. Time-dependent mobility and recombination of the photoinduced charge carriers in conjugated polymer/fullerene bulk heterojunction solar cells. *Phys. Rev. B*, 72:035217, 2005.

[109] J. Lorrmann, B. H. Badada, O. Inganäs, V. Dyakonov, and C. Deibel. Charge Carrier Extraction by Linearly Increasing Voltage: Analytic framework and ambipolar transients. *J. Appl. Phys.*, 108:113705, 2010.

[110] C. Deibel. Charge carrier dissociation and recombination in polymer solar cells. *Phys. Stat. Sol. A*, 206:2731, 2009.

[111] A. Wagenpfahl, C. Deibel, and V. Dyakonov. Organic solar cell efficiencies under the aspect of reduced surface recombination velocities. *IEEE J. Sel. Top. Quantum Electron.*, 2010.

[112] S. M. Tuladhar, D. Poplavskyy, S. A. Choulis, J. R. Durrant, D. D. C. Bradley, and J. Nelson. Ambipolar charge transport in films of methanofullerene and poly(polyphenylenevinylene)/methanofullerene blends. *Adv. Funct. Mater.*, 15:1171, 2005.

[113] M. Shibao, T. Morita, W. Takashima, and K. Kaneto. Ambipolar transport in field-effect transistors based on composite films of poly(3-hexylthiophene) and fullerene derivative. *Jpn. J. Appl. Phys.*, 46:L123, 2007.

[114] E. von Hauff, J. Parisi, and V. Dyakonov. Investigations of the effects of tempering and composition dependence on charge carrier field effect mobilities in polymer and fullerene films and blends. *J. Appl. Phys.*, 100:043702, 2006.

[115] J. Huang, G. Li, and Y. Yang. Influence of composition and heat-treatment on the charge transport properties of poly (3-hexylthiophene) and [6, 6]-phenyl c-butyric acid methyl ester blends. *Appl. Phys. Lett.*, 87:112105, 2005.

[116] P. M. Borsenberger, L. T. Pautmeier, and H. Bässler. Nondispersive-to-dispersive charge-transport transition in disordered molecular solids. *Phys. Rev. B*, 46:12145, 1992.

[117] C. Deibel, A. Baumann, and V. Dyakonov. Polaron recombination in pristine and annealed bulk heterojunction solar cells. *Appl. Phys. Lett.*, 93:163303, 2008.

[118] S. A. Choulis, Y. Kim, J. Nelson, D. D. C. Bradley, M. Giles, M. Shkunov, and I. McCulloch. High ambipolar and balanced carrier mobility in regioregular poly(3-hexylthiophene). *Appl. Phys. Lett.*, 85:3890, 2004.

[119] V. D. Mihailetchi, H. Xie, B. de Boer, L. M. Popescu, J. C. Hummelen, P. W. M. Blom, and L. J. A. Koster. Origin of the enhanced performance in poly(3-hexylthiophene): [6,6]-phenyl C_{61}-butyric acid methyl ester solar cells upon slow drying of the active layer. *Appl. Phys. Lett.*, 89:012107, 2006.

[120] P. M. Borsenberger. Hole transport in mixtures of 1,1-bis(di-4-tolylaminophenyl) cyclohexane and bisphenol-A-polycarbonate. *J. Appl. Phys.*, 68:5682, 1990.

[121] H. Sirringhaus, P. J. Brown, R. H. Friend, M. M. Nielsen, K. Bechgaard, B. M. W. Langeveld-Voss, A. J. H. Spiering, R. A. J. Janssen, E. W. Meijer, P. Herwig, and D. M. de Leeuw. Two-dimensional charge transport in self-organized, high-mobility conjugated polymers. *Nature*, 401:685, 1999.

[122] M. C. J. M. Vissenberg and M. Matters. Theory of the field-effect mobility in amorphous organic transistors. *Phys. Rev. B*, 57:12964, 1998.

[123] V. Ambegaokar, B. I. Halperin, and J. S. Langer. Hopping conductivity in disordered systems. *Phys. Rev. B*, 4:2612, 1971.

[124] C. Deibel, A. Baumann, J. Lorrmann, and V. Dyakonov. Polaron pair dissociation and polaron recombination in polymer: Fullerene solar cells. *J. Mater. Res.*, 1031:21, 2008.

[125] J. Lorrmann. Ladungstransport in ungeordneten organischen Halbleitern, unveröffentlichte Diplomarbeit, Universität Würzburg, 2008.

[126] H. Iino and J. Hanna. Ambipolar charge carrier transport in liquid crystals. *Opto-Electronics Review*, 13:295, 2005.

[127] J. Y. Kim, S. H. Kim, H.-H. Lee, K. Lee, W. Ma, X. Gong, and A. J. Heeger. New architecture for high-efficiency polymer photovoltaic cells using solution-based titanium oxide as an optical spacer. *Adv. Mater.*, 18:572, 2006.

[128] G. Juška, K. Arlauskas, J. Stuchlik, and R. Osterbacka. Non-Langevin bimolecular recombination in low-mobility materials. *J. Non-Cryst. Sol.*, 352:1167, 2006.

[129] J. M. Frost, M. A. Faist, and J. Nelson. Energetic disorder in higher fullerene adducts: A quantum chemical and voltammetric study. *Adv. Mater.*, 22:4881, 2010.

[130] C. G. Shuttle, B. O'Regan, A. M. Ballantyne, J. Nelson, D. D. C. Bradley, and J. R. Durrant. Bimolecular recombination losses in polythiophene: Fullerene solar cells. *Phys. Rev. B*, 78:113201, 2008.

[131] F. C. Jamieson, T. Agostinelli, H. Azimi, J. Nelson, and J. Durrant. Field-Dependent Charge Photogeneration in PCDTBT/PC70BM Solar Cells. *J. Phys. Chem. Lett.*, 1:3306, 2010.

[132] A. Pivrikas, R. Österbacka, G. Juška, K. Arlauskas, and H. Stubb. Time-dependent Langevin-type bimolecular charge carrier recombination in regiorandom poly(3-hexylthiophene). *Synth. Met.*, 155:242, 2005.

[133] G. Juška, K. Genevičius, N. Nekrašas, G. Sliaužys, and R. Österbacka. Two dimensional Langevin recombination in regioregular poly(3-hexylthiophene). *Appl. Phys. Lett.*, 95:013303, 2009.

[134] C. G. Shuttle, B. O'Regan, A. M. Ballantyne, J. Nelson, D. D. C. Bradley, J. de Mello, and J. R. Durrant. Experimental determination of the rate law for charge carrier decay in a polythiophene:fullerene solar cell. *Applied Physics Letters*, 92:093311, 2008.

[135] A. Foertig, A. Baumann, D. Rauh, V. Dyakonov, and C. Deibel. Charge carrier concentration and temperature dependent recombination in polymer–fullerene solar cells. *Appl. Phys. Lett.*, 95:052104, 2009.

[136] V. I. Arkhipov, P. Heremans, E. V. Emelianova, G. J. Adriaenssens, and H. Bässler. Weak field carrier hopping in disordered organic semiconductors: the effects of deep traps and partly filled density of states distribution. *J. Phys.: Condens. Matter*, 14:9899, 2002.

[137] C. G. Shuttle, R. Hamilton, J. Nelson, B. C. O'Regan, and J. R. Durrant. Measurement of charge-density dependence of carrier mobility in an organic semiconductor blend. *Adv. Funct. Mater.*, 20:698, 2010.

[138] R. A. Marsh, C. Groves, and N. C. Greenham. A microscopic model for the behavior of nanostructured organic photovoltaic devices. *J. Appl. Phys.*, 101:083509, 2007.

[139] J. Nelson. Diffusion-limited recombination in polymer-fullerene blends and its influence on photocurrent collection. *Phys. Rev. B*, 67:155209, 2003.

[140] D. Chirvase, J. Parisi, J. C. Hummelen, and V. Dyakonov. Influence of nanomorphology on the photovoltaic action of polymer–fullerene composites. *Nanotechn.*, 15:1317, 2004.

[141] A. C. Mayer, M. F. Toney, S. R. Scully, J. Rivnay, C. J. Brabec, M. Scharber, M. Koppe, M. Heeney, I. McCulloch, and M. D. McGehee. Bimolecular crystals of fullerenes in conjugated polymers and the implications of molecular mixing for solar cells. *Adv. Funct. Mater.*, 19:1173, 2009.

[142] N. C. Cates, R. Gysel, Z. Beiley, C. E. Miller, M. F. Toney, M. Heeney, I. McCulloch, and M. D. McGehee. Tuning the properties of polymer bulk heterojunction solar cells by adjusting fullerene size to control intercalation. *Nano Lett.*, 9:4153, 2009.

[143] J. K. J. van Duren, X. Yang, J. Loos, C. W. T. Bulle-Lieuwma, A. B. Sieval, J. C. Hummelen, and R. A. J. Janssen. Relating the morphology of poly(p-phenylene vinylene) methanofullerene blends to solar-cell performance. *Adv. Funct. Mater.*, 14:425, 2004.

[144] M. Heeney, C. Bailey, K. Genevicius, M. Shkunov, D. Sparrowe, S. Tierney, and I. McCulloch. Stable polythiophene semiconductors incorporating thieno[2,3-b]thiophene. *J. Am. Chem. Soc.*, 127:1078, 2005.

[145] J. E. Kroeze, T. J. Savenije, and J. M. Warman. Contactless determination of the efficiency of photo-induced charge separation in a porphyrin–TiO_2 bilayer. *J. Photochem. Photobiol. A*, 148:49, 2002.

[146] J. E. Kroeze, T. J. Savenije, M. J. W. Vermeulen, and J. M. Warman. Contactless Determination of the Photoconductivity Action Spectrum, Exciton Diffusion Length, and Charge Separation Efficiency in Polythiophene-Sensitized TiO_2 Bilayers. *J. Phys. Chem. B*, 107:7696, 2003.

[147] A. Huijser, T. J. Savenije, J. E. Kroeze, and L. D. A. Siebbeles. Exciton Diffusion and Interfacial Charge Separation in meso-Tetraphenylporphyrin/TiO_2 Bilayers : Effect of Ethyl Substituents. *J. Phys. Chem. B*, 109:20166, 2005.

[148] T. J. Savenije, J. E. Kroeze, M. M. Wienk, J. M. Kroon, and J. M. Warman. Mobility and decay kinetics of charge carriers in photoexcited PCBM/PPV blends. *Phys. Rev. B*, 69:155205, 2004.

[149] I. McCulloch, M. Heeney, M. L. Chabinyc, D. DeLongchamp, R. J. Kline, M. Cölle, W. Duffy, D. Fischer, D. Gundlach, B. Hamadani, R. Hamilton, L. Richter, A. Salleo, M. Shkunov, D. Sparrowe, S. Tierney, and W. Zhang. Semiconducting Thienothiophene Copolymers: Design, Synthesis, Morphology, and Performance in Thin-Film Organic Transistors. *Adv. Mater.*, 21:1091, 2009.

[150] A. Sanchez-Diaz, M. Izquierdo, S. Filippone, N. Martin, and E. Palomares. The Origin of the High Voltage in DPM12/P3HT Organic Solar Cells. *Adv. Func. Mat.*, 20:2695, 2010.

[151] S. Shoaee, M. P. Eng, E. Espildora, J. L. Delgado, B. Campo, N. Martin, D. Vanderzande, and J. Durrant. Influence of nanoscale phase separation on geminate versus bimolecular recombination in P3HT:fullerene blend films. *Energy Environ. Sci.*, 3:971, 2010.

[152] W. J. Grzegorczyk, T. J. Savenije, T. E. Dykstra, J. Piris, J. M. Schins, and L. D.A. Siebbeles. Temperature-independent charge carrier photogeneration in P3HT-PCBM blends with different morphology. *J. Phys. Chem. C*, 114:5182, 2010.

[153] J. E. Parmer, A. C. Mayer, B. E. Hardin, S. R. Scully, M. D. McGehee, M. Heeney, and I. McCulloch. Organic bulk heterojunction solar cells using poly(2,5-bis(3-tetradecyllthiophen-2-yl)thieno[3,2,-b]thiophene). *Appl. Phys. Lett.*, 92:113309, 2008.

[154] T. J. Savenije, W. J. Grzegorczyk, M. Heeney, S. Tierney, I. McCulloch, and L. D. A. Siebbeles. Photoinduced Charge Carrier Generation in Blends of Poly(Thienothiophene) Derivatives and [6,6]-Pheny-C61-butyric Acid Methyl Ester: Phase segregation versus intercalation. *J. Phys. Chem. C*, 114:15116, 2010.

[155] L. J. A. Koster, V. D. Mihaletchi, and P. W. M. Blom. Bimolecular recombination in polymer/fullerene bulk heterojunction solar cells. *Appl. Phys. Lett.*, 88:052104, 2006.

[156] V. I. Arkhipov and A. Rudenko. Drift and diffusion in materials with traps II. *Phil. Mag. B*, 45:189, 1982.

[157] A. Zaban, M. Greenshtein, and J. Bisquert. Determination of the electron lifetime in nanocrystalline dye solar cells by open-circuit voltage decay measurements. *Chem. Phys. Chem.*, 4:859, 2003.

[158] J. Schafferhans, A. Baumann, A. Wagenpfahl, C. Deibel, and V. Dyakonov. Oxygen doping of P3HT:PCBM blends: Influence on trap states, charge carrier mobility and solar cell performance. *Org. Electron.*, 11:1693, 2010.

[159] A. Seemann, H.-J. Egelhaaf, C. J. Brabec, and J. A. Hauch. Influence of oxygen on semi- transparent organic solar cells with gas permeable electrodes. *Org. Electron.*, 10:1424, 2009.

[160] M. O. Reese, A. J. Morfa, M. S. White, N. Kopidakis, S. E. Shaheen, G. Rumbles, and D. S. Ginley. Pathways for the degradation of organic photovoltaic P3HT:PCBM based devices. *Sol. Ener. Mat. Sol. Cells*, 92:746, 2008.

[161] J. Schafferhans, A. Baumann, C. Deibel, and V Dyakonov. Trap distribution and the impact of oxygen-induced traps on the charge transport in poly(3-hexylthiophene). *Appl. Phys. Lett.*, 93:093303, 2008.

[162] V. Chellappan, G. M. Ng, M. J. Tan, W.-P. Goh, and F. Zhu. Imbalanced charge mobility in oxygen treated polythiophene/fullerene based bulk heterojunction solar cells. *Appl. Phys. Lett.*, 95:263305, 2009.

[163] V. I. Arkhipov, P. Heremans, E. V. Emilianova, and H. Bässler. Effect of doping on the density-of-states distribution and carrier hopping in disordered organic semiconductors. *Phys. Rev. B*, 71:045214, 2005.

[164] A. Wagenpfahl, D. Rauh, M. Binder, C. Deibel, and V. Dyakonov. S-shaped current–voltage characteristics of organic solar devices. *Phys. Rev. B*, 82:115306, 2010.

[165] K. Schulze, C. Uhrich, R. Schüppel, K. Leo, M. Pfeiffer, E. Brier, E. Reinold, and P. Bäuerle. Efficient vacuum-deposited organic solar cells based on a new low-bandgap oligothiophene and fullerene C_{60}. *Adv. Mater.*, 18:2872, 2006.

[166] A. Kumar, S. Sista, and Y. Yang. Dipole induced anomalous S-shape I-V curves in polymer solar cells. *J. Appl. Phys.*, 105:094512, 2009.

[167] S. H. Park, A. Roy, S. Beaupre, S. Cho, N. Coates, J. S. Moon, D. Moses, M. Leclerc, K. Lee, and A. J. Heeger. Bulk heterojunction solar cells

with internal quantum efficiency approaching 100%. *Nat. Photon.*, 3:297, 2009.

[168] R. Winter, M. S. Hammer, C. Deibel, and J. Pflaum. Improvemement of the P3HT field effect transistor performance using contact functionalization by small polyaromatic molecules. *Appl. Phys. Lett.*, 95:263313, 2009.

Nomenclature

ABBREVIATIONS

$E_{g,DA}$	Band gap between the HOMO of the donor and the LUMO of the acceptor
BHJ	Bulk heterojunction
CELIV	Charge carrier extraction by linearly increasing voltage
photo-CELIV	Photogenerated charge carrier extraction by linearly increasing voltage
CT	Charge-transfer
DOS	Density of states
DSSC	Dye sensitized solar cell
GDM	Gaussian disorder model
GDOS	Gaussian density of states
HOMO	Highest occupied molecular orbital
LUMO	Lowest unoccupied molecular orbital
MTR	Multiple trapping and release
OLED	Organic light emitting diode
OPV	Organic photovoltaics
OSC	Organic solar cells
OTRACE	Open circuit corrected transient charge extraction by linearly increasing voltage
PCE	Power conversion efficiency
PP	Polaron pair
PV	Photovoltaics
TOF	Time-of-Flight

MATERIALS

Al	Aluminum
Ca	Calcium
ITO	Indium tin oxide
LiF	Lithium fluoride
MDMO-PPV	Poly[2-methoxy-5-(3',7'-dimethyloctyloxy)-1,4-phenylenevinylene
MEH-PPV	Poly[2-methoxy-5-(2'-ethyl-hexyloxy)-1,4-phenylenevinylene]
P3HT	Poly(3-hexylthiophene-2,5-diyl)
pBTCT-C_{12}	Poly(2,5-bis(3-alkylthiophen-2-yl)thieno[2,3-b]thiophene)
pBTTT	Poly(2,5-bis(3-tetradecylthiophen-2-yl) thieno[3,2-b]thiophene)
$PC_{61}BM$	[6,6]-phenyl-C_{61}butyric acid methyl ester
$PC_{71}BM$	[6,6]-phenyl-C_{71} butyric acid methyl ester
bis-$PC_{61}BM$	bis-[6,6]-phenyl-C_{61}butyric acid methyl ester
PCDTBT	Poly[[9-(1-octylnonyl)-9H-carbazole-2,7-diyl]-2,5-thiophenediyl-2,1,3-benzothiadiazole-4,7-diyl-2,5-thiophenediyl]
PEDOT:PSS	Poly(3,4-ethylendioxythiophene): polystyrolsulfonate

VARIABLES

E_{tr}	Transport energy
F	Electric field
FF	Fill factor
j_{sc}	Short circuit current density
μ	Charge carrier mobility

n_{ext}	Charge carrier concentration revealed by transient extraction measurement (photo-CELIV, OTRACE)
P_{mpp}	Maximum power point
r_c	capture radius of a Coulomb sphere
t_{delay}	Delay time: time between the charge photogeneration and the charge extraction by the voltage pulse
t_p	Pulse width of the extraction pulse
τ_σ	Dielectric relaxation time
t_{tr}	Transit time
V_{oc}	Open circuit voltage
V_{bi}	Built-in field; internal electric field
V_{off}	Offset voltage
V_p	Extraction voltage pulse height

Appendix A

List of Publications

Full Papers

Paper–1 Trap distribution and the impact of oxygen-induced traps on the charge transport in poly(3-hexylthiophene), J. Schafferhans, **A. Baumann**, C. Deibel, V. Dyakonov, *Appl. Phys. Lett.* **93**, 093303 (2008).

Paper–2 Polaron Recombination in Pristine and Annealed Bulk Heterojunction Solar Cells, C. Deibel, **A. Baumann**, V. Dyakonov, *Appl. Phys. Lett.*, **93**, 163303, (2008)
Selected for the November 3, 2008 issue of Virtual Journal of Nanoscale Science & Technology.

Paper–3 Bipolar Charge Transport in Poly(3-hexylthiophene)/Methanofullerene Blends: A Ratio Dependent Study, **A. Baumann**, J. Lorrmann, C. Deibel, V. Dyakonov, *Appl. Phys. Lett.*, **93**, 252104, (2008)
Selected for the January 12, 2009 issue of Virtual Journal of Nanoscale Science & Technology.

Paper–4 Polaron Recombination in Pristine and Annealed Bulk Heterojunction Solar Cells, C. Deibel, **A. Baumann**, A. Wagenpfahl, V. Dyakonov, *Synth. Meth.*, **159**, 2345 (2009).

Paper–5 Charge Carrier Concentration and Temperature Dependent Recombination in Polymer–Fullerene Solar Cells, A. Foertig, **A. Baumann**, D. Rauh, V. Dyakonov, C. Deibel, *Appl. Phys. Lett.*, **95**, 052104, (2009)
Selected for the August 17, 2009 issue of Virtual Journal of Nanoscale Science & Technology.

Paper–6 Fullerene Dimers (C60/C70) for Energy Harvesting, J. L. Delgado, E. Espildora, M. Liedtke, A. Sperlich, D. Rauh, **A. Baumann**, C. Deibel, V. Dyakonov, N. Martin, *Chem. Eur. J.*, **15**, 13474 (2009).

Paper–7 Oxygen doping of P3HT:PCBM blends: Influence on trap states, charge carrier mobility and solar cell performance, J. Schafferhans, **A. Baumann**, A. Wagenpfahl, C. Deibel, V. Dyakonov, *Org. Electron.*, **11**, 1693 (2010).

Paper–8 Influence of Phase Segregation on the Recombination Dynamics in Bulk Heterojunction Solar Cells, **A. Baumann**, T. J. Savenije, D. H. K. Murthy, M. Heeney, V. Dyakonov, C. Deibel, *Adv. Func. Mat.*, **21**, 1687 (2011).

Paper–9 Triplet Exciton Generation in Bulk-Heterojunction Solar Cells based on Endohedral Fullerenes, M. Liedtke, A. Sperlich, H. Kraus, **A. Baumann**, C. Deibel, M. Wirix, J. Loos, C. Cardona, V. Dyakonov, *J. Am. Chem. Soc.*, **133**, 9088 (2011).

Contributions to Conferences

Talks

1. Charge Carrier mobility in organic bulk P3HT:PCBM solar cells with varied donor-acceptor ratio, **A. Baumann**, J. Lorrmann, M. Hammer, C. Deibel, V. Dyakonov, *DPG-Frühjahrstagung in Berlin*, talk, HL 289 (2008).

2. Ratio Dependent Charge Transport in Organic Bulk P3HT:PCBM Devices, **A. Baumann**, J. Lorrmann, C. Deibel, V. Dyakonov, *EMRS Spring Meeting in Strasbourg*, talk (2009).

3. Polaron Recombination Dynamics in Bulk Heterojunction Solar Cells, **A. Baumann**, S. Hafner, A. Wagenpfahl, C. Deibel, V. Dyakonov, *DPG-Frühjahrstagung in Regensburg*, talk (2010).

4. Influence of Phase Segregation on the Polaron Dynamics in Organic Solar Cells, **A. Baumann**, T. J. Savenije, D. H. K. Murthy, M. Heeney, C. Deibel, V. Dyakonov, *DPG-Frühjahrstagung in Dresden*, talk (2011).

Poster presentations

1. Bipolar Charge Transport in Poly(3-Hexyl Thiophene)/Methanofullerene Blends, **A. Baumann**, J. Lorrmann, C. Deibel, V. Dyakonov, *DPG-Frühjahrstagung in Dresden*, poster presentation (2009).

2. Origin of the Reduced Efficiency in Aged Organic Solar Cells, **A. Baumann**, J. Schafferhans, A. Wagenpfahl, C. Deibel, V. Dyakonov, *MRS Spring Meeting in San Francisco*, poster presentation (2010).

Anhang B

Danksagung

An dieser Stelle möchte ich mich bei denjenigen bedanken, die mich während meiner Arbeit tatkräftig unterstützt haben und so zu einem erfolgreichen Gelingen der Promotion beigetragen haben. Ich bedanke mich:

- In erster Linie bei Prof. Dr. Vladimir Dyakonov für die gute Betreuung und Untersützung während meiner gesamten Zeit am Lehrstuhl der EP6 einschließlich der Diplomarbeit. Vor allem die intensiven Diskussionen in Hinblick auf wissenschaftliche Veröffentlichungen, sowie die Vorbereitungen für die Vorträge bei wissenschaftlichen Tagungen waren sehr hilfreich und unterstützend.

- Prof. Dr. Bert Hecht für die interessierte Begutachtung dieser Arbeit.

- Dr. Carsten Deibel ebenfalls für die Betreuung und Unterstützung während den letzten fünf Jahren und den vielen anregenden Diskussionen. Gerade seine kritischen und sehr detaillierten Begutachtungen der experimentellen Ergebnisse hat mich während meiner Arbeit immer wieder vorangetrieben.

- der Deutschen Bundesstiftung Umwelt, die mir die Promotion durch ein Stipendium ermöglicht hat. Stellvertretend hier auch ein Dank an meine Betreuerin Christiane Grimm, die mir während meiner Förderzeit jederzeit unterstützend zur Seite stand.

- Alexander Förtig für das Korrekturlesen dieser Arbeit, den vielen hilfreichen wissenschaftlichen Diskussionen und natürlich für all die packenden Tennis-Matches.

- Volker Lorrmann für die Unterstützung im Programmieren. Danke auch für die schönen außeruniversitären Aktivitäten.

- Jens Lorrmann für die tolle Zusammenarbeit und den vielen anregenden und hilfreichen Diskussionen. Besonders seine intensive Arbeit an Simulationen zum Ladungstransport haben das grundlegende Verständnis der experimentellen Ergebnissen gefördert. Nicht zuletzt sein sehr gut durchdachtes Auswerteprogramm in Python muss hier erwähnt werden,

dass in Zukunft den kommenden Diplomanden und Doktoranden einiges an Arbeit ersparen wird. Vielen Dank dafür!

- meinen Kollegen Volker Lorrmann, Markus Mingebach und Daniel Rauh für die tolle Arbeitsatmosphäre im Büro E06.
- Dr. Tom Savenije für die interessanten fachlichen Diskussionen und die gute Zusammenarbeit während seines Aufenthaltes hier bei der EP6 vor allem während unseres gemeinsamen Projektes. Hartelijk dank!
- meinem Diplomanden Sebastian Hafner für seine Mithilfe und den vielen Diskussionen physikalischer aber auch nicht-physikalischer Natur.
- Alexander Wagenpfahl, unserem Simulanten! Es war immer interessant die physikalischen Prozesse auch einmal aus einer ganz anderen Sichtweise vorgestellt zu bekommen und zu diskutieren.
- Maria Hammer, die mich während meiner gesamten Zeit bei der EP6 im "Tran-sport" begleitet hat.
- Moritz Liedtke, den Bremen-Fan, mit dem es immer spannend war neben der Physik auch mal den vergangenen Fussballspieltag zu analysieren.
- meinen Kollegen vom Transport-Treffen Julia Schafferhans, Maria Hammer, Jens Lorrmann und den vielen Diplomanden für die interessanten Diskussionsrunden.
- Andreas Sperlich und Hannes Kraus, den wahren IT-Spezialisten. Wer weiß, wie viele wichtige Daten ohne die beiden verloren gegangen wären.
- Julien Gorenflot, unseren Franzosen! Der EMRS Konferenzbesuch mit dir in Strasbourg war super.
- Den Jungs und Mädels von der Photophysik-Gruppe Björn Gieseking, Julia Kern, Julien Gorenflot, Moritz Liedtke und ihren Diplomanden für die anregenden wissenschaftlichen Gespräche.
- nicht zuletzt der gesamten EP6 Arbeitsgruppe. Es hat mir stets Freude bereitet mit Euch zusammenzuarbeiten.

Ein besonderer Dank gilt meinen Eltern Lieselotte und Werner Baumann, die mich während meiner gesamten langen Studienzeit immer unterstützt und an mich geglaubt haben. Nicht zuletzt möchte ich meiner Freundin Heike von ganzem Herzen danken. Sie hat mir vor allem in der letzten sehr arbeitsintensiven Phase meiner Arbeit viel Verständnis entgegengebracht und mir jederzeit den Rücken gestärkt.

Anhang C

Erklärung gemäß §5(2) der Promotionsordnung

Hiermit erkläre ich, dass ich die vorliegende Arbeit selbständig und ohne fremde Hilfe unter Verwendung der angegeben Quellen und Hilfsmittel angefertigt habe.

(Andreas Baumann)
Rothenburg ob der Tauber, 11. Mai 2011